FURTHER CHARACTERIZATION OF HEART- AND SKELETAL MUSCLE-SPECIFIC MITOCHONDRIAL ASPARTYL-tRNA SYNTHETASE (DARS2) KNOCKOUT MOUSE

by

Özlem Kartal

B.S., Molecular Biology and Genetics, Boğaziçi University, 2019

Submitted to the Institute for Graduate Studies in
Science and Engineering in partial fulfillment of
the requirements for the degree of
Master of Science

Graduate Program in Molecular Biology and Genetics
Boğaziçi University

2022

ACKNOWLEDGEMENTS

I would like to express my sincere appreciation to my supervisor Şükrü Anıl Doğan for inspiring me to study mitochondria and supporting me throughout the whole process. I am grateful for all the techniques he taught me and all his advice that guided me on this journey; I will be thankful for a lifetime.

I was glad to be a part of the Doğan lab. It was an invaluable experience to witness the establishment of a new laboratory. I was lucky to have an excellent lab team. I am thankful to Semin and Mehmet for being amazing labmates, Ayşenur for being there whenever I need and Bengi, Sertan, and Erdost for all their assistance.

I also would like to thank all the MBG family for their help and supports throughout my Master's studies. I am specifically grateful to Davod and Ulduz for their help with troubleshooting. I also would like to express my respect and appreciation for all instructors contributing to me gaining a researcher perspective.

Last but not least, I would like to share my gratitude for my friends and family. I am grateful to İdris for believing me and always motivating me. I would like to thank Büşra for being on the end of the phone whenever I am stressed out. I am thankful to İdil and Merjan for easing the whole process by helping me. I also want to thank my mother, Seniha Kartal, my father, Duran Kartal, and my brother Emre Kartal for supporting me and believing in me throughout my life.

ABSTRACT

FURTHER CHARACTERIZATION OF HEART- AND SKELETAL MUSCLE-SPECIFIC MITOCHONDRIAL ASPARTYL-tRNA SYNTHETASE (DARS2) KNOCKOUT MOUSE

Mitochondrial respiratory chain defects are the primary cause of mitochondrial disorders. Mitochondria have developed various adaptive responses to counteract the effects of these defects. In this study, the heart- and skeletal muscle-specific mitochondrial aspartyl-tRNA synthetase (DARS2) knockout mouse model (hmKO) was further characterized phenotypically and molecularly by previously unchecked parameters. Phenotypic characterization demonstrated that hmKO mice have lower exercise performance, poorer coordinated activity, and weaker muscles than their wild-type littermates. Furthermore, respiratory chain deficiency led to mitochondrial dysfunction exemplified by reduced oxygen consumption rate, reactive oxygen species (ROS) flux, and ATP production. In addition, components of the mitochondrial integrated stress response (ISR^{mt}) were upregulated, while the antioxidant response was downregulated in the heart. Although there is no specific cure for mitochondrial diseases, various approaches can slow down the disease progress or attenuate the symptoms, one of which is ketogenic diet (KD). Animals were fed with KD to mitigate the effects of the severe phenotype of hmKO mice. Unfortunately, KD could not prolong the shortened lifespan and improve the exercise performance and muscle strength of hmKO animals due to our model's severe diseased phenotype.

ÖZET

KALP VE İSKELET KASINA ÖZGÜ MİTOKONDRİAL ASPARTİL-tRNA SENTETAZIN (DARS2) İLERİ KARAKTERİZASYONU

Mitokondriyal solunum zinciri kusurları, mitokondriyal bozuklukların birincil nedenidir. Mitokondri, bu kusurların etkilerine karşı koymak için çeşitli uyarlanabilir tepkiler geliştirmiştir. Bu çalışmada, kalp ve iskelet kasına özgü mitokondriyal aspartil-tRNA sentetaz (DARS2) nakavt fare modeli (hmKO), önceden kontrol edilmemiş parametrelerle fenotipik ve moleküler olarak ileri karakterize edildi. Fenotipik karakterizasyon, hmKO farelerinin, kontrollerinden daha düşük egzersiz performansına, daha zayıf koordineli aktiviteye ve daha zayıf kaslara sahip olduğunu gösterdi. Ayrıca, solunum zinciri eksikliği, azalan oksijen tüketim oranı, reaktif oksijen türleri (ROS) akışı ve ATP üretimi ile örneklenen mitokondriyal işlev bozukluğuna yol açtı. Ek olarak, kalpte mitokondriyal entegre stres yanıtının (ISR^{mt}) bileşenleri artarken antioksidan stres yanıtı azaldı. Mitokondriyal hastalıklar için kesin bir tedavi olmamakla birlikte, ketojenik diyet (KD) gibi çeşitli yöntemler hastalığın ilerlemesini yavaşlatabilir veya semptomları hafifletebilir. Hayvanlar, hmKO farelerinin şiddetli fenotipinin etkilerini hafifletmek için KD ile beslendi. Ne yazık ki KD, modelimizin aşırı hastalıklı fenotipi nedeniyle hmKO hayvanlarının kısalmış ömrünü uzatamadı ve egzersiz performansını ve kas gücünü iyileştiremedi.

TABLE OF CONTENTS

LIST OF FIGURES

LIST OF TABLES

LIST OF SYMBOLS

g	Gram
g	Gravity
kb	Kilo Base
m	Meter
m	Milli
M	Molar
mg	Milligram
ml	Milliliter
nM	Nanomolar
pmol	Picomole
rpm	Revolutions Per Minute
s	Second
U	Units
V	Volt
°C	Celcius Degree
α	Alpha
β	Beta
γ	Gamma
Δ	Delta
μl	Microliter
μM	Micromolar
Ψ	Psi

LIST OF ACRONYMS/ABBREVIATIONS

AA	Amino Acid
ADP	Adenosine Diphosphate
ARE	Antioxidant Response Element
ARS2	Mitochondrial Aminoacyl-tRNA Synthetase
ATP	Adenosine Triphosphate
BSA	Bovine Serum Albumin
CAT	Catalase
CCCP	Carbonyl Cyanide 3-Chlorophenylhydrazone
Cre	Bacteriophage P1 Derived Site-specific Recombinase
DARS2	Mitochondrial Aspartyl-tRNA Synthetase
DC	Detergent Compatible
ddH_2O	Double Distilled Water
DNA	Desoxyribonucleic Acid
dNTP	Deoxyribonucleotide Triphosphate
ECL	Enhanced Chemoluminiscence
EDTA	Ethylendiamine Tetraacetate
EGTA	Ethylene Glycol Tetraacetic Acid
EtBr	Ethidium Bromide
ETC	Electron Transport Chain
GCL	Glutamine-Cysteine Ligase
GPx	Glutathione Peroxidase-1
GS	Glutathione Synthetase
GST	Glutathione S-Transferase
H_2O_2	Hydrogen Peroxide
HCl	Hydrochloric Acid
HO-1	Heme Oxygenase-1
HRP	Horseradish Peroxidase
KCl	Potassium Chloride

K_2HPO_4	Potassium Hydrogen Phosphate
$MgCl_2$	Magnesium Dichloride
mRNA	Messenger RNA
mtDNA	Mitochondrial DNA
NaCl	Sodium Chloride
NaF	Sodium Fluoride
NQO1	Quinone Oxidoreductase 1
$O^{\cdot -}$	Superoxide
PBS	Phosphate-Buffered Saline
PCR	Polymerase Chain Reaction
pH	Potential of Hydrogen
RNA	Ribonucleic Acid
ROS	Reactive Oxygen Species
qPCR	Quantitative Polymerase Chain Reaction
SDS	Sodium Dodecyl Sulfate
SOD	Superoxide Dismutase
TEMED	Tetramethyl Ethylenediamine
Tris	2-Amino-2-(Hydroxymethyl)-1,3-Propandiole
Tris HCl	2-Amino-2-Hydroxymethyl-Propane-1,3-Diol
tRNA	Transfer RNA
TWEEN	Polyoxethylene-Sorbitan-Monolaureate

1. INTRODUCTION

1.1. Mitochondria

Mitochondria are the organelles that provide energy for almost every eukaryotic cell (Gray, 2013). The origin of the mitochondria is a prokaryote according to the endosymbiosis theory (Aanen & Eggleton, 2017). The endosymbiosis theory postulated that the mitochondria aroused from a symbiont relationship between the alphaproteobacterium and the host Asgard archaea (Roger et al., 2017). This theory has been supported by much evidence. One of the strong proofs is the physiological and biochemical similarity between the mitochondria and the prokaryotic cells (Boguszewska et al., 2020). The mitochondrial inner membrane is similar to prokaryotic membranes in composition and physical properties (Scorrano, 2013). Mitochondria use the same strategy, fission, as prokaryotes for dividing (Kuroiwa et al., 2006). Likewise, a mitochondrion has its own genome that retains a miniaturized chromosome of a prokaryotic cell, and mitochondrial DNA can translate its own proteins (Lightowlers et al., 2014; Zimorski et al., 2014). Furthermore, protein translation in mitochondria resembles bacterial protein translation in that both initiate translation with N-formyl methionyl tRNA, unlike the eukaryotic cytosolic translation (Fridovich, 1974; Kummer & Ban, 2021).

Mitochondria have a dynamic structure with balanced fusion and fission machinery, which shapes the mitochondrial compartments for responding to changing physiological conditions (Westermann, 2010). A mitochondrion consists of the inner membrane (IMM), outer membrane (OMM), and the intermembrane space that separates the IMM and OMM (Figure 1.1). The inner part of mitochondria is filled with the matrix containing mitochondrial DNA, ribosomes, RNAs, proteins, and various enzymes, which maintain the mitochondrial function (Frey & Mannella, 2000).

The mitochondrial inner membrane is folded to extend its surface; these folded structures are called cristae (Mannella, 2020). Cristae comprise the protein complexes responsible for oxidative phosphorylation (OXPHOS) (Joubert & Puff, 2021).

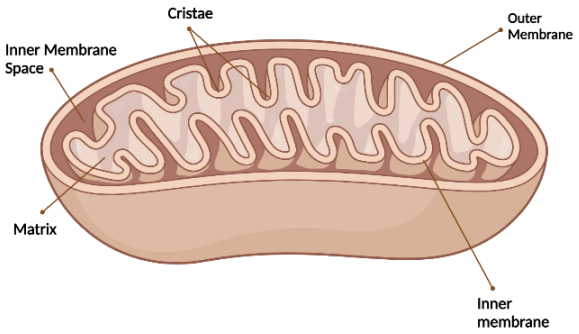

Figure 1.1. Structure of the mitochondria.

1.1.1. Electron Transport Chain

Cristae harbor the electron transport chain (ETC) that comprises five main complexes and two carriers facilitating oxidative phosphorylation (OXPHOS) (Cogliati et al., 2013). During forward electron transport (FET), complex I (NADH: ubiquinone oxidoreductase) oxidizes NADH to NAD^+ and transfers its electrons to ubiquinone (Sousa et al., 2018). Complex II (Succinate: quinone dehydrogenase) oxidizes the Krebs cycle metabolite succinate to fumarate and reduces ubiquinone to ubiquinol (Quinlan et al., 2012). Ubiquinone also receives electrons from dihydroorotate dehydrogenase (DHODH), electron transfer flavoprotein quinone oxidoreductase (ETF: QOR), and Glycerol-3-phosphate dehydrogenase (GPDH) (Scialò et al., 2017). Then, complex III accepts electrons from ubiquinol and transfers them to cytochrome c (Chandel, 2010). Cytochrome c carries 2 electrons to complex IV, and electrons reduce the final acceptor oxygen to water. This process creates a proton gradient that Complex V can utilize to produce ATP from ADP (Sousa et al., 2018). The forward electron transport process is depicted in Figure 1.2.

1.1.2. Mitochondrial Reactive Oxygen Species (mtROS)

During electron transfer, some electrons may directly leak onto oxygen instead of passing to the next carrier, which causes superoxide $O^{\cdot -}$ formation (Liu et al., 2002). Afterward, $O^{\cdot -}$ is converted to hydrogen peroxide H_2O_2 by superoxide dismutase enzymes (SODs). Both $O^{\cdot -}$ and H_2O_2 are known as reactive oxygen species (ROS); if their sources are the mitochondria, they are called the mitochondrial reactive oxygen species (mtROS) (Li et al., 2013). Complex I and complex III are the primary sources of the mtROS, but complex II can also contribute to ROS generation (Zhao et al., 2019). ROS plays a role in oxidative damage, aging, and various diseases, including ischemia, Parkinson's, and Alzheimer's diseases (Scialò et al., 2016). Recently, it has been revealed that ROS also acts as a signal molecule regulating physiologic homeostasis (Sena & Chandel, 2012). The role of ROS depends on its amount, nature, and where and when it is produced (Stefanatos & Sanz, 2018). A low amount of ROS has been associated with the signaling function, whereas a high level of ROS is considered detrimental (Scialò et al., 2017). A depiction of the forward electron transportation process and reactive oxygen species production can be found in Figure 1.2. The forward electron transport is not the only source of mitochondrial ROS. Under certain conditions, electrons are transferred back to complex I, which is called the reverse electron transfer (RET) (Selivanov et al., 2011). For instance, when Complex II is supplied with succinate, electrons are carried to ubiquinone (Q), which leads to the over-reduction of ubiquinone. Therefore, it cannot receive any electrons from Complex I, which causes electrons to move back (Scialò et al., 2017). The production of ROS by RET depends on mitochondrial membrane potential and the redox state of both the CoQ pool and the NADH pool (Robb et al., 2018). The RET-ROS plays an essential role in many biological processes. RET-ROS has been shown to activate some stress responses like mitochondrial biogenesis (Dogan et al., 2018), extend the lifespan of *Drosophila melanogaster* (Scialò et al., 2016), help myoblast differentiation (Lee et al., 20011), and trigger inflammatory responses of macrophages (Mills et al., 2016). A depiction of the reverse electron transfer process and reactive oxygen species production can be found in Figure 1.3.

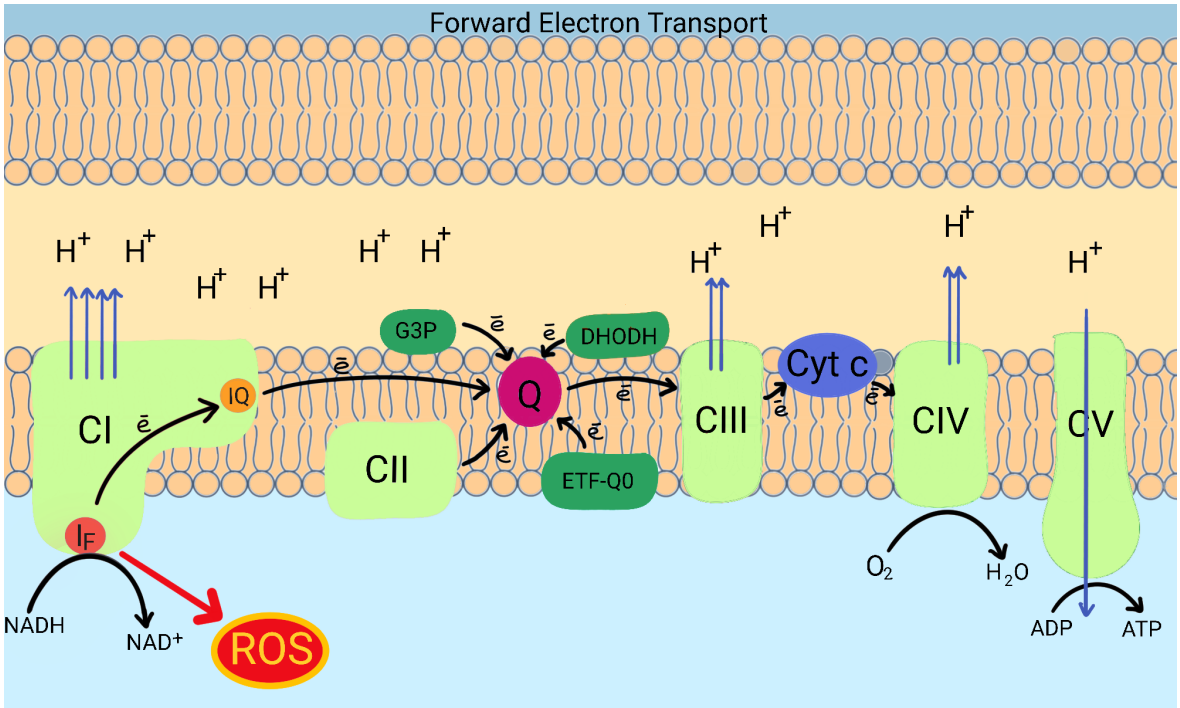

Figure 1.2. Forward electron transport (FET).

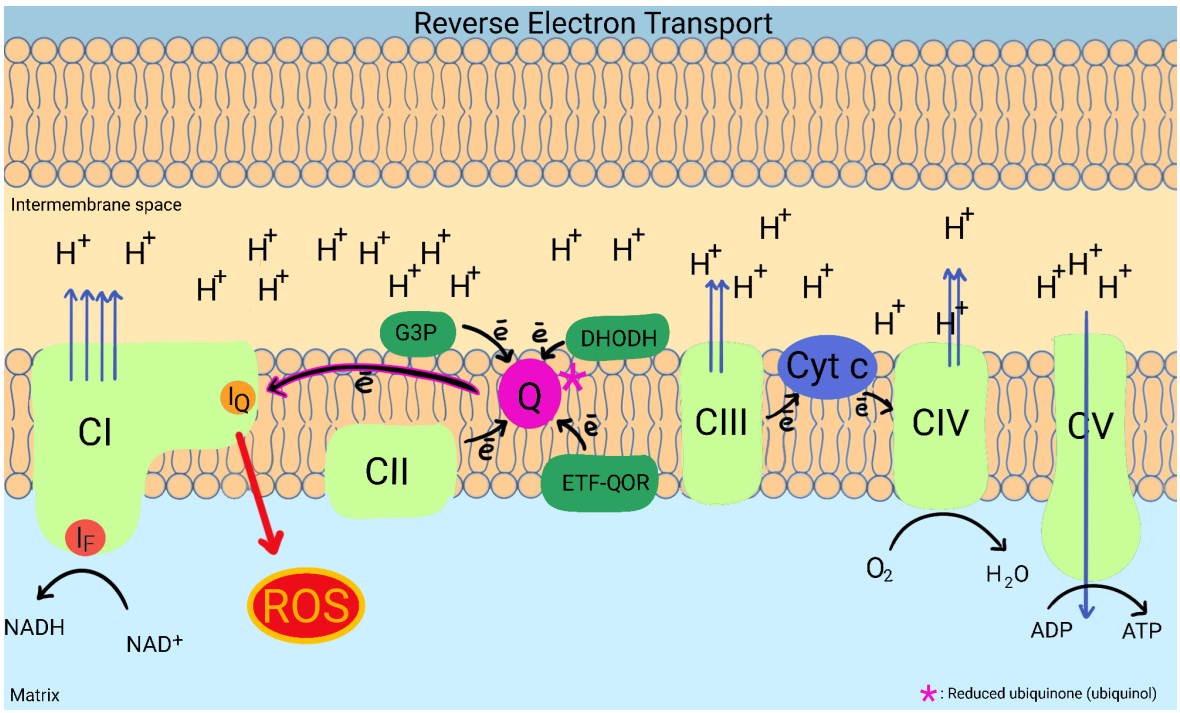

Figure 1.3. Reverse electron transport (RET).

1.1.3. Mitochondrial DNA

Human mitochondrial DNA (mtDNA) is a 16,569-kb long double-stranded circular molecule with 37 genes encoding for 22 tRNAs, 2 rRNAs, and 13 subunit proteins of the mitochondrial respiratory chain (Young & Copeland, 2016). Since only the egg cell contributes to mitochondria at fertilization, mtDNA belongs to the ovum, which means mtDNA is transmitted not according to Mendelian rules but by maternal inheritance (Giles et al., 1980). Therefore, mtDNA mutations are passed from the mother to her offspring. Likewise, only her daughters transmit mutations to the next generation (Saneto & Sedensky, 2013).

A single eukaryotic cell contains many mitochondria (up to several thousand) and each mitochondria many copies of mtDNA, which creates the concepts of homoplasmy and heteroplasmy. Homoplasmy defines the uniformity of the mitochondrial genome (Bolze et al., 2019). In contrast, heteroplasmy means the presence of more than two mitochondrial genotypes (Stewart & Chinnery, 2015). These concepts become meaningful when considering diseases that result from mtDNA mutations. Homoplasmic mutations impact all mtDNA, while heteroplasmic mutations only affect some copies (Taylor & Turnbull, 2005). If an mtDNA homoplasmic mutation causes a disease, it certainly shows its clinical effects. However, if a mutation presents in some copies (heteroplasmic mutation), its effects are determined by the ratio of healthy and mutant copies. The minimum critical level of mutant mtDNA copies required to demonstrate the clinical expression of a disease is called the threshold effect (DiMauro & Davidzon, 2005).

1.1.4. Mitochondria in Disease

A mitochondrion participates in various biological processes. It is more than a powerhouse for a cell (McBride et al., 2006). It has essential roles in cell signaling, cell growth, ion homeostasis, and the mechanism of cell survival and death (Osellame et al., 2012). Therefore, it is vital to protect mitochondrial homeostasis.

In physiological conditions, mitochondria keep their balance by biogenesis and degradation (mitochondrial autophagy; 'mitophagy') (Melser et al., 2015). The dysfunction of a mitochondrion may cause many diseases such as cancer, diabetes, cardiovascular disorders, and neurodegenerative diseases. Because mitochondria have roles in programmed cell death mechanisms, including necroptosis, apoptosis, ferroptosis, pyroptosis, and autophagy, their fitness is crucial for the homeostasis of the cell (Javadov et al., 2020). Moreover, as stated above, it produces a signaling molecule, ROS, that plays an essential role in activating stress responses, extending lifespan, and triggering inflammation as well as oxidative damage, aging, and various diseases (Dogan et al., 2018; Lee et al., 20011; Mills et al., 2016; Scialò et al., 2016).

The mitochondrial genome is more susceptible to mutations than the nuclear DNA (Lax et al., 2011). Because mtDNA is close to respiratory chain complexes, it may be damaged easily by ROS released from complexes (Santos et al., 2013). Even though it has repair systems, it cannot overcome oxidative damage all the time (Ryzhkova et al., 2018).

mtDNA mutations can be investigated under two main groups: point mutations and mtDNA rearrangements. Mitochondrial DNA point mutations might be in the genes encoding for protein, rRNA, or tRNA. Nevertheless, most point mutations causing disease has been found to be occuring in tRNA genes (Wallace et al., 1992). Mitochondrial tRNA mutations may affect all mitochondrial translation by reducing mt-tRNA availability (Tuppen et al., 2010). mtDNA point mutations result in various diseases like MELAS (Mitochondrial encephalomyopathy, lactic acidosis, and stroke-like episodes), MERRF (Myoclonus epilepsy and ragged red fibers), LHON (Leber's hereditary optic neuropathy), and NARP (Neuropathy, ataxia retinitis pigmentosa) (Taylor & Turnbull, 2005). mtDNA rearrangements are the other source of mitochondrial dysfunctions and diseases. Large-scale mtDNA rearrangements might result in deletions, hence defects in mtDNA maintenance (Rygiel et al., 2016). mtDNA rearrangement mutations lead to various mendelian, maternally inherited, and sporadic disorders such as Kearns-Sayre syndrome (KSS) (Moraes et al., 1989; Wallace, 2005).

Mitochondrial fitness can be affected by mutations not only in mtDNA but also in nuclear DNA. mtDNA encodes 13 proteins of respiratory chain complexes (Subunits of complex I: ND1-ND6 and ND4L; subunit of complex III: CYTB; subunits of complex IV: COX1-COX3; and subunits of complex V: ATP6 and ATP8); however, most genes coding for subunits of complexes are encoded by nuclear DNA (Wang et al., 2021). In addition, nuclear DNA encodes many essential genes that participate in mtDNA maintenance, replication, transcription, and translation (Rusecka et al., 2018). This study will focus on the nuclear-encoded mitochondrial enzyme, aspartyl-tRNA synthetase 2 (DARS2), a crucial player in the mitochondrial translational process.

1.1.5. Mitochondrial Aminoacyl-tRNA Synthetases

Aminoacyl-tRNA synthetases (ARSs) are responsible for ligating tRNAs with their corresponding amino acids during protein synthesis (Kwon et al., 2019). Charging tRNAs with their cognate amino acids is catalyzed in a two-step reaction by corresponding aminoacyl-tRNA synthetases (Kaiser et al., 2020). In the first step, amino acid and an ATP molecule bind to the catalytic site of the aminoacyl-tRNA synthetase, which results in hydrolysis of ATP to adenosine monophosphate (AMP) and pyrophosphate (PPi) (Figure 1.4). While amino acid is attached to the AMP in the enzyme, pyrophosphate is released from the active site. In the second step, the corresponding tRNA molecule binds to aminoacyl-tRNA synthetases, then the amino acid is transferred to tRNA from adenosine monophosphate (AMP) and the vacant AMP is released (Kaiser et al., 2020; Rubio Gomez & Ibba, 2020).

Since mitochondria can synthesize their own genes, they need aminoacyl-tRNA synthetase to charge their tRNAs with cognate amino acids (Chihade, 2020). The nucleus encodes aminoacyl-tRNA synthetase enzymes which act in the cytosol or are imported to mitochondria (Ognjenović & Simonović, 2018).

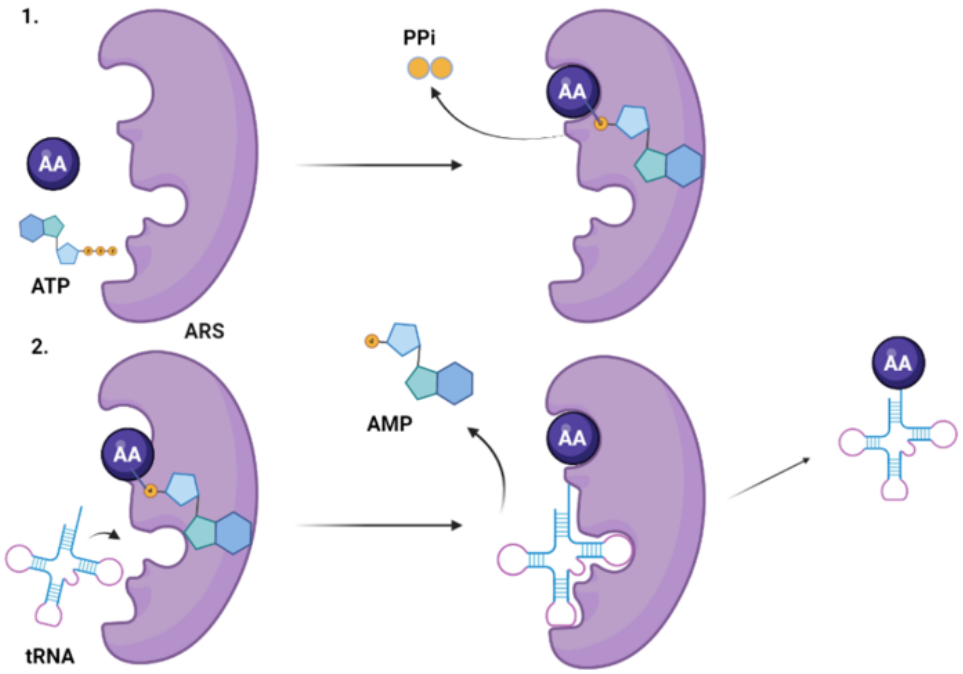

Figure 1.4. Aminoacylation reaction.

It has been shown that genes that encode mitochondrial aminoacyl-tRNA synthetases are associated with a wide range of human diseases; because mtARSs play an essential role in mitochondrial protein synthesis, their deficiency might affect mitochondrial fitness and hence human health (Figuccia et al., 2021). Mitochondrial dysfunctions primarily affect the tissues, specifically the brain, muscle, and heart, that require high energy to maintain their functions. Therefore, mitochondrial aminoacyl-tRNA synthetase mutations cause central nervous system pathologies like leukodystrophies, Perrault syndrome, and encephalopathies (Fine et al., 2019). Mitochondrial aminoacyl-tRNA synthetase genes and related diseases are listed in Table **??**. DARS2 is one of the mitochondrial aminoacyl-tRNA synthetases crucial for protein synthesis in mitochondria. It attaches the aspartate amino acid to its corresponding tRNA, as shown in Figure 1.4.

It has been proposed that almost all patients that suffer from Leukoencephalopathy with brainstem and spinal cord involvement and lactate elevation have mutations in the DARS2 gene (Scheper et al., 2007). One of these mutations is generally found in the splice site in intron 2, the upstream of exon 3, which results in a frameshift and non-functional protein. However, this mutation can be 'leaky,' meaning full-length protein can be formed by part of the mutated mRNAs with exon3 (van Berge et al., 2014).

Table 1.1. Various diseases caused by mutations in mitochondrial aminoacyl-tRNA genes.

Gene	Disease
AARS2	Perinatal or infantile mitochondrial cardiomyopathy (Götz et al., 2011)
DARS2	LBSL (Leukoencephalopathy with brain stem and spinal cord involvement and lactate elevation) (van Berge et al., 2014)
EARS2	LTBL (Early-onset Leukoencephalopathy with Thalamus and Brainstem Involvement and High Lactate) (Steenweg et al., 2012)
FARS2	Early-onset epileptic mitochondrial encephalopathy and spastic paraplegia (Barcia et al., 2021)
GARS	CMT (Charcot-Marie-Tooth disease) (Motley et al., 2011)
HARS2	PRLTS2 (Perrault syndrome 2) (Pierce et al., 2011)
KARS	CMTRIB (Charcot-Marie-Tooth disease, recessive intermediate, B) (Quadros Santos Monteiro Fonseca & Zanoteli, 2018)
LARS2	PRLTS4 (Perrault syndrome 4) (Pan et al., 2020)
YARS2	MLASA (Myopathy, Lactic Acidosis, and Sideroblastic Anemia) (Kasapkara et al., 2017)
MARS2	ARSAL (Autosomal Recessive Spastic Ataxia with Leukoencephalopathy) (Bayat et al., 2012)
RARS2	PCH6 (Pontocerebellar Hypoplasia type 6) (Nevanlinna et al., 2020)
SARS2	HUPRA (Hyperuricemia, Pulmonary hypertension, Renal failure in infancy, and Alkalosis) (Belostotsky et al., 2011)

DARS2 deficiency has been studied in various mouse models. In the heart- and skeletal muscle-specific DARS2-deficient mouse model, DARS2 depletion resulted in respiratory chain dysfunction in both tissues, and DARS2 deficient mice developed cardiac hypertrophy and muscle atrophy (Dogan et al., 2014). In forebrain-specific DARS2-deficient mice, loss of DARS2 in neurons caused strong mitochondrial dysfunction and cell death (Aradjanski et al., 2017). Another study investigated the contribution of mitochondrial metabolism to the inflammatory effects of macrophages in the wound healing process using myeloid-specific DARS2-deficient models (Willenborg et al., 2021).

1.2. Mitochondrial Stress Signaling

It is vital to ensure compatibility between mitochondrial fitness and cell to maintain mitochondrial function and meet the cell's needs (Chandel, 2014). Therefore, mitochondria developed various adaptation mechanisms to cope with the changing environmental conditions. These mechanisms include communication with the other organelles and the nucleus by signal conduction (Mick et al., 2020). Respiratory chain defects causing impaired oxidative phosphorylation and energy metabolism are the principal activators of most adaptive stress responses (Barbour & Turner, 2014). In addition, the other sources of mitochondrial stress are impaired proteostasis, excessive reactive oxygen species (ROS) production, nutrient deprivation, hypoxia, and viral infections (Camhi et al., 1995; Pakos-Zebrucka et al., 2016; Zhao, 2002). Adaptive responses that mitochondria develop to cope with stress are discussed below.

1.2.1. Retrograde Signaling

Although mitochondria synthesize their own proteins, the most considerable portion of the mitochondrial proteins is encoded in the nucleus and imported into mitochondria (da Cunha et al., 2015). Thus, communication between the nucleus and the mitochondria is essential to maintain cell homeostasis. Mitochondria communicate with the nucleus for biogenesis, homeostasis, and informing the nucleus about

mitochondrial dysfunction (Cardamone et al., 2018). The mitochondrial retrograde signaling pathway was firstly described in *Saccharomyces cerevisiae* (Rios-Anjos et al., 2017). In *Saccharomyces cerevisiae*, mitochondrial dysfunction can be sensed by Rtg2p, which activates a transcription factor complex consisting of Rtg1p and Rtg3p. Rtg1p and Rtg3p complex translocates to the nucleus and turns on the transcription of genes required for adapting to changing physiological conditions (Hill & Van Remmen, 2014; Rios-Anjos et al., 2017). The signal mechanism has become more complicated with many unknowns in higher organisms. The studies in mammalian retrograde signaling focus on mitochondrial biogenesis (Cardamone et al., 2018).

Mitochondrial biogenesis can be defined as increasing mitochondrial mass and copy number (Bhatti et al., 2017). The master regulator of mitochondrial biogenesis is the peroxisome-proliferator-activated receptor γ co-activator-1α (PGC-1α). PGC-1α activates the other transcription factors; nuclear respiratory factor 1 (NRF1) and nuclear respiratory factor 2 (NRF2). NRF1 and NRF2 are essential components of biogenesis event; they activate mitochondrial transcription factor A (TFAM), which drives mitochondrial replication and transcription (Jornayvaz & Shulman, 2010).

Mitochondrial biogenesis can be activated in response to physiological stimuli such as exercise, temperature, dietary restriction, and muscle myogenesis (Bhatti et al., 2017). It also occurs in response to mitochondrial dysfunction; upon mitochondrial respiratory chain deficiency, mitochondria activate biogenesis to compensate for energy deficit (Uittenbogaard & Chiaramello, 2014). However, it might fail to counteract deficiency, causing pathology such as cardiac hypertrophy (Rimbaud et al., 2009).

1.2.2. Antioxidant Response

Some electrons may leak from complexes during electron transport and reduce oxygen to superoxide molecules ($O^{\cdot -}$) (Liu et al., 2002). $O^{\cdot -}$ is immediately converted to H_2O_2. Both $O^{\cdot -}$ and H_2O_2 are produced by mitochondria called mitochondrial reactive oxygen species (mtROS) (Li et al., 2013). mtROS might be beneficial by

acting as a signaling molecule; however, an excessive amount of mtROS might cause oxidative damage and age-related diseases such as Parkinson's and Alzheimer's (Scialò et al., 2016). Cells developed an antioxidant response to cope with excess mtROS.

NFE2L2 (the transcription factor nuclear factor (erythroid 2)-like, also known as NRF2) is an essential player in the antioxidant response. Under physiological conditions, the level of NFE2L2 is controlled by KEAP1-induced proteasomal degradation (Wen et al., 2017). Under oxidative stress conditions, free radicals lead NFE2L2 to release from Keap1. Thus, NFE2L2 does not undergo proteasomal degradation; instead, it can translocate to the nucleus to bind antioxidant response elements (ARE). Thus, it can activate the transcription of antioxidant enzymes, glutathione peroxidase (GPx), heme oxygenase-1 (HO-1), catalase (CAT), glutathione S-transferase (GST), NAD(P)H: quinone oxidoreductase 1 (NQO1), superoxide dismutase (SOD), glutathione reductase (GR), glutathione synthetase (GS) and glutamine-cysteine ligase (GCL) (Francisqueti-Ferron et al., 2019). Activation of antioxidant response is depicted in Figure 1.5.

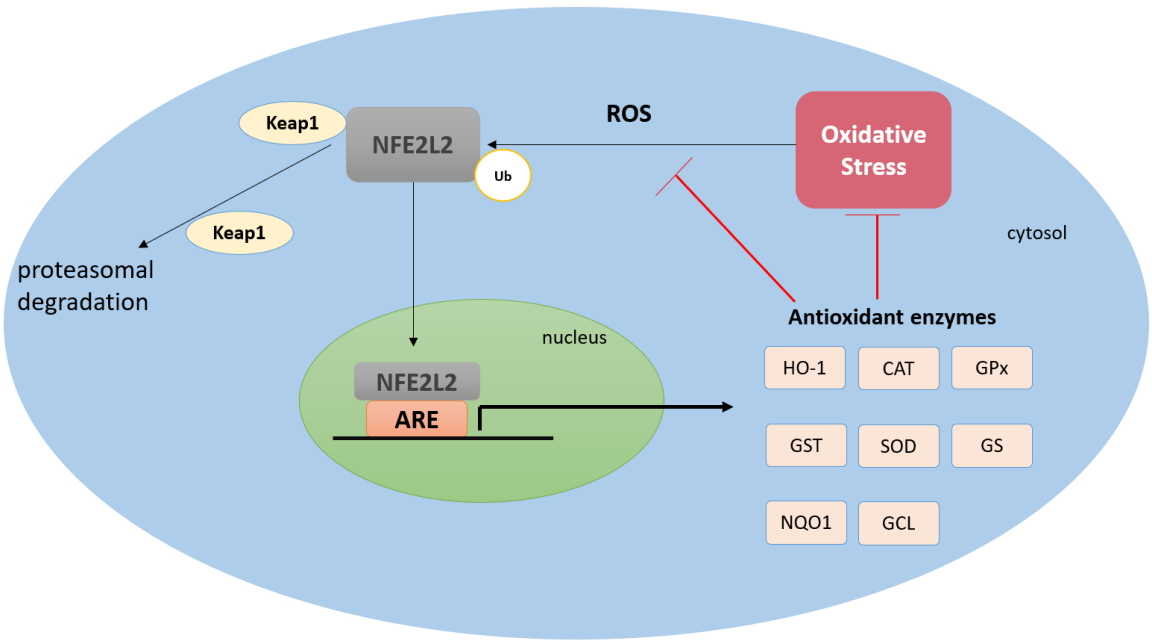

Figure 1.5. Activation of antioxidant response.

Superoxide dismutases, catalase, and glutathione peroxidase-1 are the essential components of antioxidant response. Superoxide dismutase (SODs) are ROS scavenging enzymes. They are crucial in converting superoxide molecules released from respiratory complexes to hydrogen peroxide. SOD1 (Cu/ZnSOD) regulates superoxide levels in cytosol, peroxisome, and the intermembrane space of the mitochondria (Eleutherio et al., 2021). SOD2 (MnSOD) is responsible for scavenging ROS in the mitochondrial matrix. Superoxide molecules can also be converted to other reactive species, including reactive nitrogen species (RNS) such as peroxynitrite ($ONOO^-$). Therefore, SODs also control the concentration of other reactive species (Wang et al., 2018). Glutathione peroxidase-1 (GPx-1) and catalase are the crucial components of antioxidant response. They are responsible for converting hydrogen peroxide to water; thus, they can limit the harmful effects of hydrogen peroxide by preventing its accumulation (Lubos et al., 2011; Nandi et al., 2019). A scheme showing antioxidant response reactions is depicted in Figure 1.6.

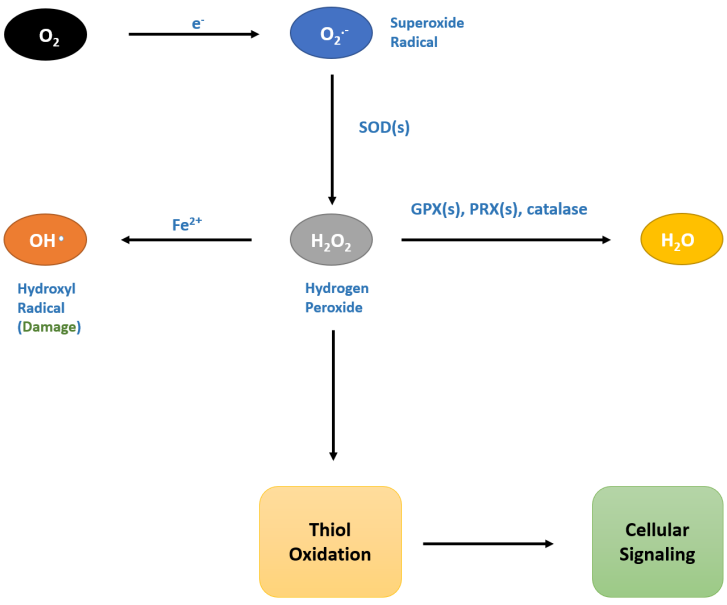

Figure 1.6. Antioxidant response reactions.

1.2.3. Mitochondrial Integrated Stress Response (ISR^{mt})

Integrated stress response (ISR) is an adaptive signaling pathway triggered in response to different physiological conditions, including hypoxia, glucose deprivation, amino acid deprivation, and pathogen infection (Pakos-Zebrucka et al., 2016). In mammalian cells, the signaling pathway is initiated by eIF2α activation; eIF2α is activated by phosphorylation. According to stimuli, eIF2α can be phosphorylated by different kinases; GCN2, PKR, HRI, and PERK. Activated eIF2α decreases global protein synthesis, whereas it also upregulates the activating transcription factor 4 (ATF4) to turn on the transcription of ISR component genes. (Pakos-Zebrucka et al., 2016). While this pathway can initiate the transcription of genes coding for metabolic rewiring proteins for all cellular compartments, it can also respond in an organelle-specific manner (Zhao, 2002).

Mitochondrial stress might result in activating mitochondrial integrated stress response (ISR^{mt}). The primary mechanism is similar to endoplasmic reticulum stress response, in which activated eIF2α promotes ATF4 translation. However, how mitochondrial stress is sensed and relayed to ATF4 is an open question (Guo et al., 2020). ATF4 upregulates its downstream genes that are essential players in ISR^{mt}. Upon mitochondrial dysfunction, ISR^{mt} activates serine and proline catabolism, the mitochondrial one-carbon pathway, and upregulates the levels of mitochondrial cytokines FGF21 (fibroblast growth factor 21) and GDF15 (growth factor 15) in affected tissues (Kühl et al., 2017; Mick et al., 2020).

Mitochondrial unfolded protein response (UPR^{mt}) is part of the ISR^{mt} (Anderson & Haynes, 2020). Mitochondrial dysfunction increases with aging, which results in the accumulation of unfolded proteins in the mitochondrial matrix (Melber & Haynes, 2018). In response to accumulated misfolded or unfolded proteins, the cell turns on the transcription of nuclear genes that encode mitochondrial proteases and chaperones. Thus, mitochondrial proteostasis can be enhanced by rewiring cellular metabolism (Anderson & Haynes, 2020).

Mitochondrial unfolded protein response (UPR^{mt}) was described firstly in *Caenorhabditis elegans* (Hill & Van Remmen, 2014). In response to mitochondrial stress, *Caenorhabditis elegans* activates UPR^{mt} in controlling ATFS-1 (activating transcription factor associated stress) (Wu et al., 2018). ATFS-1 has nuclear and mitochondrial localization signals. Under normal physiological conditions, it is degraded by the Lon protease in the mitochondria. However, it translocates to the nucleus upon mitochondrial stress and turns on the transcription of various metabolic enzymes, mitochondrial chaperons, and detoxification enzymes (Shpilka & Haynes, 2018; Wu et al., 2018).

In mammalian UPR^{mt}, mitochondrial stress activates eIF2α-induced transcription of essential UPR^{mt} transcription factors ATF4, ATF5, and CHOP (CCAAT/enhancer-binding protein homology protein). ATF4 upregulates the transcripts of various genes, including CHOP (Münch, 2018). CHOP is an essential player of mammalian UPR^{mt}; it dimerizes with C/EBPβ and activates the transcription of mitochondrial proteases and chaperones such as chaperonin 10 and chaperonin 60, mtDNAJ, and ClpP (Zhao, 2002).

1.2.4. Mitochondrial Autophagy (Mitophagy)

Autophagy is a Greek term that means "self-eating" (Chang, 2020). Self-degradation is an adaptive response that is essential for cellular homeostasis. Autophagy is a way to eliminate aggregated or misfolded proteins, pathogens, and damaged organelles such as the endoplasmic reticulum, mitochondria, and peroxisome (Glick et al., 2010). The first step of autophagy is forming double-membrane vesicles, autophagosomes. The autophagosome initiation is mediated by the ULK1 complex (ULK, FIP200, Atg101, and Atg13). Then autophagosomes are elongated by Atg12 and LC3 (microtubule-associated protein 1 light chain 3). Autophagosomes fuse with lysosomes to form autolysosomes. Degradation of macromolecules takes place in autolysosomes; they are degraded into fatty acids, nucleotides, and amino acids (Yang et al., 2015).

Mitophagy is selective autophagy in which mitochondria are degraded (Ding & Yin, 2012). Mitophagy shares the principal mechanism with autophagy. In budding yeast studies, Atg32 (autophagy-related protein) was described as a novel player in selective autophagy. It is found in the outer membrane of the mitochondria and binds to Atg11 to initiate mitophagy (Kondo-Okamoto et al., 2012). In case of mitochondrial damage, mitophagy removes dysfunctional mitochondria to keep the population of functional mitochondria at an optimal state (Killackey et al., 2020). Depolarization of mitochondria, hypoxia, or impaired OXPHOS might induce mitochondria to mitophagy (Killackey et al., 2020).

2. PURPOSE

Mitochondrial respiratory chain dysfunction is the primary cause of mitochondrial disorders. Mitochondria have developed various adaptive responses to counteract the effects of dysfunctional mitochondria. Mitochondrial aspartyl-tRNA synthetase (DARS2) deficiency has been shown to impair mitochondrial protein synthesis in the heart and skeletal muscle, preventing OXPHOS complexes from properly assembling, which results in respiratory chain defects in both the heart and skeletal muscle tissues (Dogan et al., 2014). Furthermore, the heart and skeletal muscle tissues act differently in response to DARS2 depletion; while the heart initiates adaptive stress responses, skeletal muscle uses its intrinsic mechanism to maintain protein homeostasis (Dogan et al., 2014). In this study, our overall objective was to further characterize the heart-and skeletal muscle-specific DARS2 knockout mouse model (hmKO) phenotypically and molecularly by previously unchecked parameters, and try to attenuate the effects of DARS2 depletion by ketogenic diet intervention. The first aim was to characterize the hmKO mouse model phenotypically to see how DARS2 deficiency affects the phenotype of hmKO mice. The second aim was to molecularly characterize hmKO mice by checking mitochondrial function and various stress response elements to understand the molecular effects of DARS2 depletion in the heart and skeletal muscle. The final aim was to treat hmKO mice with a well-known dietary intervention method, the ketogenic diet, to mitigate the severe phenotype of this model.

3. MATERIALS

All materials used in this study are listed below.

3.1. Biological Materials

Mouse models from C57BL/6N genetic background were transferred from Cologne Excellence Cluster in Aging and Aging-Associated Diseases (CECAD), Cologne, Germany.

3.2. Buffers and Solutions

Buffers and solutions used in this study are listed below.

Table 3.1. Buffers for Genotyping.

Buffer	**Recipe**
Tail Lysis Buffer	10 mM Tris-HCl 5 mM EDTA (pH:8) 0.2% SDS 200 mM NaCl
TBE Buffer (10X)	1 M Tris base 1 M Boric Acid 0.02 M EDTA

Table 3.2. Organ Lysis Buffer.

Buffer	**Recipe**
Organ Lysis Buffer	50 mM Hepes (pH: 7.4) 1% Triton X-100 0.1 M NaF 10 mM Na Orthovanadat 10 mM EDTA 0.1% SDS 50 mM NaCl

Table 3.3. Western Blot Buffers and Solutions.

Buffers or Solutions	**Recipe**
Ammonium Persulfate	10% APS (w/v) in ddH_2O
Blocking Buffer	1X PBST with 5% (w/v) nonfat dry milk or BSA
PBS (10X)	1.37 M NaCl 27 mM KCl 100 mM Na_2HPO_4 18 mM KH_2PO_4
PBS-T	1X PBS 0.1% Tween 20
Running Buffer	25 mM Tris 250 mM Glycine 0.2% SDS

Table 3.3. Western Blot Buffers and Solutions. (cont.)

Buffers or Solutions	**Recipe**
Transfer Buffer	25 mM Tris 200 mM Glycine 20% Methanol

Table 3.4. Western Blot Gels.

Gels	**Recipe**
10% Resolving Gel	10% Acrylamide:Bisacrylamide 375 mM Tris-HCl (pH 8.8) 0.005% TEMED 0.1% SDS 0.05% APS
12% Resolving Gel	12% Acrylamide:Bisacrylamide 375 mM Tris-HCl (pH 8.8) 0.005% TEMED 0.1% SDS 0.05% APS
5% Stacking Gel	5% Acrylamide:Bisacrylamide 0.125 mM TrisHCl (pH 6.8) 0.0075% TEMED 0.1% SDS 0.05% APS

Table 3.5. Mitochondria Respiration and Isolation Buffers.

Buffer	**Recipe**
Mito Respiration Buffer (pH: 7.2) (Medium for O2k-FluoRespirometer)	120 mM Sucrose 50 mM KCl 20 mM Tris-HCl 1 mM EGTA 4 mM KH_2PO_4 2 mM $MgCl_2$ 1% BSA (Fatty acid free)
Mito Isolation Buffer (pH: 7.2) (For heart)	100 mM Sucrose 50 mM KCl 1 mM EDTA 20 mM TES 0.2% BSA (Fatty acid free)

Table 3.5. Mitochondria Respiration and Isolation Buffers. (cont.)

Buffer	**Recipe**
Mito Isolation Buffer 1 (pH: 7.4) (For skeletal muscle)	67 mM Sucrose 50 mM KCl 50 mM Tris-HCl 10 mM EDTA 0.2% BSA (Fatty acid free)
Mito Isolation Buffer 2 (pH: 7.4) (For skeletal muscle)	250 mM Sucrose 0.3 mM EGTA-Tris 10 mM Tris-HCl

3.3. Antibodies

Antibodies used in this study are listed in table 3.6.

Table 3.6. Antibody List.

Antibody	**Supplier**	**Source**
eIF2α	Cell Signalling Technologies (9722)	Rabbit
HSC 70	Santa Cruz Biotechnology (D0318)	Mouse

Table 3.6. Antibody List. (cont.)

Antibody	**Supplier**	**Source**
LC3B	Cell Signalling Technologies (2775S)	Rabbit
NRF2	Cell Signalling Technologies (12721S)	Rabbit
Phospho-eIF2α	Cell Signalling Technologies (3398)	Rabbit
SOD2	Cell Signalling Technologies (13141S)	Rabbit
SQSTM1	Abnova (H00008878-M01)	Mouse
Total OXPHOS Cocktail	Abcam (ab110412)	Mouse
Anti-Mouse HRP-linked	Cell Signalling Technologies (7076S)	Horse
Anti-Rabbit HRP-linked	Cell Signalling Technologies (7074S)	Goat

3.4. Primers

Primers used in this study are listed in table3.7.

Table 3.7. Primer List.

Primer Code	**Sequence (5'-3')**
Aldh18a1_F	AATCAGGGCCGAGAGATGATG
Aldh18a1_R	GGCCTCTAAGACCGGAATTGC
Atf3_F	CCAGAATAAACACCTCTGCCATCG

Table 3.7. Primer List. (cont.)

Primer Code	**Sequence (5'-3')**
Atf3_R	CTTCAGCTCAGCATTCACACTCTC
Atf4_R	GTTTCCAGGTCATCCATTCG
Atf5_F	CCTTGCCCTTGCCCACCTTTGAC
Atf5_R	CCAGAGGAGGAGGCTGCTGT
Atf6_F	TCGCCTTTTAGTCCGGTTCTT
Atf6_R	GGCTCCATAGGTCTGACTCC
Catalase_F	TGGCACACTTTGACAGAGAGC
Catalase_R	CCTTTGCCTTGGAGTATCTGG
Cd36_F	TGCTGGAGCTGTTATTGGTG
Cd36_R	TGGGTTTTGCACATCAAAGA
Cdt1b_R	AACAGTGCTTGGCGGATGTG
Cdt1b_F	TCGCAGGAGAAAACACCATGT
Dars2_F	GGAATTAGCCAGGTCGTTGGA
Dars2_R	ACGAACCTTTTCCGGCTCAG
Fasn_F	CCCTTGATGAAGAGGGATCA
Fasn_R	ACTCCACAGGTGGGAACAAG
Gdf15_F	CAACCAGAGCCGAGAGGAC
Gdf15_R	TGCACGCGGTAGGCTTC
Gpx1_F	CCACCGTGTATGCCTTCTCC
Gpx1_R	AGAGAGACGCGACATTCTCAAT
Hprt_F	GCCCCATGGTTAAGGTT
Hprt_R	TTGCGCTCATAGGCTTT
Mthfd2_F	CATGGGGCATATGGGAGATAAT
Mthfd2_R	CCGGGCCGTTCGTGAGC
Nfe2I2_F	TCCATTCCCGAATTACAGTGTCT
Nfe2I2_R	GCCCACTTCTTTTTCCAGCG
Pdk4_F	CCCGCTGTCCATGAAGCAGC

Table 3.7. Primer List. (cont.)

Primer Code	**Sequence (5'-3')**
Pdk4_R	CCAATGTGGCTTGGGTTTCC
Sod1_F	CAAGCGGTGAACCAGTTGTG
Sod1_R	TGAGGTCCTGCACTGGTAC
Sod2_F	GCCTGCACTGAAGTTCAATG
Sod2_R	ATCTGTAAGCGACCTTGCTC
Pycr1_F	ATGAGCGTAGGCTTCATCGG
Pycr1_R	GTGTCAGGTTCACCCCTATCT

3.5. Chemicals

Chemicals used in this study are listed in table 3.8.

Table 3.8. Chemicals.

Chemical	**Supplier**
Acrylamide-Bisacrylamide 40% 37.5:1	Neofroxx, Germany
Adenosine 5′-diphosphate monopotassium salt dihydrate	Sigma-Aldrich, USA
Agarose	GeneOn, Germany
Ammonium persulfate	Biofroxx, Germany
Amplex™ Red Reagent	Sigma-Aldrich, USA
Antimycin A	Sigma-Aldrich, USA
BSA	Neofroxx, Germany
BSA (fatty acid free)	Sigma-Aldrich, USA
CCCP	Sigma-Aldrich, USA
di-Potassium hydrogen phoshate anhydrous	Merck, Germany
di-Sodium hydrogen phosphate	Merck, Germany

Table 3.8. Chemicals. (cont.)

Chemical	**Supplier**
dNTP Solution Set	NEB, USA
EDTA	Biofroxx, Germany
EGTA	Biofroxx, Germany
Ethanol Absolute≥ 99.9%	Isolab, Germany
Ethidium Bromide	Neofroxx, Germany
Glycine	Neofroxx, Germany
HEPES buffer	Biofroxx, Germany
Hydrogen Peroxide	Merck, Germany
K_2HPO_4	Merck, Germany
L-Malic acid	Sigma-Aldrich, USA
L-Glutamic acid, monosodium salt hydrate	Sigma-Aldrich, USA
Methanol ≥ 99.8%	Isolab, Germany
Milk Powder	Havancızade, Turkey
NuPAGE Sample Reducing Agent	Invitrogen, USA
NuPAGE LDS Sample Buffer (4X)	Invitrogen, USA
Oligomycin A	Sigma-Aldrich, USA
PageRuler Plus Prestained Protein Ladder	Thermo Fisher, USA
Ponceau S	Ecotech, Turkey
Potassium chloride	Merck, Germany
Potassium hydroxide	Sigma-Aldrich, USA
Proteinase K	Biofroxx, Germany
Rotenone	Sigma-Aldrich, USA
Safranin O	Sigma-Aldrich, USA
Sodium Chloride	Merck, Germany
Sodium Dodecyl Sulfate (SDS)	Biofroxx, Germany
Sodium Floride (NaF)	Neofroxx, Germany
Sodium Hydroxide	Merck, Germany

Table 3.8. Chemicals. (cont.)

Chemical	Supplier
Sodium phosphate dibasic dihydrate	Sigma-Aldrich, USA
Sodium pyruvate	Sigma-Aldrich, USA
Sodium Succinate dibasic hexahydrate	Sigma-Aldrich, USA
Sucrose	Caisson Labs, USA
TEMED	Neofroxx, Germany
TES	PanReac AppliChem, USA
Tris-HCl	Promega, USA
Triton X-100	Biofroxx, Germany
TWEEN20	Neofroxx, Germany

3.6. Kits and Enzymes

Kit, enzymes and reagents used in this study are listed in table 3.9.

Table 3.9. Kits, Enzymes and Reagents.

Kit, Enzyme or Reagent	Supplier
Complete, Mini, EDTA-free Protease Inhibitor Cocktail	Roche, Switzerland
DC Protein Assay Kit	Bio-Rad, USA
GeneRuler 1kb DNA ladder	Thermo Fisher, USA
GoTaq G2 DNA Polymerase	Promega, USA
Horseradish peroxidase	Sigma-Aldrich, USA
iScript™ cDNA Synthesis Kit	Bio-Rad, USA
NuPAGE Sample Reducing Agent	Sigma-Aldrich, USA
NuPAGE LDS Sample Buffer (4X)	Sigma-Aldrich, USA
PageRuler Plus Prestained Protein Ladder	Thermo Fisher, USA
RealQ Plus 2x Master Mix Green	Ampliqon, Denmark

Table 3.9.Kits, Enzymes and Reagents. (cont.)

Kit, Enzyme or Reagent	**Supplier**
Superoxide Dismutase from bovine erythrocytes	Sigma-Aldrich, USA
Subtilisin A	Sigma-Aldrich, USA
Trypsin-EDTA (0.5%)	Thermo Fisher, USA
WesternBright ECL - HRP Substrate	Advansta, USA
WesternBright Sirius Chemiluminescent Detection Kit	Advansta, USA
Zymo Research Directzol RNA MiniPrepPlus	Zymo Research, USA

3.7. Equipments and Devices

Equipments and devices used throughout this study is listed in table 3.10.

Table 3.10. Equipments and Devices.

Equipment or instrument	**Supplier**
Accu-Check Glucometer	Roche, Switzerland
Accu-Check Glucometer strips	Roche, Switzerland
Activity Cage	Ugo Basile, Italy
Agarose Gel Electrophoresis System	Analytic Jena, Germany
Autoclaves	ASB260T, Astell, UK
Centrifuge	Hitachi Koki, Japan
Cold room	Birikim Elektrik Sogutma, Turkey
Cryopure Tube	Sarstedt, Germany
Deepfreezer (-20)	Arçelik, Turkey
Deepfreezer (-80)	Thermo, UK
Dish Washer	Mielabor G7783, Miele, Germany
G-BOX Chemi XX6	Syngene, UK

Table 3.10. Equipments and Devices. (cont.)

Equipment or instrument	**Supplier**
Gel Doc XR System	Bio-Doc, Italy
Grip Strength	Ugo Basile, Italy
Heat Blocks	Analytic Jena, Germany
Ice Maker	Scotsman Inc. AF20, Italy
Laboratory Bottles	Isolab, Germany
Magnetic Fish	Isolab, Germany
Magnetic Stirrer	Chiltren, USA
Micropipettes	Axygen, USA
Micropipette Tips	Axygen, USA
Microwave Oven	Arcelik, Turkey
Nitrocelluluse Blotting Membrane	Amersham, UK
Multiwell Plates	Topscien, China
O2k-FluoRespirometer	Oroboros Instruments, Austria
Oven	Gallenkamp 300, UK
PCR Tubes (0.2ml)	Axygen, USA
Petri Dishes	Fırat Plastik, Turkey
pH Meter	Hanna Instruments, USA
Pipettor	Axygen, USA
Plate Reader	VersaMax, Molecular Devices, USA
Power Supply	BIO-RAD, USA
Real-Time Quantitative PCR System	Bioneer Exicycler, Republic of Korea
Refrigerators	Bosch, Germany
Repeater pipette	Rainin Autorep, Canada
Rotarod	Ugo Basile, Italy
Rotator	Onilab, USA
SDS-PAGE Transfer System	Bio-Rad, USA
Serological Pipettes	Sarstedt, Germany

Table 3.10. Equipments and Devices. (cont.)

Equipment or instrument	**Supplier**
Shakers	Onilab, USA
Spectrophotometer	Nanodrop ND-100 Thermo, USA
Syringes	Set inject, Turkey
Thermal Cycler	Bio-Rad, USA
Treadmill	Ugo Basile, Italy
Ultra Centrifuge	Beckman, USA
Vortex	IKA, USA
Water purification system	UTES, Turkey
Watmann Filter Paper-Extra Thick	Thermo Fisher, USA

4. METHODS

4.1. Animal Experiments

4.1.1. Animal Care

The animals were maintained in the Bogazici University Experimental Animal Breeding and Care Unit. All procedures were conducted according to the Bogazici University Animal Experiments Local Ethics Committee (BÜHADYEK), approved by the Republic of Turkey Ministry of Agriculture and Forestry. Mice were housed in well-ventilated cages in groups of 3-5 and exposed to light for 12 hours per day. The temperature of the rooms was 20°C - 24°C. Mice were fed ad-libitum. Mice were weighted in the regular intervals. For ketogenic diet intervention study animals were fed with ketogenic food (10.4% protein, 0.1%0 carbohydrate and 89.5% fat).

4.1.2. Tissue Harvesting from Mice

Mice were sacrificed by cervical dislocation. For this study, the heart and the quadriceps muscle tissues were harvested. The heart tissues were weighted immediately after harvesting. Tissues were frozen in liquid nitrogen to store until the experiment. Exceptionally, the heart was put into Mito isolation buffer, and quadriceps muscle tissues were put into ice-cold PBS-EDTA immediately after harvesting for mitochondria isolation.

4.1.3. Blood Glucose Measurement

The lateral vein of a mouse was punctured with an injection needle, and a glucose strip took a drop of blood. After placing the strip into Accu-Check Glucometer, the value of the glucose level was monitored and recorded for wild-type and hmKO animals.

4.2. Phenotypic Assays

4.2.1. Activity Cage (Horizontal and Vertical Movement Count)

Mice were placed into a special cage that had infrared lights in it. Mice moved freely in the cage in both horizontal and vertical directions, and all movements that broke the infrared rays were recorded for 30 minutes.

4.2.2. Treadmill

Before starting the experimental process, mice were adapted to the treadmill at a constant (6.5 m/min) speed for 10 minutes x 2 days. Six mice were placed into a separate lane at the same time. They were forced to run by a mild electric shock at the bottom of the platform. The speed of the platform was 6.5 m/min at the beginning; however, it accelerated to 0.5 m/min every 3 minutes. If a mouse was shocked more than 10 times in a minute, the experiment was stopped for that mouse. The distance that the mice ran was recorded.

4.2.3. Grip Strength (Whole Limb)

Mice were held from their tail and brought close to the grid. When they gripped the grid by four limbs, they were pulled away at the constant speed for each time and g force data were recorded. This procedure was repeated 5 times for each mouse at one-minute intervals.

4.2.4. Rotarod

Before starting the experimental process, mice were adapted to the rotarod. Five mice were placed into separate lanes of the rotarod; after 4 minutes, the rotarod started to turn at a constant speed for five minutes. This adaptation step was repeated one more time. For the experiment, mice were placed on the rotarod and turned at accel-

erated speed (min 2 rpm, max 50 rpm, acceleration 5 rpm) for 5 minutes. The time that mice fell was recorded, and this procedure was repeated 3 times at 20 minutes intervals.

4.3. Molecular Biology

4.3.1. DNA Isolation from Mouse Ear and Tail

The biopsies (from ear or tail) were incubated overnight in tail lysis buffer (see Table 3.1 for the recipe) at 55°C in a thermoshaker. An equivalent volume of Isopropanol was added into tubes, and DNA was precipitated by centrifuging at 4°C and the maximum speed for 20 minutes. Then the supernatant was discarded, and the pellet was washed with 70% cold EtOH by centrifuging at 4°C and the maximum speed for 15 minutes. After drying EtOH, pellets were resuspended in 50 μl ddH_2O at 37 °C in a thermoshaker for 1 h. These DNA samples were used for genotyping.

4.3.2. DNA Isolation from Mouse Tissues

The frozen tissues (heart and skeletal muscle for this study) were incubated overnight in lysis buffer at 55°C in a thermoshaker. 75 μl of 8M potassium acetate and 0.5 ml chloroform were added into tubes, and then tubes were centrifuged at 4°C for 10 minutes to precipitate DNA. Three phases were observed after centrifuging: aqueous phase (upper), interphase, and organic phase (lower). The upper phase was transferred to new tubes. Then 1 ml of absolute EtOH was added into tubes. Tubes were inverted 3-5 times, then centrifuged at 4°C and the maximum speed for 10 minutes. Afterward, the pellet was rinsed with 70% cold EtOH and centrifuged at maximum speed for 5 minutes. After drying, the pellet was resuspended in 50 μl ddH_2O. These DNA samples were used for quantifying mitochondrial DNA amount by qPCR.

4.3.3. Polymerase Chain Reaction (PCR)

PCR experiments for genotyping were conducted by using Cre and Dars2 primers (see Table 3.7 for the primer sequences) to detect wild type and knockout mice. The reaction components and conditions are listed in the table 4.1 and 4.2 respectively.

Table 4.1. PCR components.

Component	**Volume**
DNA	1 μl
GoTaq® Buffer	4 μl
dNTP Mix (1.25 mM)	1 μl
Forward Primer (10μm)	0.8 μl
Reverse Primer (10 μm)	0.8 μl
MgCl2	1.2 μl
GoTaq® DNAPolymerase	0.1 μl
ddH2O	11.1 μl
Total	20 μl

Table 4.2. PCR conditions.

Step	**Temperature**	**Time**	**cycle**
Initial Denaturation	95 °C	2 minutes	1
Denaturation	95 °C	30 seconds	35 cycles
Annealing	55-60 °C	30 minutes	
Extension	72 °C	1 minute	
Final Extension	72 °C	5 minutes	1

1% agarose gel was prepared with TBE buffer. 1kb DNA ladder was loaded into first well, other wells were loaded with samples, including negative and positive controls. Gel electrophoresis was performed at 120V for 25 min. After running, gel was incubated in EtBr for 30 minutes. Lastly, gel was monitored by Gel Doc XR System.

4.3.4. Total RNA Isolation from Mouse Tissues

600 μl of TRIzol reagent was put into tubes with magnetic beads (Roche) on ice. Approximately 50 mg of each sample tissue (heart and quadriceps muscle for this study) were placed into. Samples were homogenized at 6500rpm for 1 minute (2 x 30 seconds) by MagNa LYser. RNA was isolated from homogenized tissues using the RNA isolation kit (Zymo Research Directzol RNA MiniPrepPlus kits).

4.3.5. Quantitative Reverse Transcription PCR

After isolating total RNA, the concentration, purity, and integrity of each sample were measured by nanodrop. Samples were used to synthesize of cDNA according to cDNA synthesis kit (iScript™ cDNA Synthesis Kit) procedure is given table 4.3 and 4.4.

Table 4.3. cDNA synthesis components.

Component	**Volume**
5X iScript Reaction Mix	4 μl
iScript Reverse Transcriptase	1 μl
Nuclease-free water	Variable
RNA template	Variable
Total	20 μl

Table 4.4. cDNA synthesis conditions.

Step	**Temperature**	**Time**	**Cycle**
Priming	25 °C	5 minutes	1
Reverse transcription	46 °C	20 minutes	1
RT inactivation	95 °C	1 minute	1

For qPCR procedure the appropriate primers (see Table 3.7 for the primer sequences) were used. Hprt and RNaseP was used as reference genes. qPCR procedure was performed according to manufacturer's procedure as shown in Tables 4.5 and 4.6.

Table 4.5. qPCR components.

Component	**Volume**
RealQ Plus 2x Master Mix Green	5 μl
Forward Primer	0.25 μl
Reverse Primer	0.25 μl
Nuclease-free water	2.5 μl
Template DNA (20 ng)	2 μl
Total	10 μl

Table 4.6. qPCR conditions.

Step	**Temperature**	**Time**	**Cycle**
Initial Denaturation	95 °C	15 minutes	1
Denaturation	95 °C	15 seconds	40 cycles
Annealing	60 °C	15 minutes	
Extension	72 °C	30 seconds	

4.4. Biochemistry

4.4.1. Protein Isolation from Mouse Tissues

500 μl of organ lysis buffer (see Table 3.2 for the recipe) was put into tubes magnetic beads tubses (Roche). Approximately 50 mg of each sample tissue (heart and skeletal muscle for this study) was placed into the magnetic bead tubes. Samples were homogenized at 6500rpm for 2 x 30 seconds by MagNa LYser. After homogenization, samples were centrifuged at maximum speed for 45 minutes at 4 °C. Supernatants were transferred into new Eppendorf tubes to store. Also, samples were diluted 1:10 and 1:20 to measure concentration with DC protein assay according to the manufacturer's instructions. Finally, samples were stored at -80 °C.

4.4.2. Western Blotting

Sample preparation: reaction tubes were prepared with 50 μg protein, 4X sample buffer, ddH_2O and 10X reducing agent in total 11 μl. Then they were incubated at 70 °C for 10 minutes.

Gel loading: Gels were casted as two layers: resolving and stacking (see Table 3.4 for the recipe). First line of the gels was loaded with protein ladder, other wells were loaded with 10 μl samples. Gel was run at 80 V for 40 minutes and 120 V for 1 hour.

Wet transfer: Gel was transferred to nitrocellulose membrane using transfer buffer (see Table 3.3 for the recipe). Transfer conditions were 100 V for at least 2 hours. After transfer, membrane was rinsed with PBS-T for 3 x 5 minutes using orbital shaker. Blocking: Membrane was blocked with 5% milk powder in 5ml PBS-T for 1 hour. Then membrane was rinsed again with PBS-T for 3 x 5 minutes using orbital shaker.

Primary antibody incubation: Membrane was incubated in 1:1000 (mostly) diluted antibody with 5 ml of 5% milk powder in PBS-T for overnight at 4°C. After 16-18 hours, membrane was washed with PBS-T for 3x5 minutes using orbital shaker.

Secondary antibody incubation: Membrane was incubated into 1:2000 diluted HRP-linked secondary antibody with 5 ml of 5% milk powder in PBS-T for 1 hour at room temperature. Membrane was washed again with PBS-T for 3 x 5 minutes.

Visualization: Membrane was incubated with ECL or Sirius reagents for 2 minutes. Proteins were visualized with chemiluminescence visualization system (Syngene G-Box instrument).

Analysis: All visual images were analyzed using ImageJ software.

4.4.3. Mitochondria Isolation from Heart

Mouse heart was harvested and put into 5 ml of mitochondria isolation buffer with 0.02% BSA (fatty acid free) (see Table 3.5 for the recipe) in 50 ml falcon. Tissue was transferred to petri dish and cut into small pieces with razor. Small tissue pieces were poured into glass homogenizer tube and 1mg/ml Subtilisin A was added into glass tube. Tissue was homogenized by hand until the solution turn into homogenous. Solution was transferred 50 ml falcon and centrifuged at 8500 g for 5 minutes at 4 °C. Supernatant was discarded, and pellet was resuspended with 30 ml mitochondria isolation buffer with 0.02% BSA (fatty acid free). It was centrifuged at 800 g for 5 minutes at 4 °C, then supernatant was transferred into new falcon and centrifuged at 8500 g for 5 minutes at 4 °C. Pellet was resuspended with mitochondria isolation buffer without BSA. Finally, Concentration was measured according to DC protein assay procedure.

4.4.4. Mitochondria Isolation from Skeletal Muscle

Quadriceps muscle tissue from the two legs of a mouse was harvested and put into cold PBS-EDTA containing falcon. Tissues were cut into small pieces with a razor in a petri dish. Pieces were transferred to a new falcon with 0.05% trypsin to be incubated for 30 minutes on ice. After 30 minutes, it was centrifuged at 200g for 5 minutes at 4°C. The supernatant was discarded, and the pellet was homogenized into IMB1 buffer (see Table 3.5 for the recipe) by hand into a glass homogenizer. The homogenous solution was poured back into the falcon and centrifuged at 700g for 10 minutes at 4 °C. The supernatant was transferred to the new falcon and centrifuged at 8000g for 10 minutes at 4°C. Then, the supernatant was discarded, and the pellet was resuspended in IBM2 buffer (see Table 3.5 for the recipe).

4.4.5. Oxygen Consumption Rate and H_2O_2 Production Measurement

Oxygen consumption rate and H_2O_2 measurement were performed simultaneously using Oroboros-O2k instrument. During all experiments 0.13 mg mitochondria (isolated from heart or skeletal muscle) was used. Firstly, chambers were filled by mitochondria respiration buffer (see Table 3.5 for the recipe) and air calibration and H_2O_2 calibration was performed according to instrument protocols. Then, mitochondria were added to two chambers (one for control). For measuring H_2O_2 production during forward electron transport, SUIT006-D048 protocol was conducted. In short, 5 mM Pyruvate, 2 mM Malate, 2.5 mM ADP,5 nM Oligomycin, *0.5 μM FCCP (*multiple step) and 2.5 μM Antimycin A were added with 3 steps H_2O_2 titration (0.1 μM for each). For measuring H_2O_2 production during reverse electron transport, SUIT026-D064 protocol was conducted. The protocol consists of eight steps including three steps H_2O_2 titration (0.1 μM for each). In short, after adding mitochondria, 10 mM Succinate, 0.5 μM Rotenone, 2.5 mM 2.5 ADP, and 2.5 μM Antimycin A were added into each chamber. Excel templates that manufacturer offers were used to data analysis.

4.4.6. Membrane Potential Measurement with Safranin

Membrane potential measurement with Oroboros-O2k instrument was performed using safranin. After safranin calibration, 0.13 mg mitochondria (isolated form heart of skeletal muscle) were added into each chamber. Afterward, SUIT021-D036 protocol was conducted. In short, 10 mM Glutamate, 2 mM Malate, 2.5 mM ADP, 10 mM Succinate, 0.5 μM Rotenone, 5 nM Oligomycin, *0.5 μM FCCP (*multiple step) and 2.5 μM Antimycin A were added into the chambers. Excel templates that manufacturer offers were used to data analysis.

5. RESULTS

5.1. Generation of Mitochondrial Aspartyl-tRNA Synthetase Mouse Model

Mitochondrial aspartyl-tRNA synthetase (*Dars2*) gene targeting was carried out by the Knockout Mouse Project (KOMP) Repository (further information available at http://www.knockoutmouse.org, Project ID: 41773). The targeted *Dars2* gene had LoxP sites between the 2nd intron and 3rd exon (Figure 5.1).

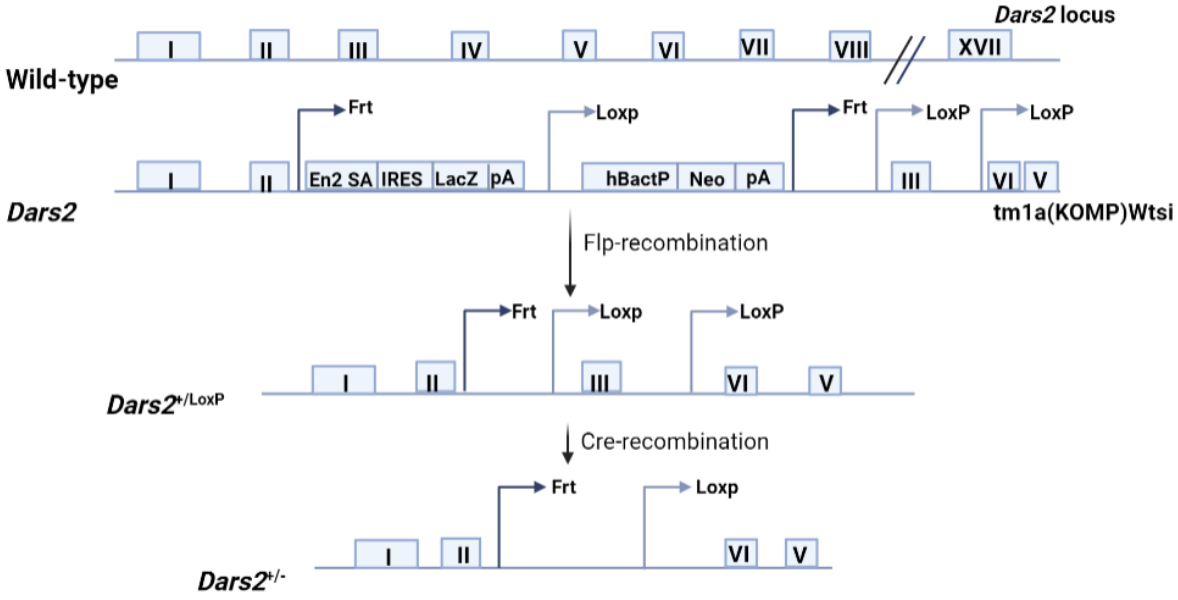

Figure 5.1. Generation of $Dars2^{+/-}$ mouse.

The whole-body knockout of DARS2 was embryonic lethal (Dogan et al., 2014) thus *Dars2* was conditionally disrupted by Cre-recombinase mediated excision (Figure 5.1). Dogan et al. generated a heart and skeletal muscle-specific DARS2 knockout mouse model by mating floxed DARS2 mouse ($Dars2^{flox/flox}$) with transgenic mice expressing Cre recombinase under the muscle creatine kinase promoter (Ckmm-cre). We transferred both the $Dars2^{flox/flox}$ and Ckmm-cre mice from Cologne Excellence

Cluster in Aging and Aging-Associated Diseases (CECAD), Cologne, Germany. By mating these mice, we have re-generated the heart and skeletal muscle-specific DARS2 knockout mouse at Bogazici University Experimental Animal Breeding and Care Unit. The mating strategy was as follows: $Dars2^{+/flox}$, +/Ckmm-cre mice were mated with $Dars2^{flox/flox}$ mice and heart- and skeletal muscle-specific $Dars2$ knock-out mice were obtained (hereafter they will be called as hmKO mice). Representative genotyping PCR results showing the wild-type ($Dars2^{flox/flox}$), heterozygous ($Dars2^{+/flox}$,+/Ckmm-cre), and homozygous ($Dars2^{flox/flox}$,+/Ckmm-cre) mice can be found in Figure 5.2. After genotyping, $Dars2$ transcript levels were quantified to confirm $Dars2$ gene disruption (Figure 5.3).

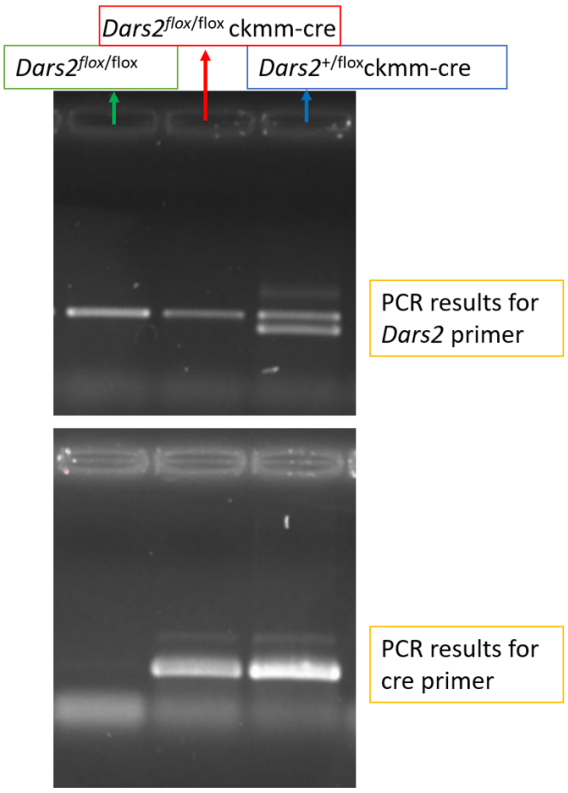

Figure 5.2. Genotyping PCR for $Dars2^{flox/flox}$, $Dars2^{+/flox}$,+/Ckmm-cre and $Dars2^{flox/flox}$,+/Ckmm-cre mice.

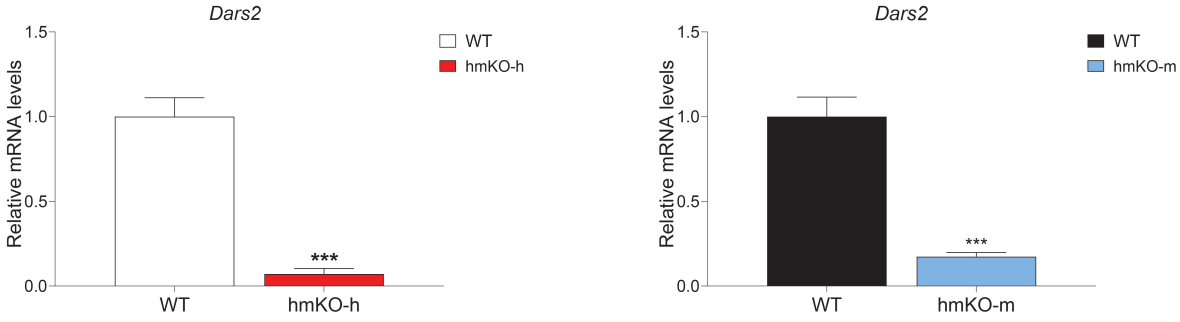

Figure 5.3. *Dars2* transcript levels in the (a) heart and (b) quadriceps tissues. Error bars represent mean ± SEM. (Student's t test: ***p<0.001)

hmKO mice had severe mitochondrial dysfunction in both heart and skeletal muscle, which shortened their lifespan to 6 - 7 weeks (Dogan et al., 2014). Cardiac hypertrophy and skeletal muscle atrophy was apparent (Dogan et al., 2014). As animal models being re-generated at different facilities / countries might not always recapitulate the main findings of the original model, we first wanted to confirm the model by checking their survival probability and body weights. As the lifespan data was correlative with the 2014 model, we continued our investigations into body weights. The weight data of all animals were recorded from 4- to 6-week-old age and divided into two groups according to their sexes. In contrast to their wild-type littermates, hmKO mice did not really gain any weight after weaning (Figure 5.4). While the weight of female hmKO mice showed a significant difference according to their wild-type littermates at 4 weeks, males were significantly lighter when they were 5 weeks old (Figure 5.4). This severity might be the results of the muscle creatine kinase promoter's activity, which is fully active in skeletal muscle and heart after embryonic day 15.5 (Lyons et al., 1991).

DARS2-deficient mice had increasing heart size due to cardiomyopathy (Dogan et al., 2014). To validate and quantify this increase, the hearts of both wild-type and hmKO animals were weighted after sacrification and normalized with their body weight. Data confirmed that hmKO mice have one-and-a-half-time larger heart-to-body weight ratio than wild-type mice (Figure 5.5).

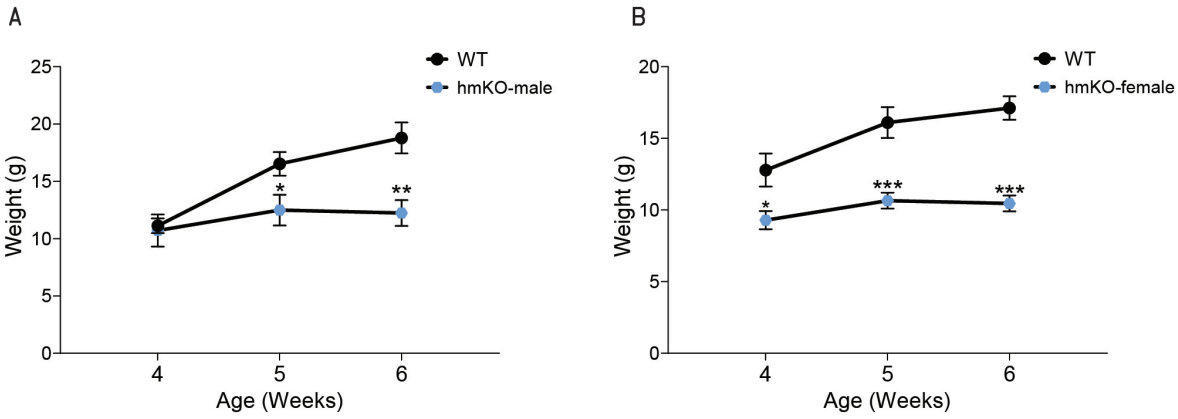

Figure 5.4. Weight curves of (a) male and (b) female animals (n=7-11). Error bars represent mean ± SEM. (Student's t test: *p<0.05, **p<0.01, ***p<0.001)

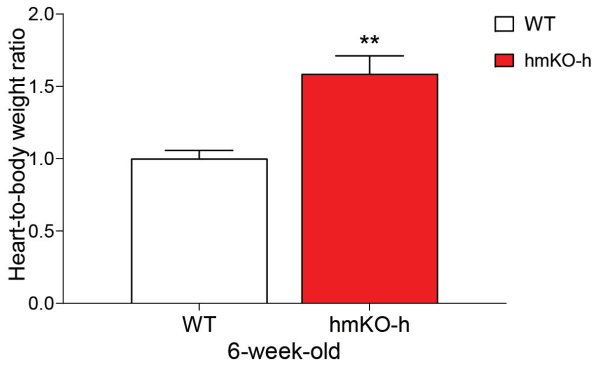

Figure 5.5. Heart-to-body weight ratio of hmKO and WT mice at 6 weeks of age. Error bars represent mean ± SEM. (Student's t test: **p<0.01)

These new results were in accordance with the published results, so we eliminated the possibility of the environmental conditions' impact on animals' phenotypes. We have decided to perform our experiments on 6-week-old mice, when they were at the end of their lifespan.

5.2. Phenotypic Characterization of hmKO Mice

To phenotypically distinguish between the wild-type and hmKO animals, we took advantage of the "Mouse Phenotyping Facility" at Bogazici University and subjected our animals to various phenotypic tests from 4 weeks of age onward. The number of animals in each test varied among the experiments; generally, each group (WT and hmKO groups) had 7-11 animals. Since male and female mice exhibit similar performance during exercises, the data was not distinguished according to their sexes.

To evaluate spontaneous coordinated activity, animals were placed into the activity cage for 30 minutes. They could move freely in the cage in both vertical and horizontal directions. In the first week of the experiment, all animals showed similar activity and movement counts in both directions (Figure 5.6a and b). However, from 5 weeks onward, hmKO mice started to display significantly less activity than wild-type littermates both vertically and horizontally (Figure 5.6a and b).

Furthermore, while vertical movement counts of wild-type animals increased with time, hmKO mice scarcely moved vertically at 6 weeks. These results suggest that hmKO mice cannot move actively, which may stem from skeletal muscle atrophy or cardiac hypertrophy.

Animals were forced to run on a treadmill to evaluate their endurance and exercise performance. During treadmill runs, hmKO mice exhausted very quickly (Figure 5.6c). They ran approximately half the distance that wild-type counterparts ran at 4 weeks (Figure 5.6c).

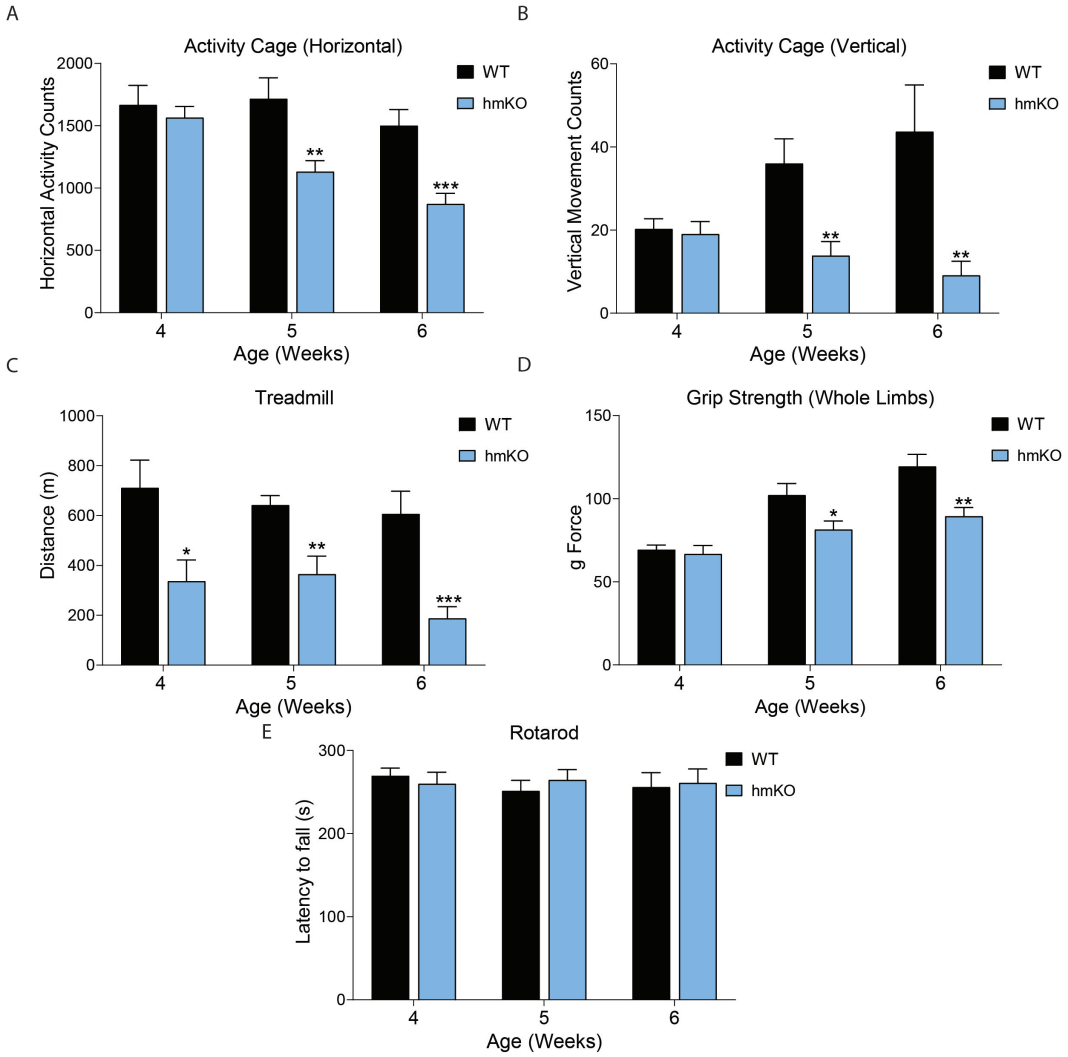

Figure 5.6. Phenotypic assay results (n=7-11). (a) Activity Cage (Horizontal), (b) Activity Cage (Vertical), (c) Treadmill, (d) Grip Strength , (e) Rotarod. Error bars represent mean ± SEM. (Student's t test: *p<0.05, **p<0.01, ***p<0.001)

The running performance of the hmKO mice worsened when they aged; when they were 6 weeks old, they ran about 200 meters, while wild-type mice completed approximately 600 meters on treadmill (Figure 5.6c). These results indicate that hmKO mice have diminished exercise performance and endurance than the wild-type animals.

A whole limb grip strength assay was conducted to measure and compare the muscle strengths of the hmKO and wild-type mice. At 4 weeks, hmKO mice and wild-type mice exhibited similar force; however, hmKO mice could apply less force at their 5th and 6th weeks of age (Figure 5.6d). This data supports the notion that hmKO mice have weaker muscles than their wild-type counterparts.

Lastly, mice were tested on the Rota-Rod to measure their motor coordination and the ability to balance. From the beginning of the experiment, both hmKO and wild-type mice showed a similar level of latency to fall (Figure 5.6e). Although hmKO mice showed less activity and performance and had weaker muscles than the wild-type animals, their motor coordination and balance abilities were indistinguishable.

5.3. Molecular Characterization of Mitochondrial Dysfunction in hmKO Mice

In the heart, DARS2 deficiency results in increased mass in mitochondria and hence elevated levels of mitochondrial mRNA transcripts (Dogan et al., 2014). We performed a qPCR experiment for quantifying *CoxI* transcripts level of mtDNA in both heart and skeletal muscle tissues. In the heart, the mtDNA-transcripts level was about threefold that of wild-type mice (Figure 5.7a). However, in quadriceps tissue, we did not observe any change (Figure 5.7b). These results are correlative with the increased level of mitochondrial mass in cardiomyocytes.

DARS2-deficiency in heart and skeletal muscle leads to mitochondrial dysfunction by decreasing the amount of fully assembled OXPHOS complexes as exemplified by Blue-Native PAGE (Dogan et al., 2014). However, OXPHOS subunits of hmKO mice were not checked by Western blotting. To confirm the reduction in the relative protein levels of the subunits, we have used Total OXPHOS Cocktail antibody (Figure 5.8). Heart tissue homogenates were used from 6-week-old WT and hmKO mice. As expected, the protein levels of the NDUFA9 subunit of complex I, the UQRC2 subunit

of complex III, and the COXIV subunit of complex IV reduced in the DARS2-deficient hearts significantly, whereas the levels of the SDHA subunit of complex II and ATP5A subunit of complex V did not change (Figure 5.8).

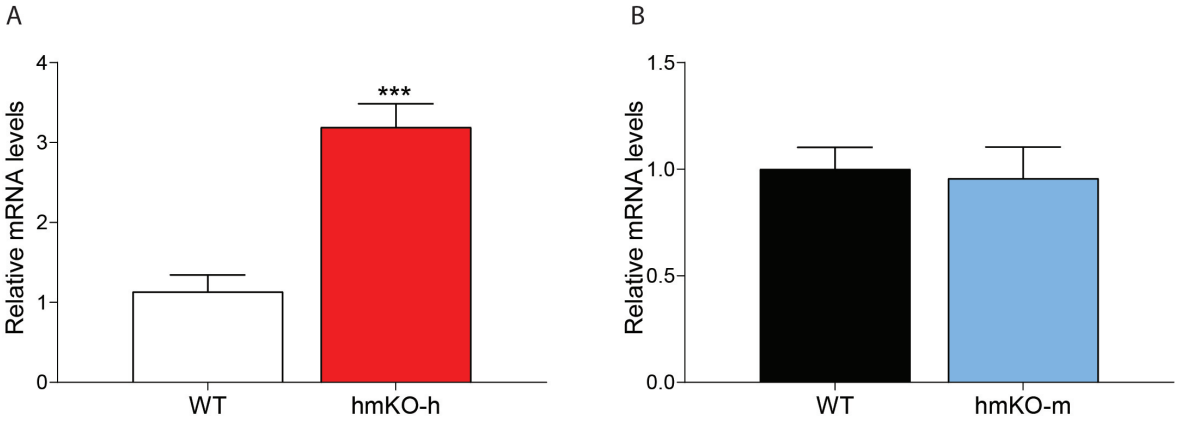

Figure 5.7. mtDNA-transcript level quantification of (a) heart and (b) quadriceps tissues. Error bars represent mean ± SEM. (Student's t test: ***p<0.001)

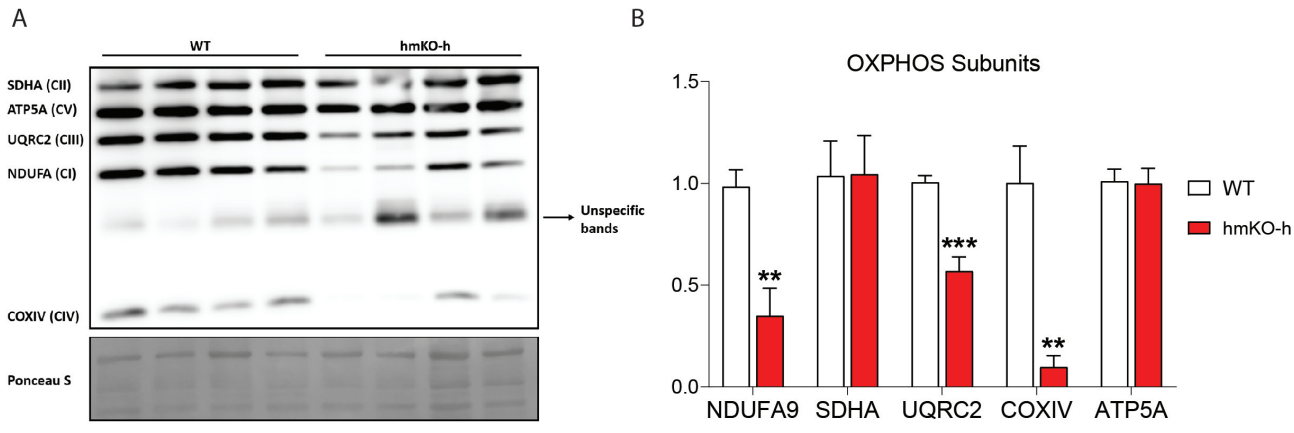

Figure 5.8. Protein levels of OXPHOS subunits in the heart. Error bars represent mean ± SEM. (Student's t **p<0.01, ***p<0.001)

Oroboros O2k-Fluorespirometer enables the quantitative measurement of respiration of living mitochondria for two samples at a time. In a closed chamber, mitochondrial respirometry can deduce the rate at which oxygen concentration decreases as a result of oxygen usage in the system. Thus, oxygen consumption rate can give a direct readout for mitochondrial dysfunction. The oxygen consumption rate of the heart mitochondria was measured using Oroboros O2k-FluoRespirometer to see whether OXPHOS deficiency affects the respiration of the mitochondria.

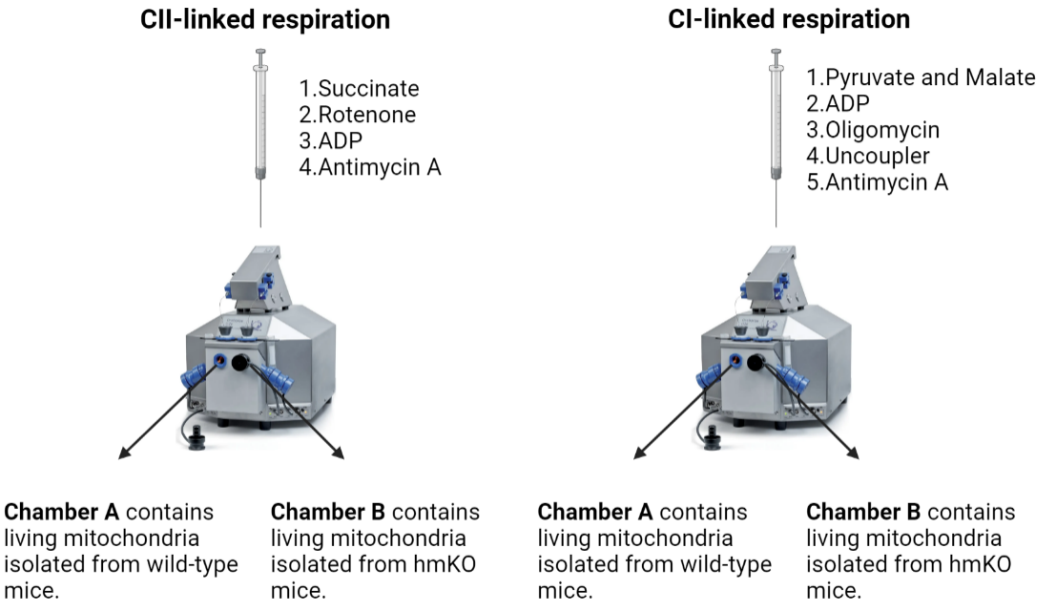

Figure 5.9. Experimental setup for the measurement of CI- and CII-linked respiration.

Respiration of the heart mitochondria was evaluated for different respiration states (Figure 5.9) with different substrates and inhibitors (Figure 5.10). Firstly, mitochondria were supplied with succinate, a Complex II substrate, followed by the Complex I inhibitor, rotenone, to detect CII-linked respiration. Then, mitochondria were supplied with a high concentration of ADP to evaluate the respiration level in state 3 (ADP-stimulated respiration). hmKO mice had a lower ADP-stimulated oxygen consumption rate (Figure 5.11). The heart mitochondria of hmKO mice showed less respiration than wild type heart mitochondria in CII-linked respiration (Figure 5.11).

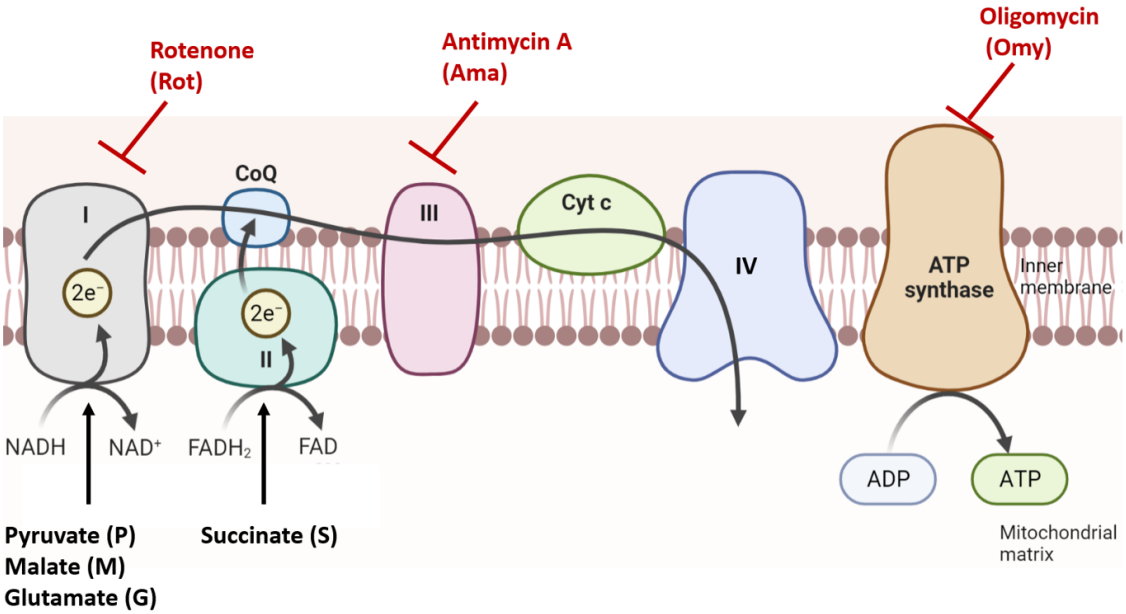

Figure 5.10. Representation of substrates and inhibitors of OXPHOS complexes.

Mitochondria were fed with complex I substrates, pyruvate and malate, to evaluate the level of complex I-linked respiration. While the respiration levels were similar between hmKO and wild-type mice when fed with the substrates, the hmKO mice displayed a lower oxygen consumption rate in state 3 (ADP-stimulated respiration).

State 4 respiration levels of mitochondria were evaluated by inhibiting ATP synthase with oligomycin. Although DARS2-deficient mitochondria tended to respire less, there were no significant differences in oxygen consumption rate in state 4. Lastly, uncoupled respiration level was measured in the presence of a mitochondrial uncoupler. Heart mitochondria of hmKO mice had a lower oxygen consumption rate than wild-type mitochondria in response to multiple titrations of uncoupler CCCP. These data suggest that the respiration of heart mitochondria of hmKO mice is affected by the DARS2 deficiency. As a result, hmKO mice consumes less oxygen, hence decreased oxygen consumption rate.

Oxygen consumption rate can provide information with relative ATP level. Thus, after analyzing the oxygen consumption rate of each sample, we calculated the oxygen

consumption rate-dependent ATP levels. We used the net OXPHOS capacity equation to calculate the ATP level. According to the equation, leak respiration rate (respiration rate of mitochondria in the presence of complex I/ complex II substrates and absence of ADP) was subtracted from ADP-stimulated oxygen consumption rate (OXPHOS capacity), which gave net OXPHOS capacity (OCR-related ATP level) (Gnaiger, 2020).

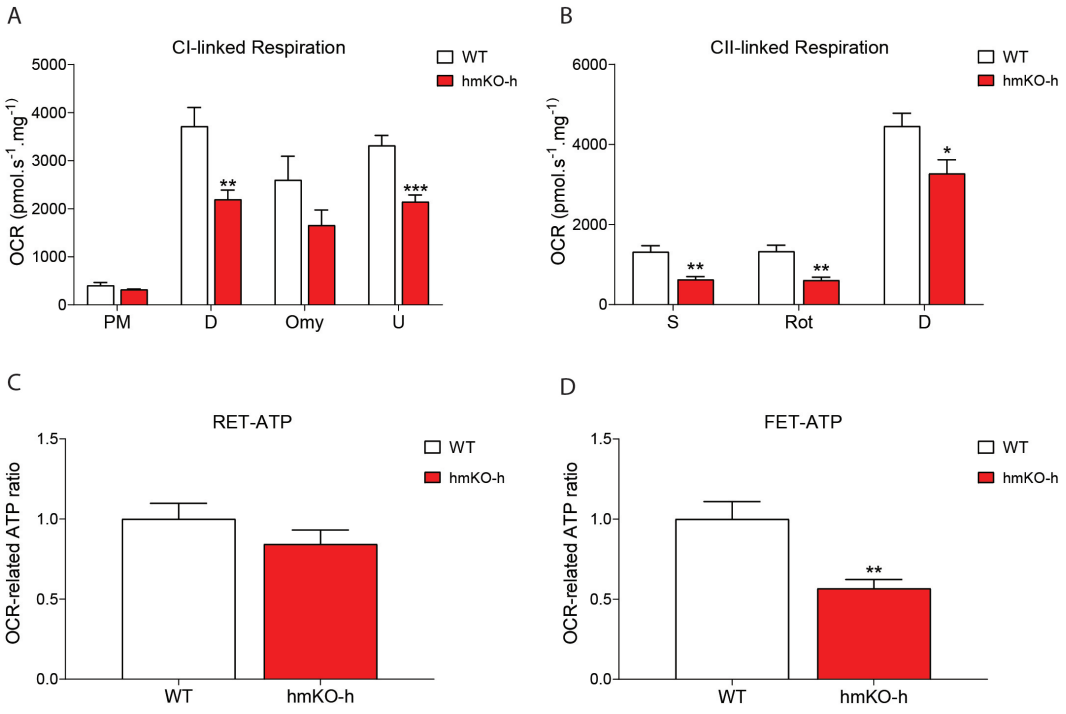

Figure 5.11. Oxygen consumption rate (OCR) of OCR-related ATP ratio of (a,c) CII-linked and (b,d) CI-linked respiration in the heart. Error bars represent mean ± SEM. (Student's t test: *p<0.05, **p<0.01, ***p<0.001)

Firstly, we calculated the OCR-related ATP level of heart mitochondria for both CI- and CII-linked respiration. While CI-linked respiration-related ATP levels of hmKO mitochondria diminished, CII-linked respiration-related ATP levels did not change significantly despite a downward tendency (Figure 5.11c and d). It is worth noting that this result does not give information about ATP production rate directly but relatively.

Similar to heart, to evaluate the impact of DARS2 deficiency on skeletal muscle mitochondria, the quadriceps proteins of the muscle were used to perform Western blots with the total OXPHOS antibody cocktail. Like the heart mitochondria, the levels of complex I subunit NDUFA9, complex III subunit UQRC2, and complex IV subunit COXIV decreased in hmKO mice mitochondria while the levels of SDHA subunit of complex II and ATP5A subunit of complex V were steady Figure 5.12.

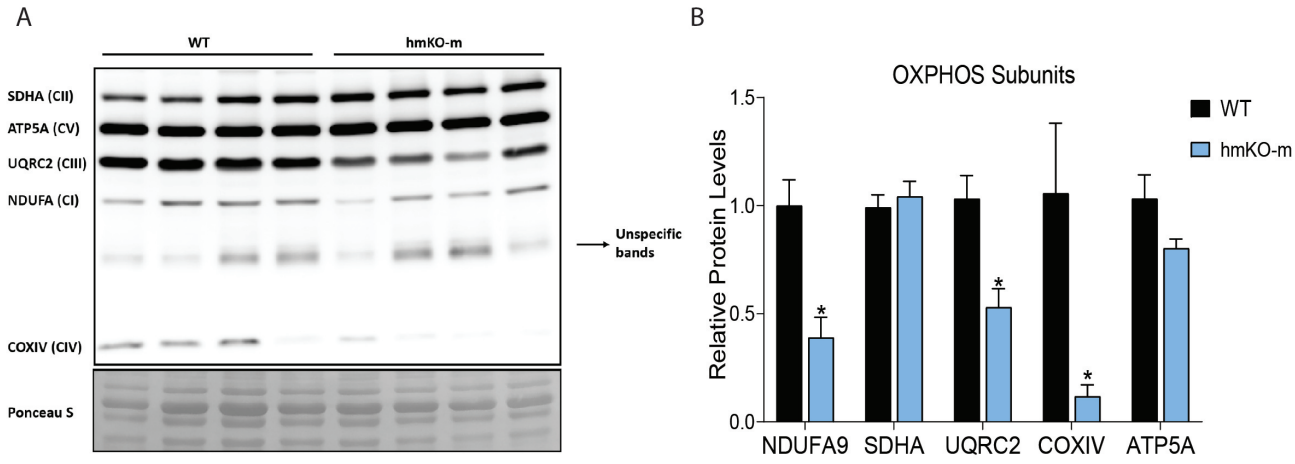

Figure 5.12. Protein levels of OXPHOS subunits in the quadriceps. Error bars represent mean ± SEM. (Student's t test: *p<0.05)

Afterward, the oxygen consumption rate of the quadriceps' mitochondria was evaluated by Oroboros-O2k FloRespirometer. Firstly, mitochondria were fed with succinate to measure complex II-linked respiration. When mitochondria were supplied with ADP, ADP-stimulated respiration (state 3 respiration) level tended to decrease in hmKO skeletal muscle mitochondria; however, it was not significant (Figure 5.13a). This data shows that complex II-linked respiration of hmKO quadriceps' mitochondria is similar to wild-type quadriceps' mitochondria.

After CII-linked respiration measurement, chambers were cleaned, and living mitochondria were added into respiratory buffer-filled chambers. Then, mitochondria were fed with complex I substrates, pyruvate and malate, to measure complex I-linked

respiration. Although there was a reduction tendency, the oxygen consumption rate of hmKO mitochondria did not show a significant difference in response to ADP stimulation (state 3), oligomycin inhibition (state 4), and uncoupler titration (uncoupler state) (Figure 5.13b).

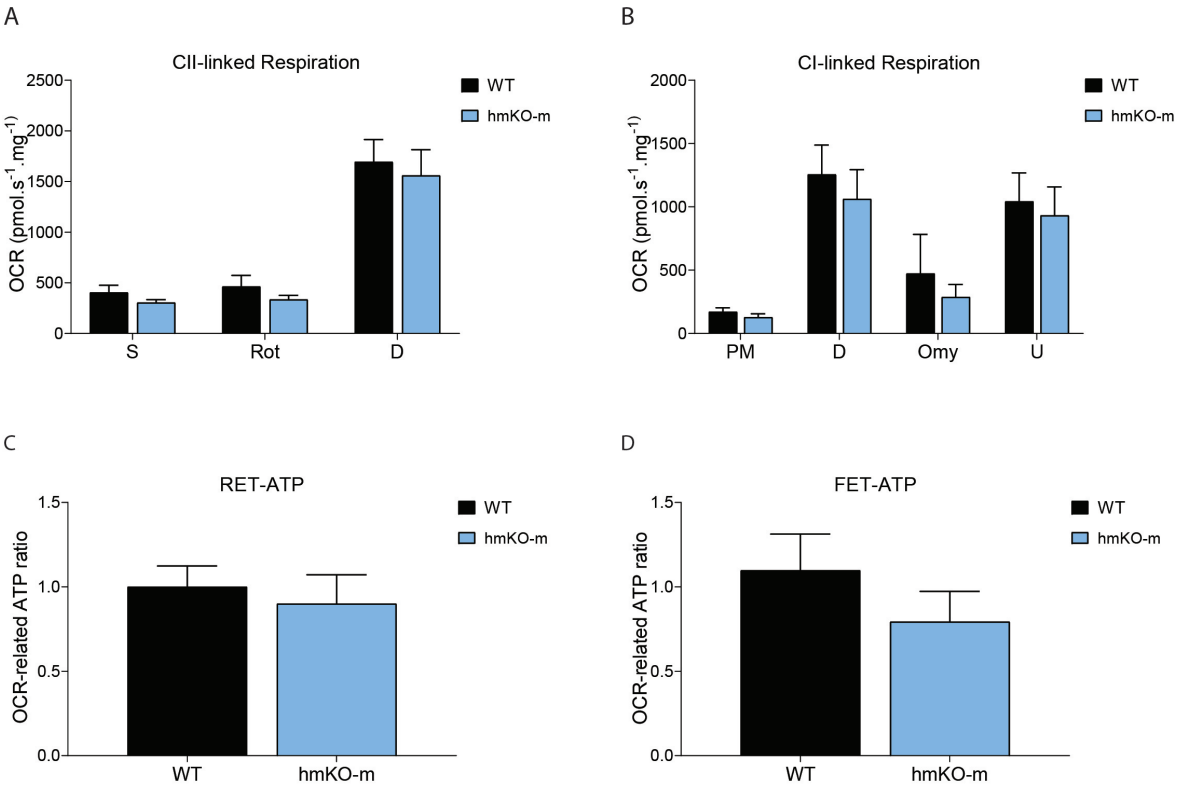

Figure 5.13. Oxygen consumption rate (OCR) and OCR-related ATP ratio of (a,c) CII-linked and (b,d) CI-linked respiration in the quadriceps. Error bars represent mean ± SEM.

The oxygen consumption results were used to calculate OCR-related ATP levels for both CI- and CII-linked respiration. Results were correlative with oxygen consumption rate data. Although hmKO quadriceps' mitochondria tended to display a decreased level of ATP, a significant reduction was not observed for both FET- and RET-related ATP levels.

5.4. Stress Responses

5.4.1. Antioxidant Response

Mitochondrial dysfunction can be associated with increased reactive oxygen species (ROS) generation that causes antioxidant response upregulation. To see whether the antioxidant response in hmKO hearts was increased, antioxidant-response related elements were checked. In response to oxidative stress, NFE2L2 translocates into the nucleus and binds to the antioxidant response element (ARE) to initiate the transcription of antioxidant genes (Tonelli et al., 2018). We performed Western blotting and qPCR to quantify the protein and mRNA levels of *Nfe2l2*, respectively. The protein level of NFE2L2 did not show a significant difference between hmKO and wild-type mice, whereas hmKO mice had significantly reduced *Nfe2l2* mRNA levels (Figure 5.14a and b). Then, we checked the mitochondrial ROS scavenging enzymes. SOD2 plays a crucial role in converting superoxide ($O^{\cdot -}$) that is produced from the electron transport chain to hydrogen peroxide (H_2O_2) (Wang et al., 2018). While the protein level was steady, the mRNA level of *Sod*2 decreased in hmKO mice (Figure 5.14c). SOD1 is also a ROS scavenging enzyme responsible for converting superoxide to hydrogen peroxide in the cytosol and mitochondrial intermembrane space (Eleutherio et al., 2021). When we quantified the transcripts of *Sod*1 in the heart of hmKO and wild-type mice, we did not observe any significant change (Figure 5.14c). Lastly, the mRNA levels of *Catalase and Gpx-1* were quantified by qPCR. CATALASE and GPX-1 are crucial antioxidant enzymes that prevent hydrogen peroxide accumulation by converting it to water (Lubos et al., 2011; Nandi et al., 2019). While the *Gpx-1* levels were significantly downregulated in hmKO mice, the *catalase* level did not change significantly (Figure 5.14c). These results suggest that the heart of the hmKO mouse model does not upregulate antioxidant response as a result of mitochondrial dysfunction.

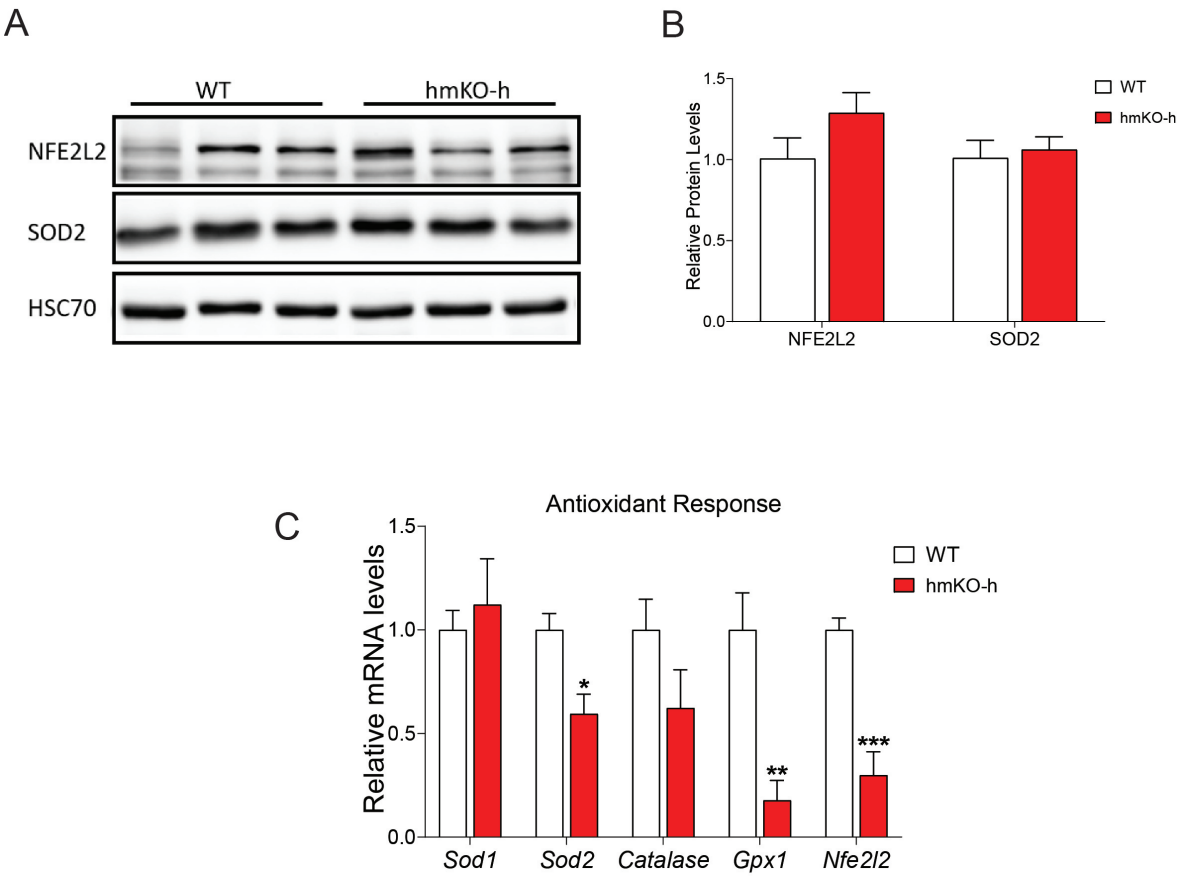

Figure 5.14. Antioxidant response in hmKO heart. Error bars represent mean ± SEM. (Student's t test: *p<0.05, **p<0.01, ***p<0.001)

Previously, it has been demonstrated that heart and quadriceps tissues react differently to DARS2 deficiency (Dogan et al., 2014). Therefore, as a next step, quadriceps tissues were investigated to understand whether the antioxidant response is upregulated in response to mitochondrial dysfunction. When we checked the protein levels of NFE2L2 and SOD2, we encountered a similar profile with the heart results. Both NFE2L2 and SOD2 levels did not change (Figure 5.15a and b). However, in contrast to the heart, their mRNA level also stayed the same between hmKO and wild-type mice (Figure 5.15c). Then, the mRNA expression level of other antioxidant elements was quantified by qPCR. While *Sod*1 and *Gpx*1 did not display a significant change, the *Catalase* level in hmKO quadriceps increased significantly (Figure 5.15c).

This results show that except for *Catalase*, there is no upregulation of antioxidant response in skeletal muscle tissues in hmKO mice.

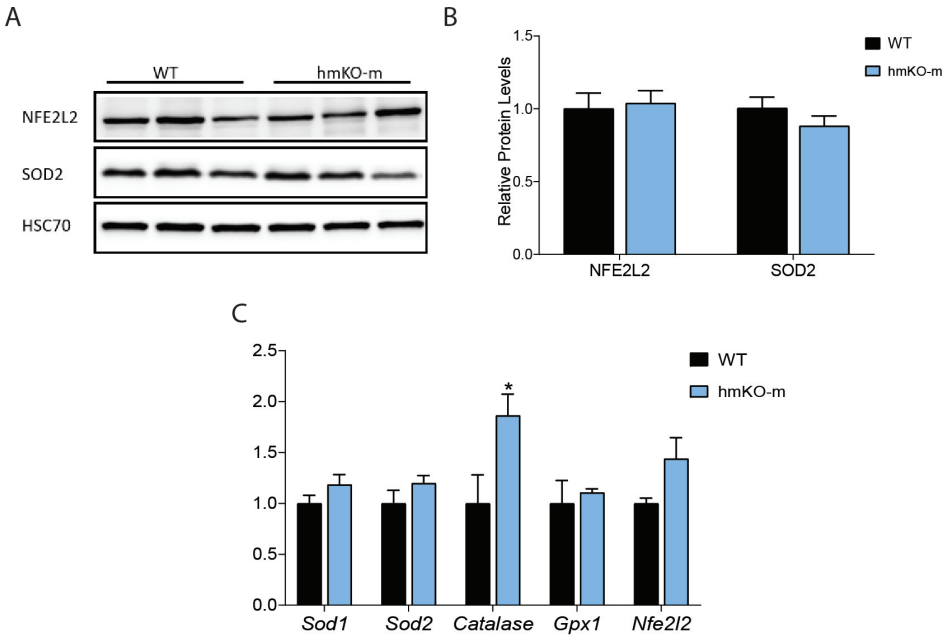

Figure 5.15. Antioxidant response in hmKO quadriceps. Error bars represent mean ± SEM. (Student's t test: *p<0.05)

During electron transportation, some electrons may leak and reduce oxygen (O_2) to superoxide ($O^{\cdot -}$) (Ray et al., 2012). Superoxide molecules are converted to hydrogen peroxide (H_2O_2) immediately by superoxide dismutase enzymes (SODs) (Murphy, 2009). So, measuring H_2O_2 production gives information about mitochondrial reactive oxygen species generation.

Oroboros-O2k Fluorespirometer instrument provides simultaneous measurement of oxygen consumption rate and H_2O_2 flux in living mitochondria of two samples. Therefore, the H_2O_2 production rate was measured with CI-linked and CII-linked respirations. When mitochondria are fed with succinate, the complex II substrate, electrons tend to move reverse because of the over-reduction of ubiquinone (Wright et al., 2022). Reverse electron transport (RET) is the source of RET-ROS. When the

heart mitochondria were fed with succinate, hmKO mitochondria showed less H_2O_2 flux according to wild-type mitochondria (Figure 5.16a). However, the difference became insignificant when the medium was supplied with complex I inhibitor rotenone (Figure 5.16a). Although there is a downward trend in response to ADP stimulation, hmKO mitochondria produced a similar level of H_2O_2 to wild-type mitochondria (Figure 5.16a). Likewise, when mitochondria were supplied with complex III inhibitor, Antimycin A, hmKO heart mitochondria produced a lower but insignificant amount of H_2O_2 than wild-type heart mitochondria (Figure 5.16a).

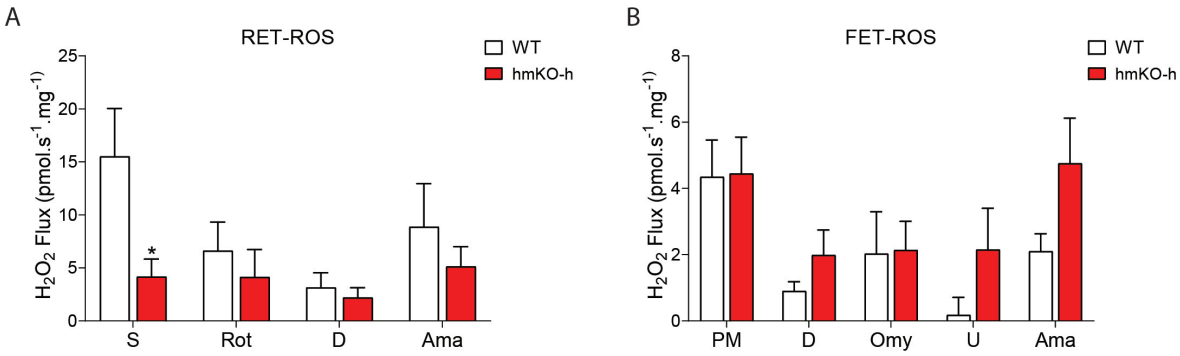

Figure 5.16. Production level of (a) reverse electron derived-ROS (RET-ROS) and (b) Forward electron derived ROS (FET-ROS) in the heart mitochondria. Error bars represent mean ± SEM. (Student's t test: *p<0.05)

In a separate experiment, mitochondria were fed with complex I substrates, pyruvate and malate, to measure the FET-ROS production rate. When the medium was supplied with pyruvate and malate, hmKO and wild-type heart mitochondria produced a similar amount of FET-ROS (Figure 5.16b). The difference in H_2O_2 production upon ADP stimulation between hmKO and wild-type mitochondria was insignificant (Figure 5.16b). When mitochondria were fed with oligomycin, uncoupler, and antimycin A, respectively, hmKO and wild-type mitochondria generated comparable amount of H_2O_2 (Figure 5.16b).

Reverse electron transport depends on mitochondrial membrane potential ($\Delta\Psi$), reduction might inhibit the reverse electron transport process (Komlódi et al., 2018). Therefore, we checked the level of membrane potential in freshly isolated heart mitochondria.

The membrane potential is measured with Safranin using Oroboros O2k- Fluo-Respirometer. Safranin is a lipophilic cationic dye located across the inner mitochondrial membrane when the inside is negatively charged (Figueira et al., 2012). Safranin can be transported to the inside of the mitochondria by electroporation upon the change in mitochondrial membrane potential, which quenches the fluorescence signal (Krumschnabel et al., 2014). Therefore, membrane potential can be detected using safranin dye in Oroboros O2k-Fluorespirometer.

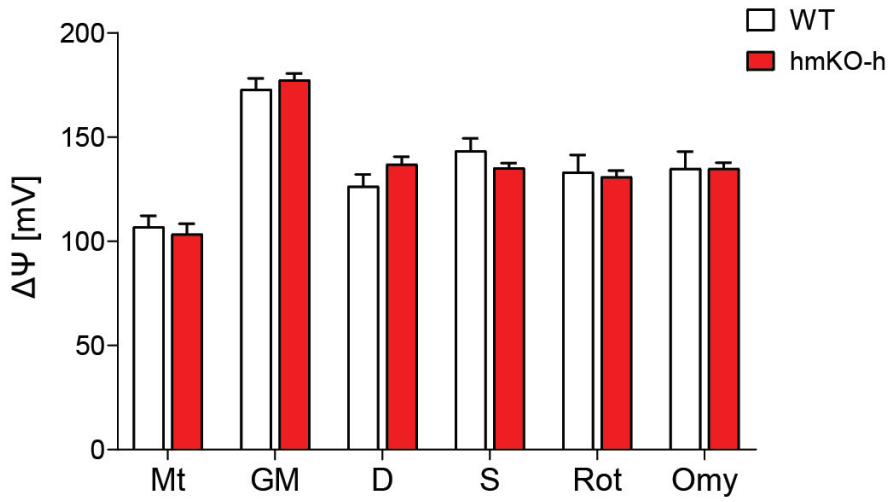

Figure 5.17. Membrane potential of the heart mitochondria. Error bars represent mean ± SEM.

Mitochondria were fed with complex I substrates, glutamate, and malate to evaluate the membrane potential level during the forward electron transport. Then, membrane potential was checked in response to ADP stimulation. To measure mitochondrial membrane potential during succinate-driven electron transport, complex II substrate, succinate, and complex I inhibitor, rotenone, was added to the medium. Afterward,

the complex V inhibitor, oligomycin, was supplied to the mitochondria. When we evaluated the membrane potential levels for each step, we did not see any changes between isolated heart mitochondria of hmKO and wild-type mice (Figure 5.17).

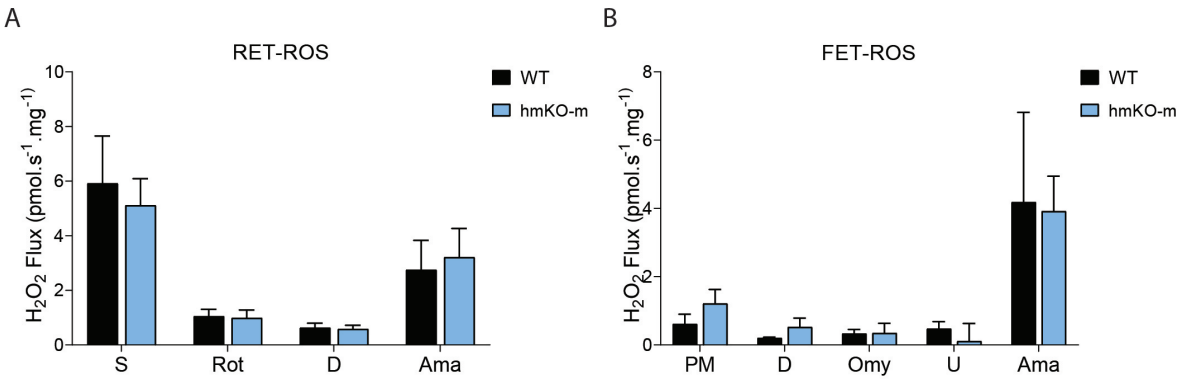

Figure 5.18. Production level of (a) reverse electron derived-ROS (RET-ROS) and (b) Forward electron derived ROS (FET-ROS) in the quadriceps' mitochondria. Error bars represent mean ± SEM.

Afterward, we checked H_2O_2 production in quadriceps tissues. Mitochondria were fed with complex II substrate, succinate, to measure RET-derived ROS. Although quadriceps mitochondria of hmKO mice tended to show a lower level of H_2O_2 production in response to substrate addition, there was no significant difference between control and hmKO mitochondria (Figure 5.18a). When rotenone and ADP were added to the medium, both hmKO and wild-type mitochondria displayed a similar level of H_2O_2 flux (Figure 5.18a). In response to complex V inhibition with oligomycin, the H_2O_2 level was upregulated; however, there was no significant change between hmKO and wild-type mitochondria (Figure 5.18a).

In a separate experiment, we supplied mitochondria with pyruvate and malate to measure forward electron-derived ROS. In response to substrate addition, hmKO quadriceps mitochondria showed an insignificant increase in H2O2 flux (Figure 5.18b). Similarly, upon ADP stimulation, both hmKO and wild-type mitochondria displayed a similar amount of H2O2 production (Figure 5.18b).

The change in H2O2 flux in hmKO mitochondria was insignificant after adding oligomycin, uncoupler, and antimycin, respectively (Figure 5.18B).

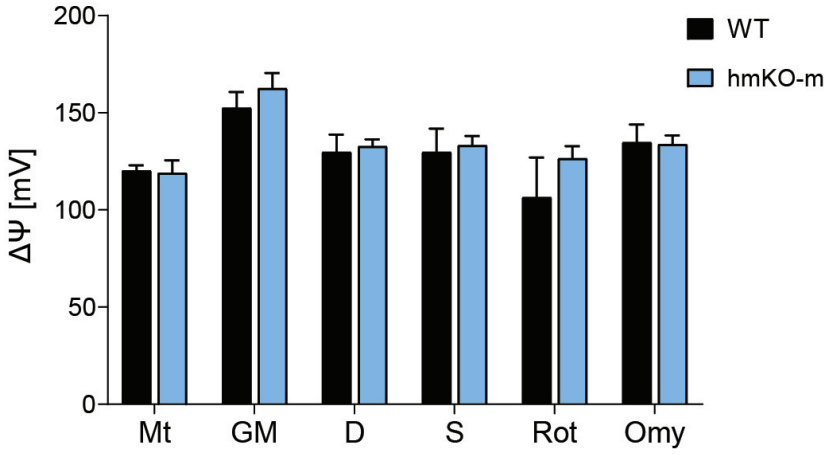

Figure 5.19. Membrane potential of the quadriceps mitochondria. Error bars represent mean ± SEM.

Membrane potential levels were also measured for mitochondria isolated from quadriceps tissue. The membrane potential of hmKO and wild-type mitochondria demonstrated a similar profile for each step as in heart tissue (Figure 5.19).

5.4.2. Mitochondrial Integrated Stress Response (ISR^{mt})

Eukaryotic cells have various signaling pathways to activate in response to pathological conditions or physiological changes; integrated stress response (ISR) is one of them. It is activated against extrinsic stresses such as starvation (including amino acid and glucose deprivation), hypoxia, and viral infection, as well as intrinsic factors like unfolded proteins in the endoplasmic reticulum (Pakos-Zebrucka et al., 2016). Mitochondrial stress can induce mitochondrial integrated stress response (ISR^{mt}).Integrating stress response is characterized by activating the eukaryotic initiation translation factor 2α (eIF2α) by phosphorylation. Thus, activated eIF2α diminishes the new protein synthesis while upregulating particular transcripts involved in signaling pathways (Dalton et al., 2012).

We conducted a Western blot experiment for both eIF2α and phosphorylated-eIF2α proteins to see activated eIF2α levels in the heart. The ratio of phosphorylated eIF2α to eIF2α was highly upregulated in hmKO cardiomyocytes, as shown in Figure5.20. This result suggests that the ISR^{mt} is activated in the hmKO heart in response to mitochondrial dysfunction.

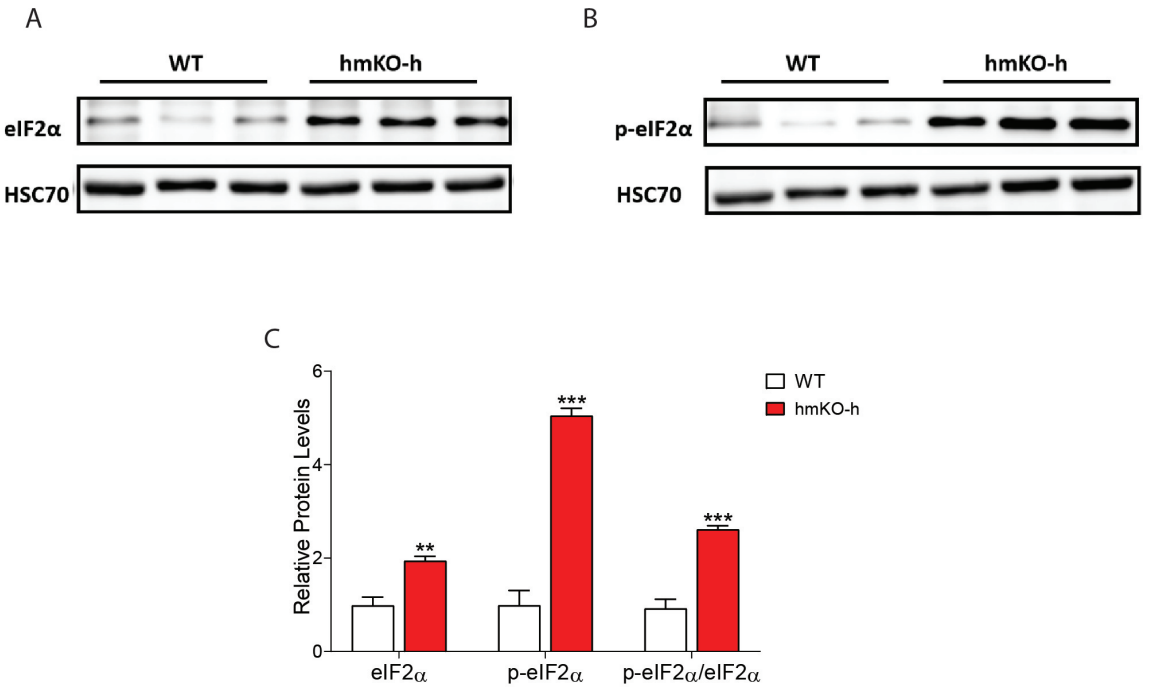

Figure 5.20. Western blot result of (a) eIF2α and (b) p-eIF2α proteins and (c) quantification of protein levels of in the heart. Error bars represent mean $\pm$ SEM. (Student's t test: **p<0.01, ***p<0.001)

The ISR^{mt} is accompanied by the activation of components of various signaling pathways. Therefore, we checked the transcript level of genes that play essential roles in integrated stress response, including;

(i) components of unfolded protein responses (UPRmt), such as *Atf3* (activated transcription factor 3), *Atf4* (activated transcription factor 4),*Atf5* (activated transcription factor5), and *Atf6* (activated transcription factor6),

(ii)a player of the folate cycle *Mthfd2* (methylene tetrahydrofolate dehydrogenase 2),

(iii) the critical enzymes for proline biosynthesis *Aldh18A1* (delta-1-pyrroline-5-carboxylate synthase) and *Pycr1* (mitochondrial pyrroline-5-carboxylate reductase 1),

(iv) metabolic hormones, mitokines,*Fgf21* (fibroblast growth factor 21) and *Gdf15* (growth differentiation factor 15).

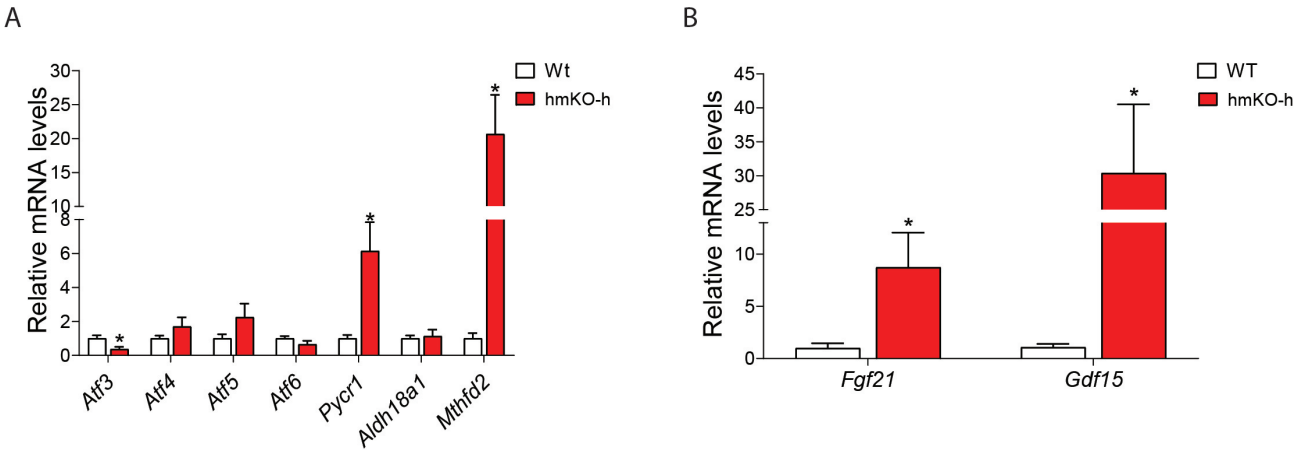

Figure 5.21. Transcript levels of (a) integrated stress response components and (b) mitokines in the heart. Error bars represent mean ± SEM. (Student's t test: *p<0.05)

Although *Atf4* and *Atf5* levels revealed an upward trend; there was no significant increase of their transcript levels. However, both *Pycr1* and *Mthfd2* transcripts were highly upregulated in hmKO cardiomyocytes (Figure 5.21a). Moreover, *Gdf15* levels of hmKO were about 30-times higher than wild-type mice, while *Fgf21* levels were

about 9-times higher(Figure 5.21b). These data indicate that hmKO mice upregulate the transcription of several components of ISR^{mt} in the heart upon mitochondrial dysfunction.

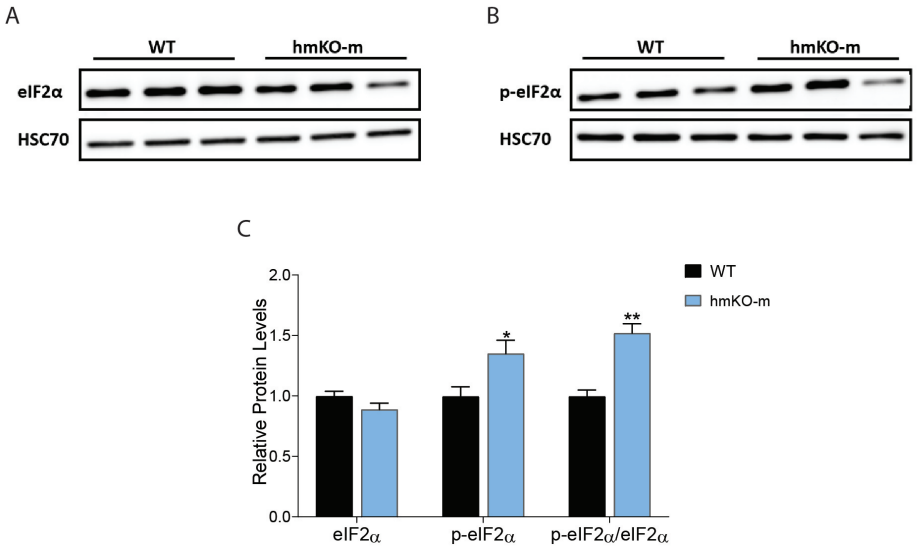

Figure 5.22. Western blot results of (a) eIF2α and (b) p-eIF2α proteins and (c) quantification of protein levels of in the quadriceps. Error bars represent mean ± SEM. (Student's t test: *p<0.05, **p<0.01)

ISR^{mt} activation was also investigated in quadriceps tissue of hmKO animals. eIF2α activation was detected in quadriceps tissue as in heart (Figure 5.22). As Dogan et al. demonstrated that the level of components of unfolded protein response and metabolic hormone *Fgf21* do not change in hmKO skeletal muscle tissue (Dogan et al., 2014), we have not re-checked these parameters.

5.5. The Effects of Dietary Intervention on hmKO Mice

Mitochondrial dysfunction leads to severe consequences, specifically for the high-energy demanding tissues like the heart, brain, liver, and skeletal muscle (Fine et al., 2019). A healthy mitochondrion should supply the energy demand using cellular energy sources such as glucose or lipids by adapting fuel oxidation according to fuel availability (Zhang et al., 2014). Although there is no specific cure for mitochondrial

diseases, various treatments are available to ameliorate the symptoms (Liufu & Wang, 2021). Ketogenic diet (KD) intervention is one of the helpful ways to attenuate the impacts of mitochondrial dysfunction. A ketogenic diet (KD) contains a high amount of fat and a low amount of carbohydrates; thus, it shifts metabolism from carbohydrate to fat oxidation (β-oxidation) (Zweers et al., 2021).

To test whether KD can ameliorate the phenotype of the DARS2-deficient mice, the animals were fed with KD ad-libitum after weaning (from 3 weeks onward). Afterward, they have been characterized phenotypically and molecularly.

5.5.1. Phenotypic Characterization of of KD-fed hmKO Mice

If KD improves the phenotype of hmKO mice, lifespan could be the first indication. Unfortunately, we have not observed any impact of KD on the median and/or maximal lifespan of the animals. hmKOs had severe health problems when they were 6 weeks old as their chow-diet (CD)-fed counterparts and they had to be culled at this age. Therefore, KD did not impact the lifespan of KD-fed hmKO animals.

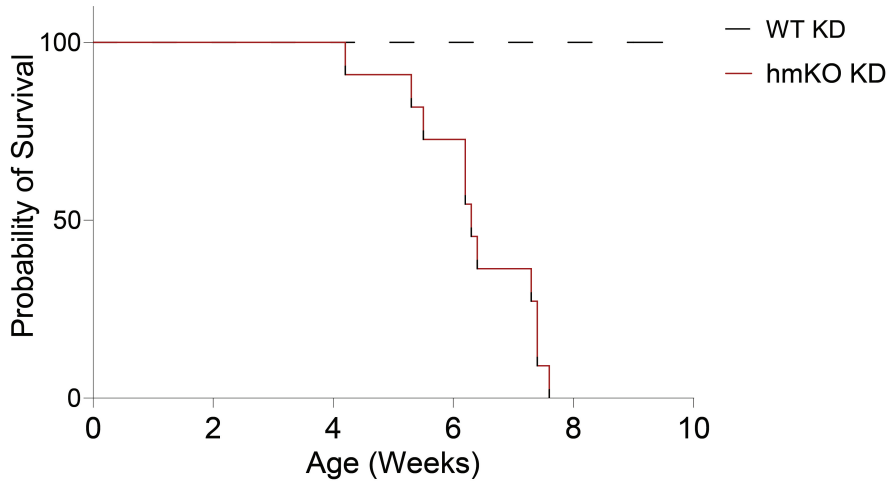

Figure 5.23. Survival curve of KD-fed animals

The weight data were recorded from 4- to 6-week-old age and divided into two groups according to their sexes. KD did not impact the weights of the wild-type animals; CD-fed and KD-fed wild-type mice were of similar weights (Figure 5.24). Likewise, KD could not attenuate the weight loss of hmKO mice. While female KD-fed hmKO had a similar weight to wild-type animals at 4-week-old age, they started to lose weight like CD-fed hmKO mice after 5 weeks (Figure 5.24). As female hmKO, male hmKO mice did not gain weight regardless of their diet (Figure 5.24). This data shows that a high-fat, low-carbohydrate diet cannot provide hmKO mice with weight gain.

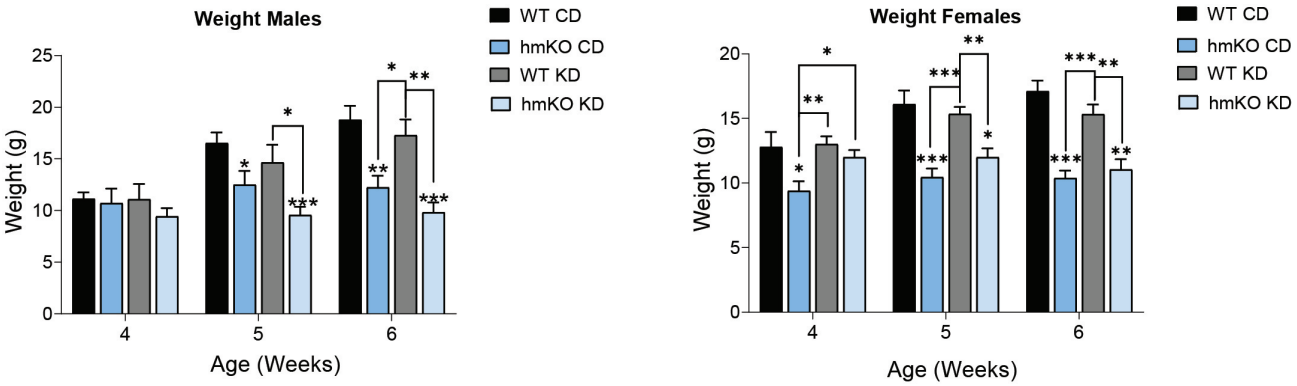

Figure 5.24. Weight curves of (a) male and (b) female CD- and KD-fed mice. Error bars represent mean ± SEM. (Student's t test: *p<0.05, **p<0.01, ***p<0.001)

To evaluate the effect of KD on coordinated activity, animals were subjected to the activity cage test. KD did not alter the activity level of wild-type mice; KD-fed wild-type animals were as active as CD-fed wilt-types in both directions (Figure 5.25). In the first week of the experiment, KD-fed hmKO mice could not move as much as their CD-fed littermates in the horizontal direction (Figure 5.25a). However, their vertical activity counts were similar (Figure 5.25b). In both directions, KD-fed hmKO displayed a similar activity level to CD-fed hmKO mice for the experiment's second and last week (Figure 5.25a and b). These data suggest that KD cannot ameliorate the poor coordination activity of hmKO.

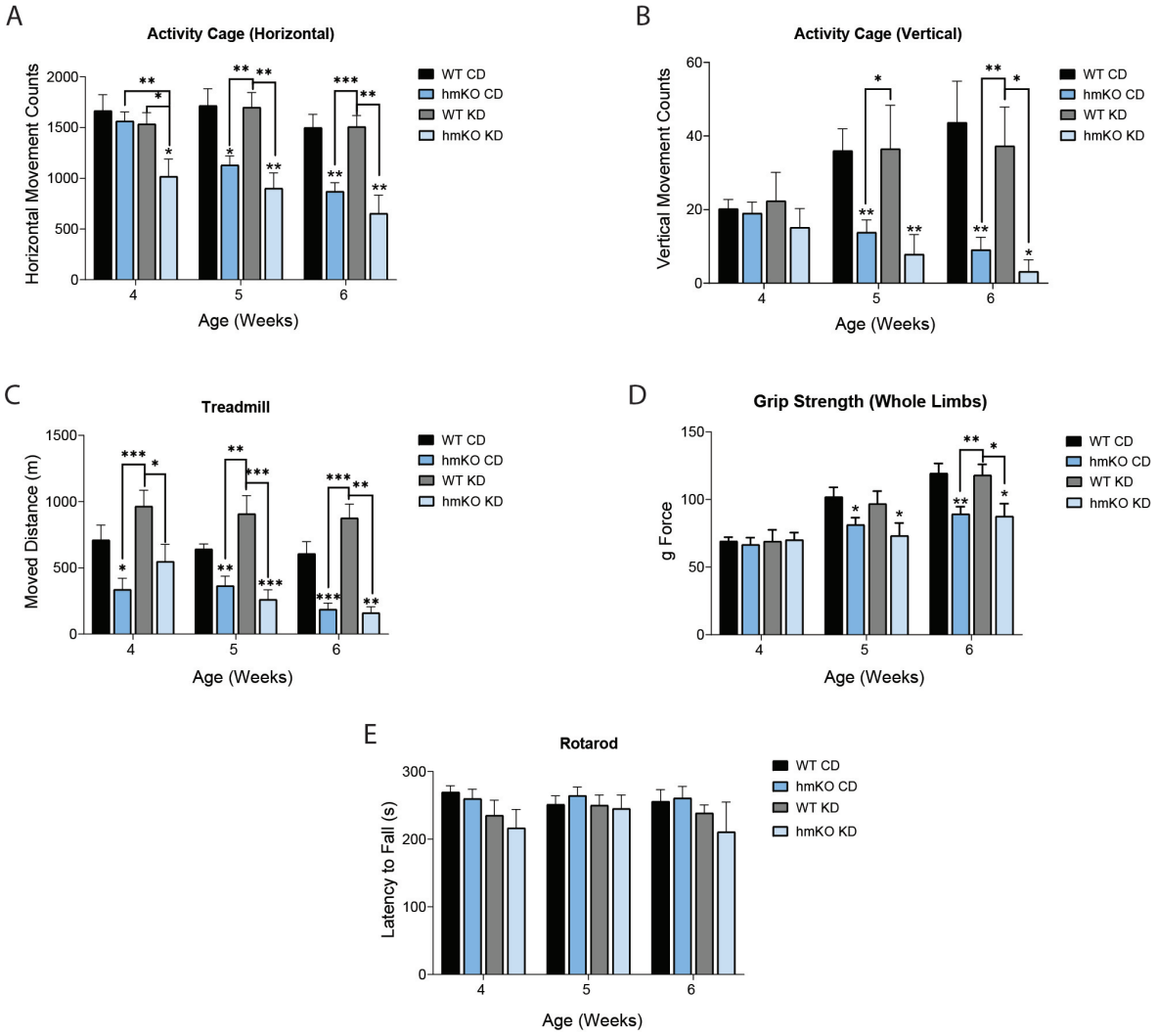

Figure 5.25. Phenotypic assay results (n=7-11). (a) Activity Cage (Horizontal), (b) Activity Cage (Vertical), (c) Treadmill, (d) Grip Strength (Whole Limb), (e) Rotarod. Error bars represent mean ± SEM. (Student's t test: *p<0.05, **p<0.01, ***p<0.001)

KD-fed animals and their CD-fed counterparts were forced to run on a treadmill to evaluate the impact of KD on endurance and exercise performance. KD diet did not affect the running performance of wild-type mice; KD-fed animals ran as much as their CD-fed littermates (Figure 5.25c). Moreover, KD did not improve the performance of hmKO mice; they showed diminished exercise performance when they aged like their CD-fed counterparts. As a result, KD cannot ameliorate the endurance and exercise

performance of hmKO mice. A whole limb grip strength assay was conducted to see whether KD influenced the muscle strength. Wild-type mice exerted similar effort regardless of the type of the diet (Figure 5.25d). While all mice exhibited similar force at 4 weeks, KD- and CD-fed hmKO could apply less force at their 5th and 6th weeks of age (Figure 5.25d). This data demonstrates that KD cannot enhance the muscle strength of hmKO mice.

Finally, mice were tested on Rota-Rod to evaluate their motor coordination and balance ability. For three weeks, all mice showed similar performance on Rota-Rod (Figure 5.25e).

These phenotypic data suggest that KD did not ameliorate the phenotypic effects of DARS2 deficiency. KD-fed mice had weaker muscle, poor exercise performance, and worse coordinated activity than wild-type animals like their CD-fed littermates.

5.5.2. Molecular Characterization of KD-fed hmKO Mice

KD shifts metabolism from carbohydrate to fat oxidation, thus, we checked the level of genes that have an essential role in fatty-acid metabolism for the heart tissue. *Fasn* is one of them; it encodes fatty acid synthase protein that facilitates the fatty acid synthesis from acetyl-CoA and malonyl-CoA in the presence of NADPH (Bueno et al., 2019). While its level stayed steady between CD-fed hmKO and wild-type animals, it was highly upregulated in response to KD (Figure 5.26). KD-fed hmKO had a lower expression of *Fasn* than their KD-fed littermates (Figure 5.26). This data indicates that KD increases the transcript level of the fatty acid synthase enzyme. *Cpt1b* encodes carnitine palmitoyltransferase, a rate-limiting enzyme of the β-oxidation pathway in muscle mitochondria responsible for transferring long-chain fatty acids across the outer membrane (Maples et al., 2015). *Cptb1b* transcript levels did not change when animals were fed with KD (Figure 5.26). *Pdk4* encodes pyruvate dehydrogenase kinase (PDK4) found in the mitochondrial matrix. PDK4 phosphorylates one of the pyruvate dehydrogenase complex subunits, thereby inhibiting its function. Thus, fatty acid uti-

lization can be preferred over glucose catabolism (Zhang et al., 2014). mRNA levels of KD-fed mice were highly upregulated according to CD-fed counterparts (Figure 5.26). KD-fed hmKO and wild-type animals had almost the same amount of *Pdk4* mRNA (Figure 5.26). This data supports the notion that KD activates *Pdk4* to inactivate glucose catabolism. CD36 is a membrane glycoprotein as a scavenger receptor and a fatty acid translocator responsible for the transportation of fatty acid; it also engages in muscle lipid uptake (Niculite et al., 2019). The transcripts level of *Cd36* did not differ in animal groups (Figure 5.26). Together, these data show that not all but some genes that are crucial for fatty oxidation were upregulated in response to KD in heart.

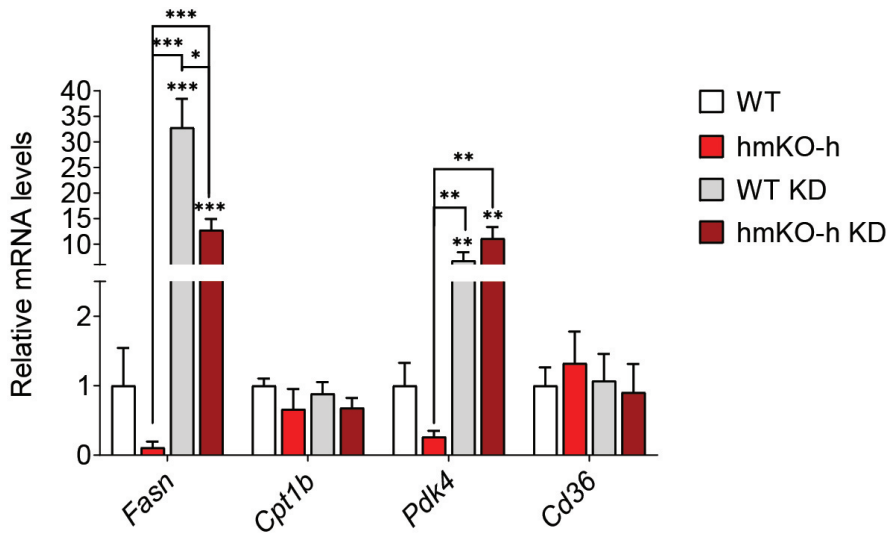

Figure 5.26. The transcript levels of fatty acid oxidation markers in the heart. Error bars represent mean ± SEM. (Student's t test: *p<0.05, **p<0.01, ***p<0.001)

We also checked the fatty acid oxidation markers in quadriceps tissue. While the transcript levels of *Fasn*,*Cpt1b*, and *Pdk4* did not change among groups, the *Cd36* level was significantly elevated in Cd- and KD-fed hmKO mice (Figure 5.27). Furthermore, KD increases the *Cd36* level in hmKO mice (Figure 5.27). These data demonstrate that despite the upregulation of the gene responsible for fatty acid uptake, the levels of remaining fatty acid oxidation pathway components do not change.

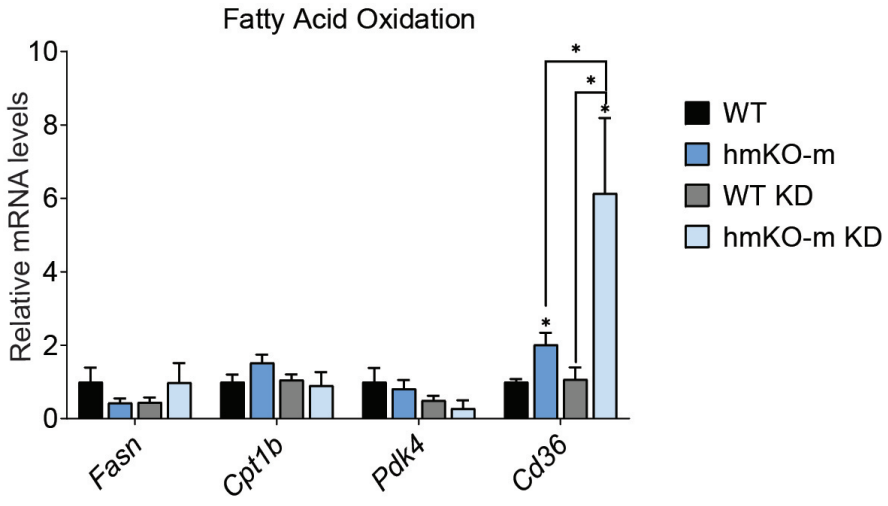

Figure 5.27. The transcript levels of fatty acid oxidation markers in the quadriceps. Error bars represent mean ± SEM. (Student's t test: *p<0.05)

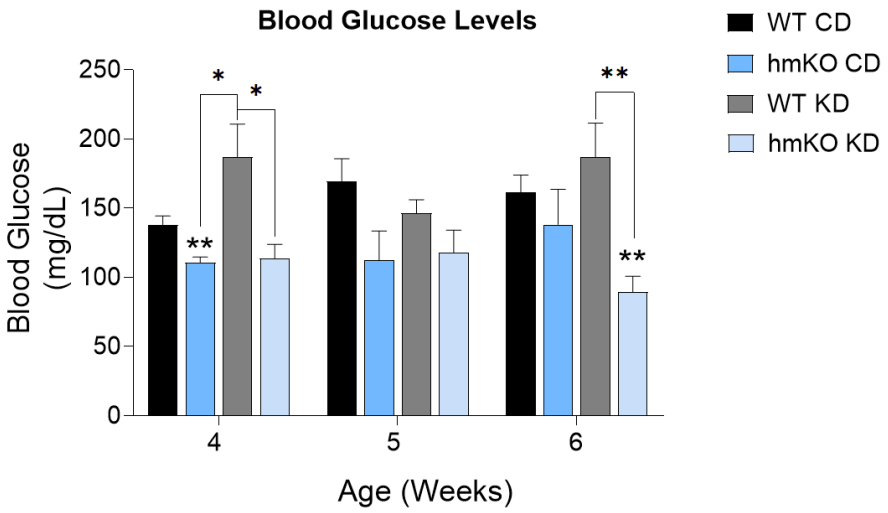

Figure 5.28. The blood glucose levels of CD- and KD-fed mice. Error bars represent mean ± SEM. (Student's t test: *p<0.05, **p<0.01)

We measured the blood glucose level of CD- and KD-fed animals to see whether KD could change energy source of mitochondria from glucose to fatty acid. We did not detect significance difference in blood glucose levels between CD- and KD-fed animals (Figure 5.28)

5.6. Stress Responses in KD-fed hmKO mice

We quantified the mRNA levels of various genes to investigate the impacts of KD on antioxidant response in heart tissue. KD-fed mice had a higher level of *Sod1* than their counterparts. In contrast, they showed a reduced level of *Sod2* (Figure 5.29), which may result from more need for superoxide conversion in the cytosol or mitochondrial intermembrane space than in the matrix. While *Catalase* levels diminished in KD-fed wild type according to CD-fed counterparts, its level remained almost the same in CD- and KD-fed hmKO (Figure 5.29). KD decreased both the *Gpx-1* and *Nfe2l2* levels in both wild-type and hmKO animals, CD- and KD-fed hmKO had the similar level of Gpx1 and Nfe2l2 (Figure 5.29). These data suggest that antioxidant components except for *Sod1* decrease in response to KD, meaning that KD reduces the antioxidant response in heart.

Antioxidant response elements were also quantified for quadriceps tissue. *Sod1*, *Sod2*, and *Nfe2l2* levels significantly decreased, whereas *Catalase* levels increased in KD-fed hmKO and wild-type animals according to their counterparts (Figure 5.30). While KD resulted in a reduced transcript level of *Gpx-1* in wild-type mice, its level did not differ in hmKO (Figure 5.30). This data indicates that antioxidant response components except for *Catalase* are downregulated in quadriceps tissue of the hmKO mice.

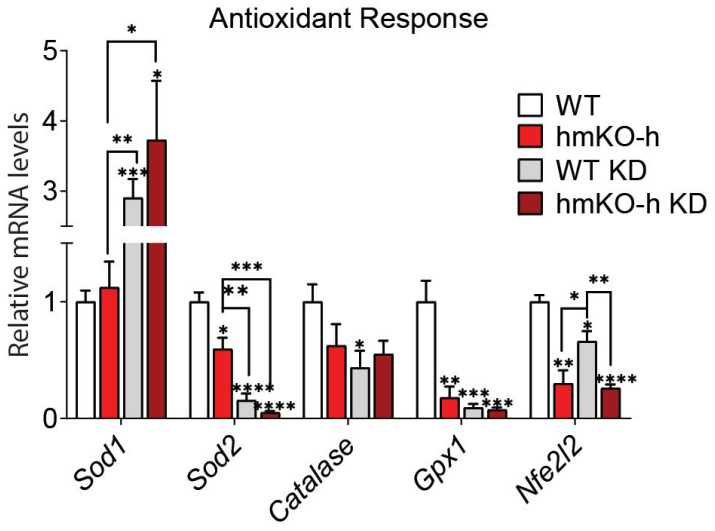

Figure 5.29. The transcript levels of antioxidant markers in the heart. Error bars represent mean ± SEM. (Student's t test: *p<0.05, **p<0.01, ***p<0.001,****p<0.0001)

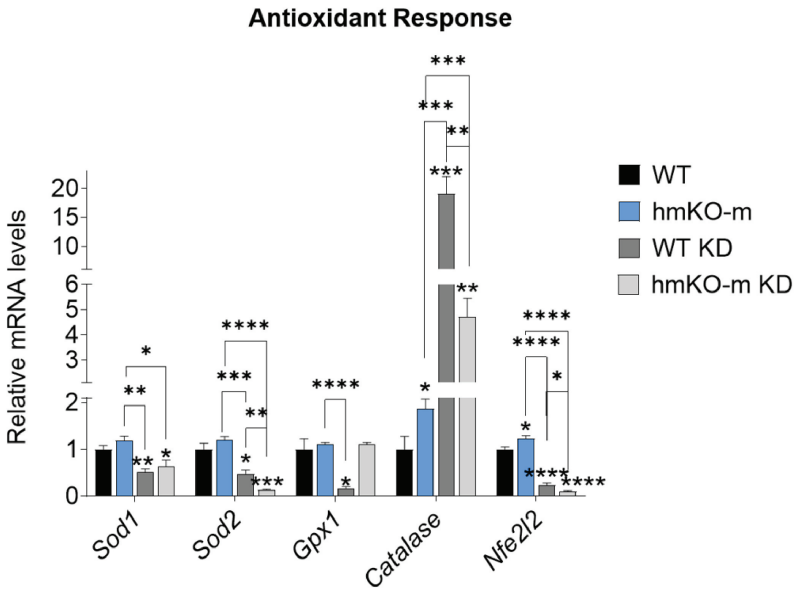

Figure 5.30. The transcript levels of antioxidant markers in the quadriceps. ***p<0.001)

6. DISCUSSION

Mitochondria are membrane-bound organelles found in almost every eukaryotic cell. They function as a powerhouse of the cells by producing most of the energy that cells need (Gray, 2013). The inner membrane of the mitochondria has folded structures named cristae. The mitochondrial respiratory complexes are localized in the cristae and carry electrons to produce energy by oxidative phosphorylation (Joubert & Puff, 2021). Moreover, mitochondria are responsible for many essential cellular processes; they have crucial roles in cell growth, cell signaling, ion homeostasis, and cell survival and death mechanisms. Thus, mitochondrial dysfunctions result in various disorders (Osellame et al., 2012). Respiratory chain dysfunctions are the primary source of mitochondrial diseases, specifically affecting high-energy demanding tissues and organs (Schlieben & Prokisch, 2020).

This study aimed to further characterize a DARS2-deficient mouse model that shows mitochondrial dysfunction due to respiratory chain defects. This mouse model has been studied before by Dogan et al., and they found that DARS2 deficiency impairs protein synthesis in the heart and quadriceps mitochondria, preventing OXPHOS complexes from properly assembling; therefore, both tissues show respiratory chain defects (2014). Furthermore, it has been revealed that in response to DARS2 depletion, the heart and skeletal muscle tissues act differently; while the heart initiates adaptive stress responses, skeletal muscle uses its intrinsic mechanism to maintain protein homeostasis.

In this study, we further characterized the heart- and skeletal muscle-specific DARS2-deficient mouse model (hmKO) phenotypically and molecularly by previously unchecked parameters. To generate hmKO mice, we disrupted the *Dars2* gene in heart and skeletal muscle tissues by expressing Cre under the muscle creatine kinase (Ckmm) promoter. DARS2$^{flox/flox}$ and Ckmm-cre mice were transferred from Cologne Excellence Cluster in Aging and Aging-Associated Diseases (CECAD), Cologne, Germany.

We generated DARS2$^{flox/flox}$,+/Ckmm-cre (hmKO) mice by mating DARS2$^{+/flox}$,+/Ckmm-cre and DARS2$^{flox/flox}$ mice at Bogazici University Experimental Animal Breeding and Care Unit. After re-generating hmKO animals, we checked the main findings of the model to see whether different facilities/countries have an impact on the phenotype of hmKO. The lifespan of the model was about 6-7 weeks, which is correlative with the previous findings. The mice exhibited severe symptoms after 6 weeks. We also recorded the weights of 4- to 6-week-old mice; as expected, DARS2-deficiency resulted in weight loss in hmKO mice. In contrast to their wild-type counterparts, they started to lose weight after five weeks. Moreover, as a sign of cardiomyopathy, the heart-to-body weight ratio was highly upregulated in 6-week-old hmKO mice. While their heart mass increased, their body weight decreased when they aged.

Similar to the hmKO mouse model, different knockout mouse strains were generated by disrupting essential genes that participate in mitochondrial DNA maintenance under muscle creatine kinase promoter (Kühl et al., 2017). The *Twinkle* knockout model was generated by disrupting TWINKLE helicase which is essential for mtDNA replication. TWINKLE loss led to mtDNA depletion in heart and skeletal muscle tissues. The lifespan of the TWINKLE model was 19 weeks, and mitochondrial cardiomyopathy was observed with progressive heart enlargement. Moreover, the TWINKLE-deficient model showed declined respiratory chain assembly and activity (Milenkovic et al., 2013). The *Tfam* mutant mouse model was obtained by disrupting *Tfam* coding transcription factor A, crucial for mtDNA maintenance. *Tfam* knockout mice exhibited severe mtDNA depletion and impaired respiratory chain function (Larsson et al., 1998). Further characterization of this mouse model revealed that TFAM loss caused atrioventricular heart conduction blocks, dilated cardiomyopathy, and shortened lifespan of 2-4 weeks (Wang et al., 1999). The *Polrmt* knockout mouse model was generated by disrupting the *Polrmt* gene encoding mitochondrial RNA polymerase. POLRMT-deficient heart showed severe mitochondrial dysfunction leading to dilated cardiomyopathy. The *Polrmt* mouse model had a shortened lifespan of fewer than 6 weeks (Kühl et al., 2016). The *Lrpprc* knockout mouse model was generated by disrupting the *Lrpprc*gene encoding leucine-rich pentatricopeptide repeat-containing

protein that plays an essential role in the regulation of mitochondrial mRNA stability. LRPPRC deficiency in the heart resulted in cardiomyopathy with mitochondrial chain deficiency. The lifespan of the *Lrpprc* knockout mouse had shortened to 16 weeks (Ruzzenente et al., 2012). Finally, the *Mterf4* knockout mouse model was generated by disrupting the *Mterf4* gene coding mitochondrial transcription termination factor 4, which is essential for mitochondrial translation. The maximum lifespan of this model was 21 weeks.*Mterf4* knockout mouse model displayed cardiomyopathy, increased level of mtDNA, and respiratory chain dysfunction in the heart (Cámara et al., 2011). All these models were generated by disrupting the genes that are crucial for mitochondrial maintenance under the muscle creatine kinase promoter, similar to our hmKO model. Moreover, their lifespans were significantly shorter than wild-type mice, and they all have cardiomyopathy, and mitochondrial dysfunction due to OXPHOS deficiency.

Beforehand, this mouse model has never been phenotypically characterized. Although it was obvious that they showed less activity by aging, we have evaluated their exercise capacity by various phenotypic tests. The coordinated activity, exercise performance, and muscle strength were measured by using the activity cage, treadmill, and grip strength tests, respectively. As a result of these phenotypic assays, hmKO mice have less performance and endurance, poorer coordinated activity, and weaker muscles than their wild-type littermates. These results demonstrate that cardiac hypertrophy or muscle atrophy limits the movement ability and activity of the animals. Various research suggests that exercise training can attenuate muscle atrophy. For example, the harlequin mutant mouse model (Hq mice) with respiratory chain defects because of complex I deficiency displayed amelioration in muscle strength and partial recovery of muscle atrophy in response to the treadmill, grip strength, and rotarod exercises (Fiuza-Luces et al., 2019). Another example showed that a POLG mouse model that has a defect in mitochondrial polymerase gamma gene exhibits mitochondrial dysfunction with various pathologies and accelerated aging phenotype with reduced lifespan (Safdar et al., 2011). When these models performed 5 months of endurance exercise, they showed improved OXPHOS capacity and restored mitochondrial morphology, which resulted in attenuation in sarcopenia, cardiomyopathy, and brain atrophy (Safdar et

al., 2011). These examples indicate that long-term exercise can improve the OXPHOS capacity and mitigate myopathy. However, our mouse model has a more severe phenotype with a shorter lifespan; even completing all the exercise assays was challenging for them.

After phenotypic characterization, we checked the molecular profile of the hmKO model. We quantified the mitochondrial mRNA transcript of the *CoxI* gene in heart and quadriceps tissues. hmKO heart had threefold more transcript levels than wild-type heart. In contrast, hmKO quadriceps did not change the transcript's level. The elevated mitochondrial transcript level in the heart indicates the mitochondrial mass increase. Therefore, our data support the notion that cardiomyocytes increase the number of mitochondria by biogenesis, whereas skeletal muscle maintains the mitochondria number. Increased mitochondrial mass might be the reason behind increased heart size. Similarly, in a cardiomyopathy model, a *Mterf4* knockout mouse showed increased mtDNA transcript levels (Cámara et al., 2011). However, *Twinkle*, *Tfam*, and *Polrmt* knockout cardiomyopathy models showed diminished mtDNA and transcript levels (Kühl et al., 2016; Larsson et al., 1998; Milenkovic et al., 2013). Since *Twinkle*, *Tfam*, and *Polrmt*mt genes are essential for mtDNA maintenance, *Twinkle* is crucial for mtDNA replication, and *Tfam* and *Polrmt* genes are required for mtDNA transcription; their disruption causes mtDNA depletion and hence mtDNA transcript levels. In contrast, *Mterf4* and *Dars2* are mitochondrial translation-related genes; their loss does not affect the mtDNA maintenance but increases mitochondrial biogenesis and mtDNA transcript levels.

We also investigated the impacts of respiratory chain deficiency on mitochondrial energy metabolism. First, respiratory chain deficiency was confirmed by a Western blot experiment. We used the OXPHOS cocktail antibody to see protein expression levels of subunits of each complex. The protein levels of the NDUFA9 subunit of complex I (CI), the UQRC2 subunit of complex III (CIII), and the COXIV subunit of complex IV (CIV) were diminished. In contrast, the expression levels of the SDHA subunit of complex II (CII) and ATP5A subunit of complex V did not change in both heart

and skeletal muscle tissues. CI, CIII, CIV, and CV consist of various subunits encoded by nuclear DNA (nDNA) and mitochondrial DNA (mtDNA), whereas CII does not have mitochondrial mtDNA-encoded subunits; all subunits of CII (SDHA, SDHB, SDHC, and SDHD) are encoded by nuclear DNA (Bezawork-Geleta et al., 2017). Our data confirm that translational defects resulting from DARS2 deficiency in mtDNA-encoded subunits of CI, CIII, and CIV impair the steady-state levels and possibly the assembly of complexes; therefore, the expression levels of subunits of CI, CIII, and CIV are reduced. However, complex V is not affected significantly; the reason must be that its mtDNA-encoded subunits (ATP6 and ATP8) contain only single aspartate residues (Table 6.1) (Dautant et al., 2018; The UniProt Consortium et al., 2021). Moreover, because CII does not have any mtDNA-encoded subunits, it is natural to be fully assembled, and the expression level of SDHA stays steady. In general, mitochondrial mutations bring along OXPHOS impairment. For example, the heart-and skeletal muscle-specific TFAM deficient mouse model showed respiratory chain deficiency in the heart (Wang et al., 1999) like in our model. In contrast, skeletal muscle mitochondrial respiratory chain was affected by DARS2-depletion, *Tfam* disruption did not lead to respiratory chain dysfunction in skeletal muscle (Wang et al., 1999). Moreover, other cardiomyopathy models (*Twinkle*, *Polrmt*, *Lrpprc*, and *Mterf4* knockout mice) displayed impaired respiratory chain function in their hearts; however, respiratory chain activity and protein levels were not evaluated in these models.

Table 6.1. Number of aspartate residues of OXPHOS Complexes' Subunits.

Complex	**mtDNA-encoded subunit**	**Number of aspartate residues**
COMPLEX I	ND1	3
	ND2	0
	ND3	2
	ND4	6
	ND4L	1
	ND5	12
	ND6	6
COMPLEX III	CYTB	11
COMPLEX IV	CO1	16
	CO2	11
	CO3	4
COMPLEX V	ATP6	1
	ATP8	1

After confirming respiratory chain deficiency, we measured the oxygen consumption rate of skeletal muscle and heart mitochondria (OCR). CI- and CII-linked respiration were measured separately. The idea behind measuring oxygen consumption rate is to detect oxygen utilization, hence oxidative phosphorylation capacity. When mitochondria are supplied with ADP after complex I or complex II substrates, the OCR value gives information about the OXPHOS capacity of the mitochondria (Gnaiger, 2009). As expected, hmKO heart mitochondria significantly reduced oxygen consumption rate in response to respiratory chain deficiency. However, although skeletal muscle mitochondria tend to decrease their OCR, they did not show a significant reduction. One of the explanations could be the elimination of dysfunctional mitochondria during mitochondria isolation steps, which might have led to the analysis of only healthy mitochondria in hmKO cells. Therefore, we might have observed a similar OCR result with wild-type healthy mitochondria. Another explanation could be the heterogeneity of the

skeletal muscle tissue; it contains different cell types, including connective tissue cells, which do not have active muscle creatine kinase promoters (Borg & Caulfield, 1980; Johnson et al., 1989). Therefore, isolated mitochondria from skeletal muscle comprised DARS2-deficient muscle mitochondria and healthy connective tissue mitochondria. To eliminate this heterogeneity, not the whole muscle but a single type of muscle fiber could be isolated, like in the previous study by Dogan et al. (2014). Additionally, isolation of mitochondria only from the soleus muscle might be a good approach as it has many mitochondria with high oxidative capacity (Crupi et al., 2018).

Mitochondrial respiratory chain defects are accompanied by reduced ATP production (Shepherd et al., 2006). Therefore, we calculated the OCR-related ATP ratio to see the impact of OXPHOS deficiency on energy metabolism. Following the OCR results, heart mitochondria diminished ATP production significantly, and skeletal muscle mitochondria displayed a downward trend. These data suggest that mitochondrial respiratory chain dysfunction leads to impaired oxidative phosphorylation and ATP production, specifically in the heart. Our method was used to calculate the OCR-related ATP ratio based on the finding of net OXPHOS capacity. However, there are more sensitive ways to obtain direct ATP production data of mitochondria. Using Magnesium green dye in the Oroboros O2k-FluoRespirometer system is one of them. The method relies on the different affinities of ADP and ATP to Mg^{2+}. When ADP is converted to ATP, Mg^{2+} prefers to bind to magnesium green and give fluorescence directly proportional to ATP production (Chinopoulos et al., 2014). In further experiments, this system could be utilized to obtain direct ATP production.

One of the highlights of mitochondrial dysfunction is the elevated reactive oxygen species (ROS) production. The excess amount of ROS might disrupt the redox balance and result in oxidative damage in cells. Cells can cope with the increased level of ROS by activating antioxidant stress responses (Poljsak et al., 2013). We checked antioxidant stress components to see whether mitochondrial dysfunction triggers ROS scavenging enzymes. In the hmKO heart, while the protein levels of antioxidant response elements, NFE2L2 and SOD2, did not change, their mRNA levels were reduced.

Also, the transcript levels of Gpx1 were significantly decreased. These results suggest that cardiomyocytes in hmKO mice do not upregulate the antioxidant response upon mitochondrial dysfunction, which implies lower ROS production in hmKO mitochondria. Therefore, next, we measured the ROS production of isolated heart mitochondria using the Oroboros O2k-FluoRespirometer. Since the experimental procedure is based on the measurement of H_2O_2 flux, we supplied the medium with the SOD enzyme so that $O^{\cdot -}$ molecules could be converted to H_2O_2 and included in the data. When we measured the reverse electron-related ROS (RET-ROS), we observed a decrease in ROS levels; however, there was no change in the forward electron transport-derived ROS (FET-ROS) levels. This could have been because FET produced a much lower H_2O_2 flux than RET, which might have caused reduced sensitivity in FET-ROS measurement. This data indicates that respiratory chain deficiency in hmKO mice hearts does not increase the mitochondrial ROS production. Because the major ROS generators are complex I and complex III, their deficiency might lead to a blockage of ROS production (Stefanatos & Sanz, 2018; Zhao et al., 2019).

The antioxidant elements were also quantified in skeletal muscle tissue. The levels of critical components (protein and transcript levels of NFE2L2 and SOD2 and transcript levels of Gpx1 and Sod1) did not change in hmKO. However, we observed an elevated level of Catalase mRNA. Since Catalase converts H2O2 to water in mitochondria, cytosol, and peroxisome, its increase might have stemmed from ROS produced by other compartments. We observed comparable H_2O_2 flux in the quadriceps mitochondria of hmKO and wild-type mice. Together these data show that DARS2-deficiency in the skeletal muscle does not affect the level of mitochondrial ROS; thereby, the antioxidant response is not activated.

Mitochondrial membrane potential ($\Delta\Psi$) is an essential component of the ATP and ROS production processes (Li et al., 2013; Zorova et al., 2018). It is known that reverse electron transport (RET) depends on mitochondrial membrane potential; reduction in ($\Delta\Psi$) might block RET (Komlódi et al., 2018). We measured the membrane potential of the heart and quadriceps mitochondria with CI&CII-linked respiration us-

ing Safranin dye in the Oroboros O2k-FluoRspirometer. We expected a decrease in ($\Delta\Psi$) in the heart due to the impaired mitochondrial respiratory chain and reduced ATP and RET-ROS levels. However, the membrane potential results of hmKO and wild-type mitochondria were very close, which might have resulted from the fact that the Safranin method might not be sensitive enough to measure ($\Delta\Psi$) with CI&CII-linked respiration. Safranin might inhibit the OXPHOS in a dose-dependent manner since its inhibitory effect is more apparent in CI-linked respiration; its sensitivity might favor the measurement of membrane potential in CII-linked respiration (Krumschnabel et al., 2014). To confidently conclude that there was no difference in ($\Delta\Psi$), we should employ different methods; for instance, using the TPP+ electrode would be a more accurate way to measure membrane potential with CI- and CI&CII-linked respiration (Teodoro et al., 2020).

Mitochondrial dysfunction can also trigger the mitochondrial integrated stress response (ISR^{mt}), which is characterized by the activation of eukaryotic translation initiation factor 2α (eIF2α), hence its downstream transcription factor ATF4 (Guo et al., 2020). We checked the eIF2α and phosphorylated-eIF2α levels in the heart and quadriceps. In both tissues, eIF2α was activated. However, Dogan et al. showed that the levels of (ISR^{mt}) components, including the metabolic hormone Fgf21, do not change in the skeletal muscle of hmKO mice. Therefore, we only checked for the previously not investigated parameters. The mRNA levels of Gdf15 were significantly higher in skeletal muscle, which suggests that skeletal muscle partly activates the adaptive response components. Then, we quantified the mRNA levels of (ISR^{mt}) components in the heart. We detected an increased trend in Atf4 and significant upregulation in Pycr1 and Mthfd2 transcript levels. Moreover, the heart upregulated the mRNA levels of metabolic hormones Fgf21 and Gdf15 in response to DARS2 depletion. These results suggest that hmKO heart triggers mitochondrial integrated stress response components.

Upregulated Fgf21 expression is common in many other mouse models: Deletor mice (Tyynismaa et al., 2010), skeletal muscle-specific Opa1-deficient mice (Pereira et al., 2017), neuron-specific Drp1-deficient mice (Restelli et al., 2018), Clpp-deficient mice (Becker et al., 2018), and mitochondrial DNA mutator mice (Kukat et al., 2014). Upregulated Fgf21 can provide tissues with protection against mitochondrial dysfunction. It has been demonstrated that Fgf21 protects Clpp-deficient mice hearts from the early pathological phase of cardiomyopathy by triggering the ERK1/2 signaling pathways in the case of mild mitochondrial dysfunction (Croon et al., 2022). However, in our model, Fgf21 upregulation failed to alleviate the phenotype due to strong OXPHOS deficiency.

Although cardiomyocytes initiated adaptive responses to counteract the mitochondrial dysfunction, severe phenotype and short lifespan were the apparent signs of failure. Since the heart is the most energy-demanding organ, it is foreseeable that adaptive responses cannot protect it from mitochondrial respiratory chain defects. In various cases, mitochondrial integrated stress response might even further contribute to the disease pathogenesis. For example, in the CHCHD10 mutant model with mitochondrial cardiomyopathy, chronic ISRmt disrupts metabolic homeostasis, increases oxidative stress and iron dysregulation, and ultimately leads to further mitochondrial dysfunction (Sayles et al., 2022)

HmKO mice have mitochondrial dysfunction and display a severe phenotype with cardiac hypertrophy and muscle atrophy. We applied a known intervention method, the ketogenic diet (KD), to attenuate the effects of the disease phenotype by shifting the metabolism from carbohydrate to fat oxidation. Previous studies demonstrated that KD could be beneficial in treating mitochondrial dysfunction. Ahola-Erkkilä et al. showed evidence that KD can alleviate the symptoms of myopathy in the Deletor mouse model (2010). Deletor mouse expresses a mutant *Twinkle* cDNA, which causes accumulation of deletions in mtDNA. The Deletor mouse model with a mitochondrial myopathy has subtle OXPHOS deficiency; KD attenuates the myopathy progression by changing the type of energy source the mitochondrial respiratory chain

utilizes; hence it partially compensates for the OXPHOS deficiency (Ahola-Erkkilä et al., 2010). Another example presents KD's beneficial effects on BCS1L (CIII assembly factor) knockout models with CIII deficiency and progressive hepatopathy. KD slows down the progression of hepatopathy by improving CIII assembly and activity; hence hepatocytes' mitochondrial morphology is normalized (Purhonen et al., 2017). These results suggest that KD might be a suitable treatment method for mitochondrial myopathies.

To observe whether KD might show its beneficial effects on hmKO mice, animals were fed with low carbohydrate and high-fat diet (KD) ad-libitum after weaning. Afterward, they have been phenotypically and molecularly characterized to test whether KD can alleviate the phenotype of hmKO mice. If KD lessens the severity of the phenotype of hmKO mice, the first indication would be a longer lifespan. Unfortunately, the lifespan of KD-fed animals was similar to CD-fed counterparts. This data suggested that KD did not impact the lifespan of the hmKO mice. Then, we compared the weight of all animals. KD-fed mice stop gaining weight after 5 weeks like their CD-fed littermates, another indication that KD does not affect the phenotype of hmKO mice.

To observe the manifestation of cardiac hypertrophy and muscle atrophy in CD- and KD-fed during exercise, animals, were subjected to various tests. Coordination activity, exercise performance and endurance, muscle strength, balance, and motor coordination were evaluated by activity cage, treadmill, grip strength, and Rota-Rod assays, respectively. For all tests, KD-fed animals gave similar results to their CD-fed counterparts; they showed poor activity, lower exercise performance, and weaker muscle strength. These results demonstrate that cardiac hypertrophy and muscle atrophy exert similar effects on movement, exercise capacity, and muscle strength between CD- and KD-fed hmKO mice.

After demonstrating that KD could not improve the disease phenotype of hmKO mice, we checked whether it might change some parameters in metabolic level. Firstly, we quantified the fatty acid oxidation components in the heart and quadriceps to

investigate whether KD shifts metabolism from carbohydrate to fat oxidation. We found no difference in the heart in Cpt1b and Cd36 levels, whereas KD-fed hmKO and wild-type animals had higher levels of Fasn and Pdk4 mRNAs, meaning that KD downregulates the glucose catabolism by upregulating Pdk4 and increase the fatty acid synthesis by upregulating Fasn. In quadriceps, KD only upregulated the transcript level of Cd36 responsible for fatty acid uptake. These results suggest that in our model, KD activates some but not all genes that are essential players in fatty acid oxidation. In addition, heart and skeletal muscle activating different genes might indicate that KD stimulates gene expression in a tissue-specific manner.

Furthermore, we measured animals' blood glucose levels weekly to investigate glucose utilization in response to KD. KD was expected to cause an increase in blood glucose levels by leading to fatty acid utilization over glucose oxidation. However, our data showed that KD-fed hmKO animals showed similar blood glucose levels to their CD-fed counterparts and lower blood glucose levels than their wild-type littermates. Also, we did not observe any significant changes in the blood glucose levels of the wild-type animals upon KD, which might have resulted from the short period of KD treatment (3 weeks). Since KD could not extend the lifespan of hmKO animals, we terminated the KD intervention at the end of the 6th week, which might mean that a 3-week KD treatment is insufficient to see its effects. However, due to our model's severe diseased phenotype and short lifespan, we could not prolong the KD. Therefore, KD might alleviate the progress of myopathy with a milder phenotype (like in Deletor and BCS1L mouse models) and longer lifespan but cannot be effective against severe phenotypes.

It has been proposed that KD has an impact on oxidative stress, so to evaluate the impacts of KD on antioxidant response, we quantified the genes that play essential roles in ROS scavenging. We observed a general downregulation in transcription levels of most of the genes in heart and quadriceps tissues. This result suggests that KD lowers the ROS production, which might point to worsened respiratory chain deficiency. Since ROS is produced mainly from CI and CIII, reducing their activity would

produce less ROS. To justify this deduction, protein and activity levels of OXPHOS complexes could be evaluated and compared with CD-fed animals. Since KD promotes beta-oxidation, it stimulates the upregulation of ketone bodies to be used as an energy source. Ketone bodies can increase succinate biosynthesis, which results in an elevation in the CII-linked respiration (Viscomi & Zeviani, 2020). Also, it has been shown that a high ketone level can stimulate the expression of OXPHOS genes (Nunnari & Suomalainen, 2012). However, in hmKO mice, our observation did not indicate the OXPHOS improvement; therefore, the level of ketone bodies might not have been upregulated. To justify this conclusion, the level of ketone bodies could be checked. In addition, C-II linked respiration, and ROS production would be measured to show whether KD stimulates the ketone body level to promote succinate synthesis and hence succinate-driven respiration. Moreover, mitochondrial biogenesis markers and circulating levels of mitokines could be checked to show whether KD impacts biogenesis and how it influences cardiomyopathy progression. The heart and skeletal muscle tissues could be investigated separately for each case to observe the effects of KD in a tissue-specific manner.

We treated animals with the ketogenic diet (KD) to alleviate the symptoms. However, it could not slow down the progression of dysfunction due to the severity of the phenotype. Apart from the therapeutic effect of KD, there also have been examples demonstrating that KD worsens the disease or does not affect the progression. For instance, in Mpv17- deficient mouse model that has mtDNA depletion in the liver, KD leads to the progression of liver cirrhosis (Bottani et al., 2014). On the other hand, the beneficial effect of KD in the Deletor mouse model encouraged researchers to study human patients. Patients with mitochondrial myopathy and ophthalmoplegia were on a modified Atkins ketogenic diet within this pilot study. However, all patients suffered from muscle pain due to muscle damage after 10-14 days; therefore, the diet was terminated. Surprisingly, 2 years after this short-term study, the same patients displayed improved muscle strength, which suggests that a short-term KD activates muscle regeneration in the long term (Ahola et al., 2016). This result suggests that short-term KD would improve the phenotype in a long-term duration; however, since

hmKO animals have 6-7 weeks lifespan, it is not possible to observe the long-term effects of KD. As a future study, new methods could be developed to counteract the effects of this severe phenotype. New treatments should focus on improving OXPHOS activity to maintain energy metabolism and decrease disease severity.

REFERENCES

Aanen, D. K. and P. Eggleton, 2017, "Symbiogenesis: Beyond the Endosymbiosis Theory?", *Journal of Theoretical Biology*, Vol. 434, pp. 99–103.

Ahola, S., M. Auranen, P. Isohanni, S. Niemisalo, N. Urho, J. Buzkova, V. Velagapudi, N. Lundbom, A. Hakkarainen, T. Muurinen, P. Piirilä,, K. H. Pietiläinen and A. Suomalainen, 2016, "Modified Atkins Diet Induces Subacute Selective Ragged-Red-Fiber Lysis in Mitochondrial Myopathy Patients", *EMBO Molecular Medicine*, Vol. 8, No. 11, pp. 1234–1247.

Ahola-Erkkilä, S., C. J. Carroll, K. Peltola-Mjösund, V. Tulkki, I. Mattila, T. Seppänen-Laakso, M. Orešič, H. Tyynismaa and A. Suomalainen, 2010, "Ketogenic Diet Slows Down Mitochondrial Myopathy Progression in Mice", *Human Molecular Genetics*, Vol. 19, No. 10, pp. 1974–1984.

Anderson, N. S. and C. M. Haynes, 2020, "Folding the Mitochondrial UPR into the Integrated Stress Response", *Trends in Cell Biology*, Vol. 30, No. 6, pp. 428–439.

Aradjanski, M., S. A. Dogan, S. Lotter, S. Wang, S. Hermans, R. Wi- bom, E. Rugarli and A. Trifunovic, 2017, "DARS2 Protects against Neuroinflammation and Apoptotic Neuronal Loss, but Is Dispensable for Myelin Producing Cells", *Human Molecular Genetics*, Vol. 26, No. 21, pp. 4181–4189.

Barbour, J. A. and N. Turner, 2014, "Mitochondrial Stress Signaling Promotes Cellular Adaptations", *International Journal of Cell Biology*, Vol. 2014, pp. 1-12.

Barcia, G., M. Rio, Z. Assouline, C. Zangarelli, C.-J. Roux, P. de Lonlay, J. Steffann, I. Desguerre, A. Munnich, J.-P. Bonnefont, N. Boddaert, A. Rötig, M. D. Metodiev and B. Ruzzenente, 2021, "Novel FARS2 Variants in Patients with Early Onset Encephalopathy with or without Epilepsy Associated with Long Survival",*European Journal of Human Genetics*, Vol. 29, No. 3, pp. 533–538.

Bayat, V., I. Thiffault, M. Jaiswal, M. Tétreault, T. Donti, F. Sasarman, G. Bernard, J. Demers-Lamarche, M.-J. Dicaire, J. Mathieu, M. Vanasse, J.- P. Bouchard, M.-F. Rioux, C. M. Lourenco, Z. Li, C. Haueter, E. A. Shoubridge,B. H. Graham, B. Brais and H. J. Bellen, 2012, "Mutations in the Mitochondrial Methionyl-tRNA Synthetase Cause a Neurodegenerative Phenotype in Flies and a Recessive Ataxia (ARSAL) in Humans", *PLoS Biology*, Vol. 10, No. 3, p. e1001288.

Becker, C., A. Kukat, K. Szczepanowska, S. Hermans, K. Senft, C. P. Brandscheid, P. Maiti and A. Trifunovic, 2018, "CLPP Deficiency Protects against Metabolic Syndrome but Hinders Adaptive Thermogenesis", *EMBO Reports*, Vol. 19, No. 5.

Belostotsky, R., E. Ben-Shalom, C. Rinat, R. Becker-Cohen, S. Feinstein, S. Zeligson, R. Segel, O. Elpeleg, S. Nassar and Y. Frishberg, 2011, "Mutations in the Mitochondrial Seryl-tRNA Synthetase Cause Hyperuricemia, Pulmonary Hypertension, Renal Failure in Infancy and Alkalosis, HUPRA Syndrome", *The American Journal of Human Genetics*, Vol. 88, No. 2, pp. 193–200.

Bezawork-Geleta, A., J. Rohlena, L. Dong, K. Pacak and J. Neuzil, 2017, "Mitochondrial Complex II: At the Crossroads", *Trends in Biochemical Sciences* Vol. 42, No. 4, pp. 312–325.

Bhatti, J., S. Kumar, M. Vijayan, G. Bhatti and P. Reddy, 2017, "Therapeutic Strategies for Mitochondrial Dysfunction and Oxidative Stress in Age-Related Metabolic Disorders", *Progress in Molecular Biology and Translational Science*, Vol. 146, pp. 13–46.

Boguszewska, K., M. Szewczuk, J. Kaźmierczak-Barańska and B. T. Karwowski, 2020, "The Similarities Between Human Mitochondria and Bacteria in the Context of Structure, Genome, and Base Excision Repair System", *Molecules*, Vol. 25, No. 12, p. 2857.

Bolze, A., F. Mendez, S. White, F. Tanudjaja, M. Isaksson, R. Jiang, A. D. Rossi, E. T. Cirulli, M. Rashkin, W. J. Metcalf, J. J. Grzymski, W. Lee, J. T. Lu and N. L. Washington, "A Catalog of Homoplasmic and Heteroplasmic Mitochondrial DNA Variants in Humans", bioRxiv 798264.

Borg, T. K. and J. B. Caulfield, 1980, "Morphology of Connective Tissue in Skeletal Muscle", *Tissue and Cell*, Vol. 12, No. 1, pp. 197–207.

Bottani, E., C. Giordano, G. Civiletto, I. Di Meo, A. Auricchio, E. Ciusani, S. Marchet, C. Lamperti, G. d'Amati, C. Viscomi and M. Zeviani, 2014, "AAV-Mediated Liver-Specific MPV17 Expression Restores mtDNA Levels and Prevents Diet-Induced Liver Failure", *Molecular Therapy*, Vol. 22, No. 1, pp. 10–17.

Bueno, M. J., V. Jimenez-Renard, S. Samino, J. Capellades, A. Junza, M. L. López-Rodríguez, J. Garcia-Carceles, I. Lopez-Fabuel, J. P. Bolanos, N. S. Chandel, O. Yanes, R. Colomer and M. Quintela-Fandino, 2019, "Essentiality of Fatty Acid Synthase in the 2D to Anchorage-Independent Growth Transition in Transforming Cells", *Nature Communications*, Vol. 10, No. 1, p. 5011.

Camara, Y., J. Asin-Cayuela, C. B. Park, M. D. Metodiev, Y. Shi, B. Ruzzenente, C. Kukat, B. Habermann, R. Wibom, K. Hultenby, T. Franz, H. Erdjument-Bromage, P. Tempst, B. M. Hallberg, C. M. Gustafsson and N.-G. Larsson, 2011, "MTERF4 Regulates Translation by Targeting the Methyltransferase NSUN4 to the Mammalian Mitochondrial Ribosome", *Cell Metabolism*, Vol. 13, No. 5, pp. 527–539.

Camhi, S. L., P. Lee and A. M. Choi, 1995, "The Oxidative Stress Response", *New Horizons (Baltimore, Md.)*, Vol. 3, No. 2, pp. 170–182.

Cardamone, M. D., B. Tanasa, C. T. Cederquist, J. Huang, K. Mahdaviani, W. Li, M. G. Rosenfeld, M. Liesa and V. Perissi, 2018, "Mitochondrial Retrograde Signaling in Mammals Is Mediated by the Transcriptional Cofactor GPS2 via Direct Mitochondria-to-Nucleus Translocation", *Molecular Cell*, Vol. 69, No. 5, pp. 757–772.e7.

Chandel, N. S., 2010, "Mitochondrial complex III: An Essential Component of Universal Oxygen Sensing Machinery?", *Respiratory Physiology Neurobiology*, Vol. 174, No. 3, pp. 175–181.

Chandel, N. S., 2014, "Mitochondria as Signaling Organelles", *BMC Biology*, Vol. 12, No. 1, p. 34.

Chang, N. C., 2020, "Autophagy and Stem Cells: Self-Eating for Self-Renewal", *Frontiers in Cell and Developmental Biology*, Vol. 8, p. 138.

Chihade, J., 2020, "Mitochondrial Aminoacyl-tRNA Synthetases", *The Enzymes*, Vol. 48, pp. 175–206.

Chinopoulos, C., G. Kiss, H. Kawamata and A. A. Starkov, 2014, "Measurement of ADP–ATP Exchange in Relation to Mitochondrial Transmembrane Potential and Oxygen Consumption", *Methods in Enzymology*, Vol. 542, pp. 333–348.

Cogliati, S., C. Frezza, M. E. Soriano, T. Varanita, R. Quintana-Cabrera, M. Corrado, S. Cipolat, V. Costa, A. Casarin, L. C. Gomes, E. Perales-Clemente, L. Salviati, P. Fernandez-Silva, J. A. Enriquez and L. Scorrano, 2013, "Mitochondrial Cristae Shape Determines Respiratory Chain Supercomplexes Assembly and Respiratory Efficiency", *Cell*, Vol. 155, No. 1, pp. 160–171.

Croon, M., K. Szczepanowska, M. Popovic, C. Lienkamp, K. Senft, C. P. Brandscheid, T. Bock, L. Gnatzy-Feik, A. Ashurov, R. J. Acton, H. Kaul, C. Pujol, S. Rosenkranz, M. Krüger and A. Trifunovic, 2022, "FGF21 Modulates Mitochondrial Stress Response in Cardiomyocytes Only under Mild Mitochondrial Dysfunction", *Science Advances*, Vol. 8, No. 14, p. eabn7105.

Crupi, A. N., J. S. Nunnelee, D. J. Taylor, A. Thomas, J.-P. Vit, C. E. Riera, R. A. Gottlieb and H. S. Goodridge, 2018, "Oxidative Muscles have Better Mitochondrial Homeostasis Than Glycolytic Muscles Throughout Life and Maintain Mitochondrial Function During Aging", *Aging*, Vol. 10, No. 11, pp. 3327–3352.

da Cunha, F. M., N. Q. Torelli and A. J. Kowaltowski, 2015, "Mitochondrial Retrograde Signaling: Triggers, Pathways, and Outcomes", *Oxidative Medicine and Cellular Longevity*, Vol. 2015, pp. 1–10.

Dalton, L. E., E. Healey, J. Irving and S. J. Marciniak, 2012, "Phosphoproteins in Stress-Induced Disease", *Progress in Molecular Biology and Translational Science*, Vol. 106, pp. 189–221.

Dautant, A., T. Meier, A. Hahn, D. Tribouillard-Tanvier, J.-P. di Rago and R. Kucharczyk, 2018, "ATP Synthase Diseases of Mitochondrial Genetic Origin", *Frontiers in Physiology*, Vol. 9, p. 329.

DiMauro, S. and G. Davidzon, 2005, "Mitochondrial DNA and Disease", *Annals of Medicine*, Vol. 37, No. 3, pp. 222–232.

Ding, W.-X. and X.-M. Yin, 2012, "Mitophagy: Mechanisms, Pathophysiological Roles, and Analysis", *Biol Chem*, Vol. 393, No. 7, pp. 547–564.

Dogan, S. A., C. Pujol, P. Maiti, A. Kukat, S. Wang, S. Hermans, K. Senft, R. Wibom, E. I. Rugarli and A. Trifunovic, 2014, "Tissue-Specific Loss of DARS2 Activates Stress Responses Independently of Respiratory Chain Deficiency in the Heart",*Cell Metabolism*, Vol. 19, No. 3, pp. 458–469.

Dogan, S. A., R. Cerutti, C. Benincá, G. Brea-Calvo, H. T. Jacobs, M. Zeviani, M. Szibor and C. Viscomi, 2018, "Perturbed Redox Signaling Exacerbates a Mitochondrial Myopathy", *Cell Metabolism*, Vol. 28, No. 5, pp. 764–775.

Eleutherio, E. C. A., R. S. Silva Magalhães, A. de Araújo Brasil, J. R. Monteiro Neto and L. de Holanda Paranhos, 2021, "SOD1, More Than Just an Antioxidant", *Archives of Biochemistry and Biophysics*, Vol. 697, p. 108701.

Figuccia, S., A. Degiorgi, C. Ceccatelli Berti, E. Baruffini, C. Dallabona and P. Goffrini, 2021, "Mitochondrial Aminoacyl-tRNA Synthetase and Disease: The Yeast Contribution for Functional Analysis of Novel Variants", *International Journal of Molecular Sciences*, Vol. 22, No. 9, p. 4524.

Figueira, T. R., D. R. Melo, A. E. Vercesi and R. F. Castilho, 2012, "Safranine as a Fluorescent Probe for the Evaluation of Mitochondrial Membrane Potential in Isolated Organelles and Permeabilized Cells", C. M. Palmeira and A. J. Moreno (Editors), *Mitochondrial Bioenergetics*, Vol. 810, pp. 103–117.

Fine, A. S., C. L. Nemeth, M. L. Kaufman and A. Fatemi, 2019, "Mitochondrial Aminoacyl-tRNA Synthetase Disorders: An Emerging Group of Developmental Disorders of Myelination", *Journal of Neurodevelopmental Disorders*, Vol. 11, No. 1, p. 29

Fiuza-Luces, C., P. L. Valenzuela, S. Laine-Menéndez, M. Fernández-de la Torre, V. Bermejo-Gómez, L. Rufián-Vazquez, J. Arenas, M. A. Martín, A. Lucia and M. Morán, 2019, "Physical Exercise and Mitochondrial Disease: Insights From a Mouse Model", *Frontiers in Neurology*, Vol. 10, p. 790.

Francisqueti-Ferron, F. V., A. J. T. Ferron, J. L. Garcia, C. C. V. d. A. Silva, M. R. Costa, C. S. Gregolin, F. Moreto, A. L. A. Ferreira, I. O. Minatel and C. R. Correa, 2019, "Basic Concepts on the Role of Nuclear Factor Erythroid-Derived 2-Like 2 (Nrf2) in Age-Related Diseases", *International Journal of Molecular Sciences*, Vol. 20, No. 13, p. 3208.

Frey, T. G. and C. A. Mannella, 2000, "The Internal Structure of Mitochondria", *Trends in Biochemical Sciences*, Vol. 25, No. 7, pp. 319–324.

Fridovich, I., 1974, "Evidence for the Symbiotic Origin of Mitochondria", *Life Sciences*, Vol. 14, No. 5, pp. 819–826.

Giles, R. E., H. Blanc, H. M. Cann and D. C. Wallace, 1980, "Maternal Inheritance of Human Mitochondrial DNA.", *Proceedings of the National Academy of Sciences*, Vol. 77, No. 11, pp. 6715–6719.

Glick, D., S. Barth and K. F. Macleod, 2010, "Autophagy: Cellular and Molecular Mechanisms", *The Journal of Pathology*, Vol. 221, No. 1, pp. 3–12.

Gnaiger, E., 2009, "Capacity of Oxidative Phosphorylation in Human Skeletal Muscle", *The International Journal of Biochemistry & Cell Biology*, Vol. 41, No. 10, pp. 1837–1845.

Gnaiger, E., 2020, *Mitochondrial Pathways and Respiratory Control: An Introduction to OXPHOS Analysis*, Fifth Edition, Bioenerg Commun.

Götz, A., H. Tyynismaa, L. Euro, P. Ellonen, T. Hyötyläinen, T. Ojala, R. Hämäläinen, J. Tommiska, T. Raivio, M. Oresic, R. Karikoski, O. Tammela, K. O. Simola, A. Paetau, T. Tyni and A. Suomalainen, 2011, "Exome Sequencing Identifies Mitochondrial Alanyl-tRNA Synthetase Mutations in Infantile Mitochondrial Cardiomyopathy", *The American Journal of Human Genetics*, Vol. 88, No. 5, pp. 635–642.

Graham, B. H., K. G. Waymire, B. Cottrell, I. A. Trounce, G. R. MacGregor and D. C. Wallace, 1997, "A Mouse Model for Mitochondrial Myopathy and Cardiomyopathy Resulting from a Deficiency in the Heart/Muscle Isoform of the Adenine Nucleotide Translocator", *Nature Genetics*, Vol. 16, No. 3, pp. 226–234.

Gray, M., 2013, "Mitochondria",*Brenner's Encyclopedia of Genetics*, pp. 430–432.

Guo, X., G. Aviles, Y. Liu, R. Tian, B. A. Unger, Y.-H. T. Lin, A. P. Wiita, K. Xu, M. A. Correia and M. Kampmann, 2020, "Mitochondrial Stress Is Relayed to the Cytosol by an OMA1–DELE1–HRI Pathway", *Nature*, Vol. 579, No. 7799, pp. 427–432.

Hansson, A., N. Hance, E. Dufour, A. Rantanen, K. Hultenby, D. A. Clayton, R. Wibom and N.-G. Larsson, 2004, "A Switch in Metabolism Precedes Increased Mitochondrial Biogenesis in Respiratory Chain-Deficient Mouse Hearts", *Proceedings of the National Academy of Sciences*, Vol. 101, No. 9, pp. 3136–3141.

Hill, S. and H. Van Remmen, 2014, "Mitochondrial Stress Signaling in Longevity: A New Role for Mitochondrial Function in Aging", *Redox Biology*, Vol. 2, pp. 936–944.

Javadov, S., A. V. Kozlov and A. K. S. Camara, 2020, "Mitochondria in Health and Diseases", *Cells*, Vol. 9, No. 5, p. 1177.

Johnson, J. E., B. J. Wold and S. D. Hauschka, 1989, "Muscle Creatine Kinase Sequence Elements Regulating Skeletal and Cardiac Muscle Expression in Transgenic Mice.", *Molecular and Cellular Biology*, Vol. 9, No. 8, pp. 3393–3399.

Jornayvaz, F. R. and G. I. Shulman, 2010, "Regulation of Mitochondrial Biogenesis", *Essays in Biochemistry*, Vol. 47, pp. 69–84.

Joubert, F. and N. Puff, 2021, "Mitochondrial Cristae Architecture and Functions: Lessons from Minimal Model Systems", *Membranes*, Vol. 11, No. 7, p. 465.

Kaiser, F., S. Krautwurst, S. Salentin, V. J. Haupt, C. Leberecht, S. Bittrich, D. Labudde and M. Schroeder, 2020, "The Structural Basis of the Genetic Code: Amino Acid Recognition by Aminoacyl-tRNA Synthetases", *Scientific Reports*, Vol. 10, No. 1, p. 12647.

Kasapkara, Ç. S., L. Tümer, N. Zanetti, F. Ezgü, E. Lamantea and M. Zeviani, 2017, "A Myopathy, Lactic Acidosis, Sideroblastic Anemia (Mlasa) Case Due to a Novel Pus1 Mutation", *Turkish Journal of Hematology.* Vol. 34, No. 4, pp. 376-377.

Killackey, S. A., D. J. Philpott and S. E. Girardin, 2020, "Mitophagy Pathways in Health and Disease", *Journal of Cell Biology*, Vol. 219, No. 11, p. e202004029.

Komlódi, T., F. F. Geibl, M. Sassani, A. Ambrus and L. Tretter, 2018, "Membrane Potential and delta pH Dependency of Reverse Electron Transport-Associated Hydrogen Peroxide Production in Brain and Heart Mitochondria", *Journal of Bioenergetics and Biomembranes*, Vol. 50, No. 5, pp. 355–365.

Kondo-Okamoto, N., N. N. Noda, S. W. Suzuki, H. Nakatogawa, I. Takahashi, M. Matsunami, A. Hashimoto, F. Inagaki, Y. Ohsumi and K. Okamoto, 2012, "Autophagy-related Protein 32 Acts as Autophagic Degron and Directly Initiates Mitophagy", *Journal of Biological Chemistry*, Vol. 287, No. 13, pp. 10631–10638.

Krumschnabel, G., A. Eigentler, M. Fasching and E. Gnaiger, 2014, "Use of Safranin for the Assessment of Mitochondrial Membrane Potential by High-Resolution Respirometry and Fluorometry", *Methods in Enzymology*, Vol. 542, pp. 163–181.

Kühl, I., M. Miranda, I. Atanassov, I. Kuznetsova, Y. Hinze, A. Mourier, A. Filipovska and N.-G. Larsson, 2017, "Transcriptomic and Proteomic Landscape of Mitochondrial Dysfunction Reveals Secondary Coenzyme Q Deficiency in Mammals", *eLife*, Vol. 6, p. e30952.

Kühl, I., M. Miranda, V. Posse, D. Milenkovic, A. Mourier, S. J. Siira, N. A. Bonekamp, U. Neumann, A. Filipovska, P. L. Polosa, C. M. Gustafsson and N.-G. Larsson, 2016, "POLRMT Regulates the Switch Between Replication Primer Formation and Gene Expression of Mammalian mtDNA", *Science Advances*, Vol. 2, No. 8, p. e1600963.

Kukat, A., S. A. Dogan, D. Edgar, A. Mourier, C. Jacoby, P. Maiti, J. Mauer, C. Becker, K. Senft, R. Wibom, A. P. Kudin, K. Hultenby, U. Flögel, S. Rosenkranz, D. Ricquier, W. S. Kunz and A. Trifunovic, 2014, "Loss of UCP2 Attenuates Mitochondrial Dysfunction without Altering ROS Production and Uncoupling Activity", *PLoS Genetics*, Vol. 10, No. 6, p. e100438.

Kummer, E. and N. Ban, 2021, "Mechanisms and Regulation of Protein Synthesis in Mitochondria", *Nature Reviews Molecular Cell Biology*, Vol. 22, No. 5, pp. 307–325.

Kuroiwa, T., K. Nishida, Y. Yoshida, T. Fujiwara, T. Mori, H. Kuroiwa and O. Misumi, 2006, "Structure, Function and Evolution of the Mitochondrial Division apparatus", *BiochimicaBiochimica et Biophysica Acta (BBA) - Molecular Cell Research*, Vol. 1763, No. 5-6, pp. 510–521.

Kwon, N. H., P. L. Fox and S. Kim, 2019, "Aminoacyl-tRNA Synthetases as Therapeutic Targets", *Nature Reviews Drug Discovery*, Vol. 18, No. 8, pp. 629–650.

Larsson, N.-G., J. Wang, H. Wilhelmsson, A. Oldfors, P. Rustin, M. Lewandoski, G. S. Barsh and D. A. Clayton, 1998, "Mitochondrial Transcription Factor A Is Necessary for mtDNA Maintance and Embryogenesis in Mice", *Nature Genetics*, Vol. 18, No. 3, pp. 231–236.

Lax, N. Z., D. M. Turnbull and A. K. Reeve, 2011, "Mitochondrial Mutations: Newly Discovered Players in Neuronal Degeneration", *The Neuroscientist*, Vol. 17, No. 6, pp. 645–658.

Lee, S., E. Tak, J. Lee, M. Rashid, M. P. Murphy, J. Ha and S. S. Kim, 2011, "Mitochondrial H2O2 Generated from Electron Transport Chain Complex I Stimulates Muscle Differentiation", *Cell Research*, Vol. 21, No. 5, pp. 817–834.

Li, X., P. Fang, J. Mai, E. T. Choi, H. Wang and X.-f. Yang, 2013, "Targeting Mitochondrial Reactive Oxygen Species as Novel Therapy for Inflammatory Diseases and Cancers", *Journal of Hematology & Oncology*, Vol. 6, No. 1, p. 19.

Lightowlers, R. N., A. Rozanska and Z. M. Chrzanowska-Lightowlers, 2014, "Mitochondrial Protein Synthesis: Figuring the Fundamentals, Complexities and Complications, of Mammalian Mitochondrial Translation", *FEBS Letters*, Vol. 588, No. 15, pp. 2496–2503.

Liu, Y., G. Fiskum and D. Schubert, 2002, "Generation of Reactive Oxygen Species by the Mitochondrial Electron Transport Chain", *Journal of Neurochemistry*, Vol. 80, No. 5, pp. 780–787.

Liufu, T. and Z. Wang, 2021, "Treatment for Mitochondrial Diseases", *Reviews in the Neurosciences*, Vol. 32, No. 1, pp. 35–47.

Lubos, E., J. Loscalzo and D. E. Handy, 2011, "Glutathione Peroxidase-1 in Health and Disease: From Molecular Mechanisms to Therapeutic Opportunities", *Antioxidants & Redox Signaling*, Vol. 15, No. 7, pp. 1957–1997.

Lyons, G., S. Muhlebach, A. Moser, R. Masood, B. Paterson, M. Buckingham and J. Perriard, 1991, "Developmental Regulation of Creatine Kinase Gene Expression by Myogenic Factors in Embryonic Mouse and Chick Skeletal Muscle", *Development*, Vol. 113, No. 3, pp. 1017–1029.

Mannella, C. A., 2020, "Consequences of Folding the Mitochondrial Inner Membrane", *Frontiers in Physiology*, Vol. 11, p. 536.

Maples, J. M., J. J. Brault, C. A. Witczak, S. Park, M. J. Hubal, T. M. Weber, J. A. Houmard and B. M. Shewchuk, 2015, "Differential Epigenetic and Transcriptional Response of the Skeletal Muscle Carnitine Palmitoyltransferase 1B (CPT1B) Gene to Lipid Exposure with Obesity", *American Journal of Physiology- Endocrinology and Metabolism*, Vol. 309, No. 4, pp. E345–E356.

McBride, H. M., M. Neuspiel and S. Wasiak, 2006, "Mitochondria: More Than Just a Powerhouse", *Current Biology*, Vol. 16, No. 14, pp. R551–R560.

Melber, A. and C. M. Haynes, 2018, "UPRmt Regulation and Output: A Stress Response Mediated by Mitochondrial-Nuclear Communication", *Cell Research*, Vol. 28, No. 3, pp. 281–295.

Melser, S., J. Lavie and G. Bénard, 2015, "Mitochondrial Degradation and Energy Metabolism", *Biochimica et Biophysica Acta (BBA) - Molecular Cell Research*, Vol. 1853, No. 10, pp. 2812–2821.

Mick, E., D. V. Titov, O. S. Skinner, R. Sharma, A. A. Jourdain and V. K. Mootha, 2020, "Distinct Mitochondrial Defects Trigger the Integrated Stress Response Depending on the Metabolic State of the Cell", *ELife*, Vol. 9, p. e49178.

Milenkovic, D., S. Matic, I. Kuhl, B. Ruzzenente, C. Freyer, E. Jemt, C. B. Park, M. Falkenberg and N.-G. Larsson, 2013, "TWINKLE Is an Essential Mitochondrial Helicase Required for Synthesis of Nascent D-loop Strands and Complete mtDNA Replication", *Human Molecular Genetics*, Vol. 22, No. 10, pp. 1983–1993.

Mills, E. L., B. Kelly, A. Logan, A. S. Costa, M. Varma, C. E. Bryant, P. Tourlomousis, J. H. M. Däbritz, E. Gottlieb, I. Latorre, S. C. Corr, G. McManus, D. Ryan, H. T. Jacobs, M. Szibor, R. J. Xavier, T. Braun, C. Frezza, M. P. Murphy and L. A. O'Neill, 2016, "Succinate Dehy- drogenase Supports Metabolic Repurposing of Mitochondria to Drive Inflam- matory Macrophages", *Cell*, Vol. 167, No. 2, pp. 457–470.e13,

Moraes, C. T., S. DiMauro, M. Zeviani, A. Lombes, S. Shanske, A. F. Miranda, H. Nakase, E. Bonilla, L. C. Werneck, S. Servidei, I. Nonaka, Y. Koga, A. J. Spiro, A. K. W. Brownell, B. Schmidt, D. L. Schotland, M. Zupanc, D. C. DeVivo, E. A. Schon and L. P. Rowland, 1989, "Mitochondrial DNA Deletions in Progressive External Ophthalmoplegia and Kearns-Sayre Syndrome", *New England Journal of Medicine*, Vol. 320, No. 20, pp. 1293–1299.

Motley, W. W., K. L. Seburn, M. H. Nawaz, K. E. Miers, J. Cheng, A. Antonellis, E. D. Green, K. Talbot, X.-L. Yang, K. H. Fischbeck and R. W. Burgess, 2011, "Charcot-Marie-Tooth–Linked Mutant GARS Is Toxic to Peripheral Neurons Independent of Wild-Type GARS Levels", *PLoS Genetics*, Vol. 7, No. 12, p. e1002399.

Münch, C., 2018, "The Different Axes of the Mammalian Mitochondrial Unfolded Protein Response", *BMC Biology*, Vol. 16, No. 1, p. 81.

Murphy, M. P., 2009, "How Mitochondria Produce Reactive Oxygen Species", *Biochemical Journal*, Vol. 417, No. 1, pp. 1–13.

Nandi, A., L.-J. Yan, C. K. Jana and N. Das, 2019, "Role of Catalase in Oxidative Stress- and Age-Associated Degenerative Diseases", *Oxidative Medicine and Cellular Longevity*, Vol. 2019, pp. 1–19.

Nevanlinna, V., S. Konovalova, B. Ceulemans, M. Muona, A. Laari, T. Hilander, K. Gorski, L. Valanne, A.-K. Anttonen, H. Tyynismaa, C. Courage and A.-E. Lehesjoki, 2020, "A Patient with Pontocerebellar Hypoplasia Type 6: Novel RARS2 Mutations, Comparison to Previously Published Patients and Clinical Distinction from PEHO Syndrome", *European Journal of Medical Genetics*, Vol. 63, No. 3, p. 103766.

Niculite, C.-M., A.-M. Enciu and M. E. Hinescu, 2019, "CD 36: Focus on Epigenetic and Post-Transcriptional Regulation", *Frontiers in Genetics*, Vol. 10, p. 680.

Nunnari, J. and A. Suomalainen, 2012, "Mitochondria: In Sickness and in Health", *Cell*, Vol. 148, No. 6, pp. 1145–1159.

Ognjenović, J. and M. Simonović, 2018, "Human Aminoacyl- tRNA Synthetases in Diseases of the Nervous System", *RNA Biology*, Vol. 15, No. 4-5, pp. 623–634.

Osellame, L. D., T. S. Blacker and M. R. Duchen, 2012, "Cellular and Molecular Mechanisms of Mitochondrial Function", *Best Practice & Research Clinical Endocrinology & Metabolism*, Vol. 26, No. 6, pp. 711–723.

Pakos-Zebrucka, K., I. Koryga, K. Mnich, M. Ljujic, A. Samali and A. M. Gorman, 2016, "The Integrated Stress Response", *EMBO reports*, Vol. 17, No. 10, pp. 1374–1395.

Pan, Z., H. Xu, Y. Tian, D. Liu, H. Liu, R. Li, Q. Dou, B. Zuo, R. Zhai, W. Tang and W. Lu, 2020, "Perrault Syndrome: Clinical Report and Retrospective Analysis", *Molecular Genetics & Genomic Medicine*, Vol. 8, No. 10.

Pereira, R. O., S. M. Tadinada, F. M. Zasadny, K. J. Oliveira, K. M. P. Pires, A. Olvera, J. Jeffers, R. Souvenir, R. Mcglauflin, A. Seei, T. Funari, H. Sesaki, M. J. Potthoff, C. M. Adams, E. J. Anderson and E. D. Abel, 2017, "OPA 1 Deficiency Promotes Secretion of FGF 21 from Muscle That Prevents Obesity and Insulin Resistance", *The EMBO Journal*, Vol. 36, No. 14, pp. 2126–2145.

Pierce, S. B., K. M. Chisholm, E. D. Lynch, M. K. Lee, T. Walsh, J. M. Opitz, W. Li, R. E. Klevit and M.-C. King, 2011, "Mutations in Mitochondrial Histidyl tRNA Synthetase HARS2 Cause Ovarian Dysgenesis and Sensorineural Hearing Loss of Perrault Syndrome", *Proceedings of the National Academy of Sciences*, Vol. 108, No. 16, pp. 6543–6548.

Poljsak, B., D. Suput and I. Milisav, 2013, "Achieving the Balance between ROS and Antioxidants: When to Use the Synthetic Antioxidants", *Oxidative Medicine and Cellular Longevity*, Vol. 2013, pp. 1–11.

Purhonen, J., J. Rajendran, M. Mörgelin, K. Uusi-Rauva, S. Katayama, K. Krjutskov, E. Einarsdottir, V. Velagapudi, J. Kere, M. Jauhiainen, V. Fellman and J. Kallijärvi, 2017, "Ketogenic Diet Attenuates Hepatopathy in Mouse Model of Respiratory Chain Complex III Deficiency Caused by a Bcs1l Mutation", *Scientific Reports*, Vol. 7, No. 1, p. 957.

Quadros Santos Monteiro Fonseca, A. T. and E. Zanoteli, 2018, "Charcot-Marie-Tooth Disease", *Revista Médica Clinica Las Condes*, Vol. 29, No. 5, pp. 521–529.

Quinlan, C. L., A. L. Orr, I. V. Perevoshchikova, J. R. Treberg, B. A. Ackrell and M. D. Brand, 2012, "Mitochondrial Complex II Can Generate Reactive Oxygen Species at High Rates in Both the Forward and Reverse Reactions", *Journal of Biological Chemistry*, Vol. 287, No. 32, pp. 27255–27264.

Ray, P. D., B.-W. Huang and Y. Tsuji, 2012, "Reactive Oxygen Species (ROS) Homeostasis and Redox Regulation in Cellular Signaling", *Cellular Signalling*, Vol. 24, No. 5, pp. 981–990.

Restelli, L. M., B. Oettinghaus, M. Halliday, C. Agca, M. Licci, L. Sironi, C. Savoia, J. Hench, M. Tolnay, A. Neutzner, A. Schmidt, A. Eckert, G. Mallucci, L. Scorrano and S. Frank, 2018, "Neuronal Mitochondrial Dysfunction Activates the Integrated Stress Response to Induce Fibroblast Growth Factor 21", *Cell Reports*, Vol. 24, No. 6, pp. 1407–1414.

Rimbaud, S., A. Garnier and R. Ventura-Clapier, 2009, "Mitochondrial Biogenesis in Cardiac Pathophysiology", *Pharmacological Reports*, Vol. 61, No. 1, pp. 131–138.

Rios-Anjos, R. M., V. d. L. Camandona, L. Bleicher and J. R. Ferreira-Junior, 2017, "Structural and Functional Mapping of Rtg2p Determinants Involved in Retrograde Signaling and Aging of Saccharomyces Cerevisiae", *PLOS ONE*, Vol. 12, No. 5, p. e0177090.

Robb, E. L., A. R. Hall, T. A. Prime, S. Eaton, M. Szibor, C. Viscomi, A. M. James and M. P. Murphy, 2018, "Control of Mitochondrial Superoxide Production by Reverse Electron Transport at Complex I", *Journal of Biological Chemistry*, Vol. 293, No. 25, pp. 9869–9879.

Roger, A. J., S. A. Muñoz-Gómez and R. Kamikawa, 2017, "The Origin and Diversification of Mitochondria", *Current Biology*, Vol. 27, No. 21, pp. R1177–R1192.

Rubio Gomez, M. A. and M. Ibba, 2020, "Aminoacyl-tRNA Synthetases", *RNA*, Vol. 26, No. 8, pp. 910–936.

Rusecka, J., M. Kaliszewska, E. Bartnik and K. Tonska, 2018, "Nuclear Genes Involved in Mitochondrial Diseases Caused by Instability of Mitochondrial DNA", *Journal of Applied Genetics*, Vol. 59, No. 1, pp. 43–57.

Ruzzenente, B., M. D. Metodiev, A. Wredenberg, A. Bratic, C. B. Park, Y. C´amara, D. Milenkovic, V. Zickermann, R. Wibom, K. Hultenby, H. Erdjument-Bromage, P. Tempst, U. Brandt, J. B. Stewart, C. M. Gustafsson and N.-G. Larsson, 2012, "LRPPRC Is Necessary for Polyadenylation and Coordination of Translation of Mitochondrial mRNAs: LRPPRC Regulates Mitochondrial Translation", *The EMBO Journal*, Vol. 31, No. 2, pp. 443–456.

Rygiel, K. A., H. A. Tuppen, J. P. Grady, A. Vincent, E. L. Blakely, A. K. Reeve, R. W. Taylor, M. Picard, J. Miller and D. M. Turnbull, 2016, "Complex Mitochondrial DNA Rearrangements in Individual Cells from Patients with Sporadic Inclusion Body Myositis", *Nucleic Acids Research*, Vol. 44, No. 11, pp. 5313–5329.

Ryzhkova, A., M. Sazonova, V. Sinyov, E. Galitsyna, M. Chicheva, A. Melnichenko, A. Grechko, A. Postnov, A. Orekhov and T. Shkurat, 2018, "Mitochondrial Diseases Caused by mtDNA Mutations: A Mini-Review", *Therapeutics and Clinical Risk Management*, Vol. 14, pp. 1933–1942.

Safdar, A., J. M. Bourgeois, D. I. Ogborn, J. P. Little, B. P. Hettinga, M. Akhtar, J. E. Thompson, S. Melov, N. J. Mocellin, G. C. Kujoth, T. A. Prolla and M. A. Tarnopolsky, 2011, "Endurance Exercise Rescues Progeroid Aging and Induces Systemic Mitochondrial Rejuvenation in mtDNA Mutator Mice", *Proceedings of the National Academy of Sciences*, Vol. 108, No. 10, pp. 4135–4140.

Saneto, R. P. and M. M. Sedensky, 2013, "Mitochondrial Disease in Childhood: mtDNA Encoded", *Neurotherapeutics*, Vol. 10, No. 2, pp. 199–211.

Santos, R. X., S. C. Correia, X. Zhu, M. A. Smith, P. I. Moreira, R. J. Castellani, A. Nunomura and G. Perry, 2013, "Mitochondrial DNA Oxidative Damage and Repair in Aging and Alzheimer's Disease", *Antioxidants & Redox Signaling*, Vol. 18, No. 18, pp. 2444–2457.

Sayles, N. M., N. Southwell, K. McAvoy, K. Kim, A. Pesini, C. J. Anderson, C. Quinzii, S. Cloonan, H. Kawamata and G. Manfredi, 2022, "Mutant CHCHD10 Causes an Extensive Metabolic Rewiring That Precedes OXPHOS Dysfunction in a Murine Model of Mitochondrial Cardiomyopathy", *Cell Reports*, Vol. 38, No. 10, p. 110475.

Scheper, G. C., T. van der Klok, R. J. van Andel, C. G. M. van Berkel, M. Sissler, J. Smet, T. I. Muravina, S. V. Serkov, G. Uziel, M. Bugiani, R. Schiffmann, I. Krägeloh-Mann, J. A. M. Smeitink, C. Florentz, R. Van Coster, J. C. Pronk and M. S. van der Knaap, 2007, "Mitochondrial Aspartyl-tRNA Synthetase Deficiency Causes Leukoencephalopathy with Brain Stem and Spinal Cord Involvement and Lactate Elevation", *Nature Genetics*, Vol. 39, No. 4, pp. 534–539.

Schlieben, L. D. and H. Prokisch, 2020, "The Dimensions of Primary Mitochondrial Disorders", *Frontiers in Cell and Developmental Biology*, Vol. 8, p. 600079.

Scialò, F., D. J. Fernández-Ayala and A. Sanz, 2017, "Role of Mitochondrial Reverse Electron Transport in ROS Signaling: Potential Roles in Health and Disease", *Frontiers in Physiology*, Vol. 8, p. 428.

Scialò, F., A. Sriram, D. Fernández-Ayala, N. Gubina, M. Lõhmus, G. Nelson, A. Logan, H. M. Cooper, P. Navas, J. A. Enriquez, M. P. Murphy and A. Sanz, 2016, "Mitochondrial ROS Produced via Reverse Electron Transport Extend Animal Lifespan", *Cell Metabolism*, Vol. 23, No. 4, pp. 725–734.

Scorrano, L., 2013, "Keeping Mitochondria in Shape: A Matter of Life and Death", *European Journal of Clinical Investigation*, Vol. 43, No. 8, pp. 886–893.

Seiferling, D., K. Szczepanowska, C. Becker, K. Senft, S. Hermans, P. Maiti, T. König, A. Kukat and A. Trifunovic, 2016, "Loss of CLPP Alleviates Mitochondrial Cardiomyopathy without Affecting the Mammalian UPR mt", *EMBO Reports*, Vol. 17, No. 7, pp. 953–964,

Selivanov, V. A., T. V. Votyakova, V. N. Pivtoraiko, J. Zeak, T. Sukhomlin, M. Trucco, J. Roca and M. Cascante, 2011, "Reactive Oxygen Species Production by Forward and Reverse Electron Fluxes in the Mitochondrial Respiratory Chain", *PLoS Computational Biology*, Vol. 7, No. 3, p. e1001115.

Sena, L. A. and N. S. Chandel, 2012, "Physiological Roles of Mitochondrial Reactive Oxygen Species", *Molecular Cell*, Vol. 48, No. 2, pp. 158–167.

Shepherd, R. K., N. Checcarelli, A. Naini, D. C. De Vivo, S. DiMauro and C. M. Sue, 2006, "Measurement of ATP Production in Mitochondrial Disorders", *Journal of Inherited Metabolic Disease*, Vol. 29, No. 1, pp. 86–91.

Shpilka, T. and C. M. Haynes, 2018, "The Mitochondrial UPR: Mechanisms, Physiological Functions and Implications in Ageing", *Nature Reviews Molecular Cell Biology*, Vol. 19, No. 2, pp. 109–120.

Sousa, J. S., E. D'Imprima and J. Vonck, 2018, "Mitochondrial Respiratory Chain Complexes", J. R. Harris and E. J. Boekema (Editors), *Membrane Protein Complexes: Structure and Function*, Vol. 87, pp. 167–227.

Steenweg, M. E., D. Ghezzi, T. Haack, T. E. Abbink, D. Martinelli, C. G. van Berkel, A. Bley, L. Diogo, E. Grillo, J. Te Water Naudé, T. M. Strom, E. Bertini, H. Prokisch, M. S. van der Knaap and M. Zeviani, 2012, "Leukoencephalopathy with Thalamus and Brainstem Involvement and High Lactate 'LTBL' Caused by EARS2 Mutations", *Brain*, Vol. 135, No. 5, pp. 1387–1394.

Stefanatos, R. and A. Sanz, 2018, "The Role of Mitochondrial ROS in the Aging Brain", *FEBS Letters*, Vol. 592, No. 5, pp. 743–758.

Stewart, J. B. and P. F. Chinnery, 2015, "The Dynamics of Mitochondrial DNA Heteroplasmy: Implications for Human Health and Disease", *Nature Reviews Genetics*, Vol. 16, No. 9, pp. 530–542.

Taylor, R. W. and D. M. Turnbull, 2005, "Mitochondrial DNA Mutations in Human Disease", *Nature Reviews Genetics*, Vol. 6, No. 5, pp. 389–402.

Teodoro, J. S., I. F. Machado, A. C. Castela, A. P. Rolo and C. M. Palmeira, 2020, "The Evaluation of Mitochondrial Membrane Potential Using Fluorescent Dyes or a Membrane-Permeable Cation (TPP+) Electrode in Isolated Mitochondria and Intact Cells", S. Mishra (Editor), *Immunometabolism*, Vol. 2184, pp. 197–213.

The UniProt Consortium, A. Bateman, M.-J. Martin, S. Orchard, M. Magrane, R. Agivetova, S. Ahmad, E. Alpi, E. H. Bowler-Barnett, R. Britto, B. Bursteinas, H. Bye-A-Jee, R. Coetzee, A. Cukura, A. Da Silva, P. Denny, T. Dogan, T. Ebenezer, J. Fan, L. G. Castro, P. Garmiri, G. Georghiou, L. Gonzales, E. Hatton-Ellis, A. Hussein, A. Ignatchenko, G. Insana, R. Ishtiaq, P. Jokinen, V. Joshi, D. Jyothi, A. Lock, R. Lopez, A. Luciani, J. Luo, Y. Lussi, A. MacDougall, F. Madeira, M. Mahmoudy, M. Menchi, A. Mishra, K. Moulang, A. Nightingale, C. S. Oliveira, S. Pundir, G. Qi, S. Raj, D. Rice, M. R. Lopez, R. Saidi, J. Sampson, T. Sawford, E. Speretta, E. Turner, N. Tyagi, P. Vasudev, V. Volynkin, K. Warner, X. Watkins, R. Zaru, H. Zellner, A. Bridge, S. Poux, N. Redaschi, L. Aimo, G. Argoud-Puy,

A. Auchincloss, K. Axelsen, P. Bansal, D. Baratin, M.-C. Blatter, J. Bolleman, E. Boutet, L. Breuza, C. Casals-Casas, E. de Castro, K. C. Echioukh, E. Coudert, B. Cuche, M. Doche, D. Dornevil, A. Estreicher, M. L. Famiglietti, M. Feuermann, E. Gasteiger, S. Gehant, V. Gerritsen, A. Gos, N. Gruaz-Gumowski, U. Hinz, C. Hulo, N. Hyka-Nouspikel, F. Jungo, G. Keller, A. Kerhornou, V. Lara, P. Le Mercier, D. Lieberherr, T. Lombardot, X. Martin, P. Masson, A. Morgat, T. B. Neto, S. Paesano, I. Pedruzzi, S. Pilbout, L. Pourcel, M. Pozzato, M. Pruess, C. Rivoire, C. Sigrist, K. Sonesson, A. Stutz, S. Sundaram, M. Tognolli, L. Verbregue, C. H. Wu, C. N. Arighi, L. Arminski, C. Chen, Y. Chen, J. S. Garavelli, H. Huang, K. Laiho, P. Mc-Garvey, D. A. Natale, K. Ross, C. R. Vinayaka, Q. Wang, Y. Wang, L.-S. Yeh, J. Zhang, P. Ruch and D. Teodoro, 2021, "UniProt: The Universal Protein Knowledge-Base in 2021", *Nucleic Acids Research*, Vol. 49, No. D1, pp. D480–D489.

Tonelli, C., I. I. C. Chio and D. A. Tuveson, 2018, "Transcriptional Regulation by Nrf2", *Antioxidants & Redox Signaling*, Vol. 29, No. 17, pp. 1727–1745.

Tuppen, H. A., E. L. Blakely, D. M. Turnbull and R. W. Taylor, 2010, "Mitochondrial DNA Mutations and Human Disease", *Biochimica et Biophysica Acta (BBA) - Bioenergetics*, Vol. 1797, No. 2, pp. 113–128.

Tyynismaa, H., C. J. Carroll, N. Raimundo, S. Ahola-Erkkilä, T. Wenz, H. Ruhanen, K. Guse, A. Hemminki, K. E. Peltola-Mjøsund, V. Tulkki, M. Orešič, C. T. Moraes, K. Pietiläinen, I. Hovatta and A. Suomalainen, 2010, "Mitochondrial Myopathy Induces a Starvation-Like Response", *Human Molecular Genetics*, Vol. 19, No. 20, pp. 3948–3958.

Uittenbogaard, M. and A. Chiaramello, 2014, "Mitochondrial Biogenesis: A Therapeutic Target for Neurodevelopmental Disorders and Neurodegenerative Diseases", *Current Pharmaceutical Design*, Vol. 20, No. 35, pp. 5574–5593.

van Berge, L., E. M. Hamilton, T. Linnankivi, G. Uziel, M. E. Steenweg, P. Isohanni, N. I. Wolf, I. Krageloh-Mann, N. J. Brautaset, P. I. Andrews, B. A. de Jong, M. al Ghamdi, W. N. van Wieringen, LBSL Research Group, B. A. Tannous, E. Hulleman, T. Wurdinger, C. G. M. van Berkel, E. Polder, T. E. M. Abbink, E. A. Struys, G. C. Scheper, M. S. van der Knaap, F. Alehan, R. E. Appleton, E. Boltshauser, K. Brockmann, E. Calado, A. Carius, I. F. M. de Coo, R. van Coster, S. El-Zind, O. Erturk, L. Fadeeva, A. Feigenbaum, S. Gokben, M. Gorman, S. Gulati, P. Hnevsova, K. Joost, W. Kohler, A. Kolk, W. Kristoferitsch, E. Lemos Silveira, J. Lin, S. Lutz, C. Mendonca, C. Nuttin, T. Opladen, M. Savoiardo, R. Schiffmann, A. Seitz, S. Serkov, S. Sharma, S. Stockler, I. K. Temple, K. Uluc, S. Vojta, G. Wilms, B. Wong and Z. Yapici, 2014, "Leukoencephalopathy with Brainstem and Spinal Cord Involvement and Lactate Elevation: Clinical and Genetic Characterization and Target for Therapy", *Brain*, Vol. 137, No. 4, pp. 1019–1029.

Viscomi, C. and M. Zeviani, 2020, "Strategies for Fighting Mitochondrial Diseases", *Journal of Internal Medicine*, Vol. 287, No. 6, pp. 665–684.

Wallace, D. C., 2005, "A Mitochondrial Paradigm of Metabolic and Degenerative Diseases, Aging, and Cancer: A Dawn for Evolutionary Medicine", *Annual Review of Genetics*, Vol. 39, No. 1, pp. 359–407.

Wallace, D. C., M. T. Lott, J. M. Shoffner and M. D. Brown, 1992, "Diseases Resulting from Mitochondrial DNA Point Mutations", *Journal of Inherited Metabolic Disease*, Vol. 15, No. 4, pp. 472–479.

Wang, F., D. Zhang, D. Zhang, P. Li and Y. Gao, 2021, "Mitochondrial Protein Translation: Emerging Roles and Clinical Significance in Disease", *Frontiers in Cell and Developmental Biology*, Vol. 9, p. 675465.

Wang, J., H. Wilhelmsson, C. Graff, H. Li, A. Oldfors, P. Rustin, J. C. Brüning, C. R. Kahn, D. A. Clayton, G. S. Barsh, P. Thorén and N.-G. Larsson, 1999, "Dilated Cardiomyopathy and Atrioventricular Conduction Blocks Induced by Heart-Specific Inactivation of Mitochondrial DNA Gene Expression", *Nature Genetics*, Vol. 21, No. 1, pp. 133–137.

Wang, Y., R. Branicky, A. Noë and S. Hekimi, 2018, "Superoxide Dismutases: Dual Roles in Controlling ROS Damage and Regulating ROS Signaling", *Journal of Cell Biology*, Vol. 217, No. 6, pp. 1915–1928.

Wen, J. J., C. Porter and N. J. Garg, 2017, "Inhibition of NFE2L2-Antioxidant Response Element Pathway by Mitochondrial Reactive Oxygen Species Contributes to Development of Cardiomyopathy and Left Ventricular Dysfunction in Chagas Disease", *Antioxidants & Redox Signaling*, Vol. 27, No. 9, pp. 550–566.

Westermann, B., 2010, "Mitochondrial Fusion and Fission in Cell Life and Death", *Nature Reviews Molecular Cell Biology*, Vol. 11, No. 12, pp. 872–884.

Willenborg, S., D. E. Sanin, A. Jais, X. Ding, T. Ulas, J. Nüchel, M. Popović, T. MacVicar, T. Langer, J. L. Schultze, A. Gerbaulet, A. Roers, E. J. Pearce, J. C. Brüning, A. Trifunovic and S. A. Eming, 2021, "Mitochondrial Metabolism Coordinates Stage-Specific Repair Processes in Macrophages During Wound Healing", *Cell Metabolism*, Vol. 33, No. 12, pp. 2398–2414.e9.

Wright, J. J., O. Biner, I. Chung, N. Burger, H. R. Bridges and J. Hirst, 2022, "Reverse Electron Transfer by Respiratory Complex I Catalyzed in a Modular Proteoliposome System", *Journal of the American Chemical Society*, Vol. 144, No. 15, pp. 6791–6801.

Wu, Z., M. M. Senchuk, D. J. Dues, B. K. Johnson, J. F. Cooper, L. Lew, E. Machiela, C. E. Schaar, H. DeJonge, T. K. Blackwell and J. M. Van Raamsdonk, 2018, "Mitochondrial Unfolded Protein Response Transcription Factor ATFS-1 Promotes Longevity in a Long-Lived Mitochondrial Mutant through Activation of Stress Response Pathways", *BMC Biology*, Vol. 16, No. 1, p. 147.

Yang, X., D.-D. Yu, F. Yan, Y.-Y. Jing, Z.-P. Han, K. Sun, L. Liang, J. Hou and L.-X. Wei, 2015, "The Role of Autophagy Induced by Tumor Microenvironment in Different Cells and Stages of Cancer", *Cell & Bioscience*, Vol. 5, No. 1, p. 14.

Young, M. J. and W. C. Copeland, 2016, "Human Mitochondrial DNA Replication Machinery and Disease", *Current Opinion in Genetics & Development*, Vol. 38, pp. 52–62.

Zhang, S., M. W. Hulver, R. P. McMillan, M. A. Cline and E. R. Gilbert, 2014, "The Pivotal Role of Pyruvate Dehydrogenase Kinases in Metabolic Flexibility", *Nutrition & Metabolism*, Vol. 11, No. 1, p. 10.

Zhao, Q., 2002, "A Mitochondrial Specific Stress Response in Mammalian Cells", *The EMBO Journal*, Vol. 21, No. 17, pp. 4411–4419.

Zhao, R., S. Jiang, L. Zhang and Z. Yu, 2019 "Mitochondrial Electron Transport Chain, ROS Generation and Uncoupling (Review)", *International Journal of Molecular Medicine*.

Zimorski, V., C. Ku, W. F. Martin and S. B. Gould, 2014, "Endosymbiotic Theory for Organelle Origins", *Current Opinion in Microbiology*, Vol. 22, pp. 38–48.

Zorova, L. D., V. A. Popkov, E. Y. Plotnikov, D. N. Silachev, I. B. Pevzner, S. S. Jankauskas, V. A. Babenko, S. D. Zorov, A. V. Balakireva, M. Juhaszova, S. J. Sollott and D. B. Zorov, 2018, "Mitochondrial Membrane Potential", *Analytical Biochemistry*, Vol. 552, pp. 50–59.

Zweers, H., A. M. J. van Wegberg, M. C. H. Janssen and S. B. Wortmann, 2021, "Ketogenic Diet for Mitochondrial Disease: A Systematic Review on Efficacy and Safety", *Orphanet Journal of Rare Diseases*, Vol. 16, No. 1, p. 295.